

# UNIVERSIDAD DE SONORA

División de Ciencias Exactas y Naturales

Departamento de Física

Posgrado en Nanotecnología

Thesis

**Polymeric nanoparticles for the controlled and  
specific delivery of drugs and genes**

For the degree of:

PhD in Nanotechnology

By:

**M.C.I.Q. Cindy Alejandra Gutiérrez Valenzuela**

Dissertation Director:

**Dr. Jesús Armando Lucero Acuña**

# Universidad de Sonora

Repositorio Institucional UNISON



**"El saber de mis hijos  
hará mi grandeza"**



Excepto si se señala otra cosa, la licencia del ítem se describe como openAccess

## COMMITTEE APPROVAL

**DR. MARIO ENRIQUE ÁLVAREZ RAMOS**

Nanotechnology Graduate Program Coordinator

We, as designated committee for the examination of the PhD thesis entitled: "Polymeric nanoparticles for the controlled and specific delivery of drugs and genes", presented by:

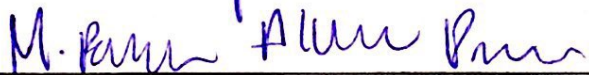
CINDY ALEJANDRA GUTIERREZ VALENZUELA

Certify that we have revised this thesis and APPROVE it as satisfying the requirements to obtain the PhD in Nanotechnology degree.



---

DR. JESÚS ARMANDO LUCERO ACUÑA



---

DR. MARIO ENRIQUE ÁLVAREZ RAMOS



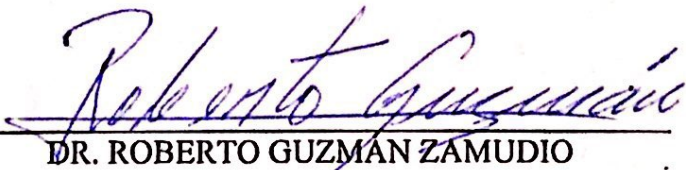
---

DRA. ADRIANA GARIBAY ESCOBAR



---

DR. REYNALDO ESQUIVEL GONZÁLEZ



---

DR. ROBERTO GUZMÁN ZAMUDIO

(EXTERNAL)

# TABLE OF CONTENTS

<b>LIST OF FIGURES .....</b>	<b>VII</b>
<b>LIST OF TABLES .....</b>	<b>XI</b>
<b>ABSTRACT.....</b>	<b>1</b>
<b>CHAPTER 1. INTRODUCTION.....</b>	<b>3</b>
1.1 Nanomedicine.....	3
1.2 Nanosystems in drug and gene delivery.....	4
1.3 Photodynamic therapy.....	6
1.4 Dissertation description.....	7
1.5 Objective .....	9
<i>1.5.1 Specific aims:.....</i>	<i>9</i>
<b>CHAPTER 2. COMPARISON OF PLGA NANOPARTICLES PREPARED BY THE TECHNIQUES OF SOLVENT EVAPORATION AND NANOPRECIPITATION.....</b>	<b>10</b>
2.1 Abstract .....	10
2.2. Introduction .....	11
2.3 Materials and Methods .....	12
<i>2.3.1 Materials.....</i>	<i>12</i>
<i>2.3.2 Preparation of PNP.....</i>	<i>12</i>
<i>2.5 Nanoparticle characterization.....</i>	<i>14</i>
2.3. Results and discussions .....	15
<i>2.3.1 PLGA Concentration .....</i>	<i>15</i>
<i>2.3.2 PVA Concentration.....</i>	<i>16</i>
<i>2.3.3 Organic to aqueous phase ratio .....</i>	<i>17</i>
<i>2.3.4 Sonicator amplitude and injection rate. ....</i>	<i>19</i>
<i>2.3.5 Agitation speed .....</i>	<i>20</i>
<i>2.3.5 Purification process.....</i>	<i>25</i>
<i>2.3.6 Cryoprotectants .....</i>	<i>26</i>

## TABLE OF CONTENTS – *Continued*

2.3.7 <i>Surface morphology</i> .....	30
2.4. Conclusion.....	31
<b>CHAPTER 3. EVALUATION OF COMBINED EMULSION PROCESS TO ENCAPSULATE METHYLENE BLUE INTO PLGA NANOPARTICLES.....</b>	<b>33</b>
3.1 Abstract .....	33
3.2. Introduction .....	34
3.3. Materials and methods .....	37
3.3.1 <i>Materials</i> .....	37
3.3.2 <i>Preparation of MB-PNP</i> .....	37
3.3.3 <i>Nanoparticle characterization</i> .....	38
3.3.4 <i>In vitro release study</i> .....	39
3.3.5 <i>Mathematical analysis of MB release</i> .....	40
3.4. Results and discussions .....	42
3.4.1 <i>Nanoparticles characterization</i> .....	42
3.4.2 <i>MB release analysis</i> .....	46
3.5. Conclusion.....	51
<b>CHAPTER 4. FOLATE FUNCTIONALIZED PLGA NANOPARTICLES LOADED WITH PLASMID PVAX1-NH36: MATHEMATICAL ANALYSIS OF RELEASE .....</b>	<b>52</b>
4.1 Abstract .....	52
4.2. Introduction .....	52
4.3 Materials and Methods .....	55
4.3.1 <i>Materials</i> .....	55
4.3.2 <i>Cell culture and pVAX1-NH36 recovery</i> .....	55
4.3.3 <i>Polymer modification</i> .....	56
4.3.4 <i>Preparation of pDNA-PNP</i> .....	57
4.3.5 <i>Nanoparticle characterization</i> .....	58
4.3.6 <i>In vitro release study</i> .....	59

## TABLE OF CONTENTS – *Continued*

4.3.7 <i>Mathematical analysis of pDNA release</i> .....	59
4.3.8 <i>Purity and integrity of plasmid</i> .....	61
4.4. Results and discussions .....	61
4.4.1 <i>Cell culture and pDNA recovery</i> .....	61
4.4.2 <i>Polymer modification</i> .....	61
4.4.3 <i>Nanoparticles characterization</i> .....	62
4.4.4 <i>Plasmid release analysis</i> .....	66
4.4.5 <i>Plasmid purity and integrity</i> .....	69
4.5 Conclusion .....	70
<b>CHAPTER 5. CONCLUSIONS</b> .....	<b>71</b>
<b>APPENDIX A. PHOTOACTIVATION OF METHYLENE BLUE IN BEAS-2B LUNG EPITHELIAL CELLS GENERATES ROS AND COMPROMISES CELL SURVIVAL</b> .....	<b>73</b>
A.1 Abstract .....	73
A.2. Background .....	73
A.3. Aims .....	74
A.4. Materials and Methods .....	74
A.4.1. DFBP Probe .....	74
A.4.2. Cell culture .....	74
A.4.3. <i>In vitro</i> PDT treatment and cell survival .....	74
A.4.4. Determination of intracellular ROS .....	75
A.5. Results and Discussion .....	75
A.6. Conclusions .....	78
<b>APPENDIX B. CELLULAR UPTAKE OF PLGA NANOPARTICLES LOADED WITH PDNA AND GFP PROTEIN EXPRESSION IN H441 CELLS</b> .....	<b>79</b>
B.1 Abstract .....	79

## TABLE OF CONTENTS – *Continued*

B.2 Introduction .....	79
B.3. Methods .....	80
B.4. Results .....	80
B.6. Conclusions .....	81
<b>CHAPTER 6. REFERENCES.....</b>	<b>82</b>

## LIST OF FIGURES

<b>Figure 2.1.</b> Nanoparticle preparation scheme by (A) simple emulsification and (B) nanoprecipitation techniques. ....	13
<b>Figure 2.2.</b> Characteristics of PLGA nanoparticles prepared by emulsification and nanoprecipitation techniques. Particle diameter and PDI of nanoparticles prepared by: (A) emulsification technique with 5 mg/mL (■), 10 mg/mL (■) and 15 mg/mL (■) PLGA concentration, and (B) nanoprecipitation technique with 5 mg/mL (■), 10 mg/mL (■) and 20 mg/mL (■) PLGA concentration. Data represent mean ± SD ( $n = 3$ ). ....	16
<b>Figure 2.3.</b> Characteristics of PLGA nanoparticles prepared by (A) emulsification and (B) nanoprecipitation techniques. Particle diameter and PDI of nanoparticles prepared with 1% (■), 3% (■) and 5% (■) PVA. Data represent mean ± SD ( $n = 3$ ). ....	18
<b>Figure 2.4.</b> Characteristics of PLGA nanoparticles prepared by emulsification and nanoprecipitation techniques. Particle diameter and PDI of nanoparticles prepared by: (A) emulsification technique with 1:1 (■), 1:2 (■) and 1:5 (■) organic:aqueous ratio and (B) nanoprecipitation technique with 1:2 (■), 1:5 (■) and 1:10 (■) organic:aqueous ratio. Data represent mean ± SD ( $n = 3$ ). ....	19
<b>Figure 2.5.</b> Characteristics of PLGA nanoparticles prepared by emulsification and nanoprecipitation techniques. Particle diameter and PDI of nanoparticles prepared by: (A) emulsification technique with 25% (■), 50% (■) and 75% (■) sonication amplitude and (B) nanoprecipitation technique with 0.6 mL/min (■), 1.2 mL/min (■) and 2.4 mL/min (■) injection speed. Data represent mean ± SD ( $n = 3$ ). ....	21
<b>Figure 2.6.</b> Characteristics of PLGA nanoparticles prepared by emulsification and nanoprecipitation techniques. Particle diameter and PDI of nanoparticles prepared by: (A) emulsification technique with a speed of agitation of 200 rpm (■), 300 rpm (■) and 400 rpm (■) and (B) nanoprecipitation technique with a speed of agitation of 200 rpm (■), 400 rpm (■) and 600 rpm (■) during solvent evaporation. Data represent mean ± SD ( $n = 3$ ). ....	22

## LIST OF FIGURES - Continued

<b>Figure 2.7.</b> Characteristics of PLGA nanoparticles during the purification process. Particle diameter (A), PDI (A) and zeta potential (B) of nanoparticles at different points of the purification process with centrifugation speed of 10,000 rpm (■), 15,000 rpm (■) and 20,000 rpm (■). Data represent mean ± SD ( <i>n</i> = 3).	26
<b>Figure 2.8.</b> Characteristics of PLGA nanoparticles when adding different ratios of cryoprotectants with respect to initial PLGA mass during dry-freezing process before lyophilization (■), sucrose (■), glucose (■) and lactose (■). Data represent mean ± SD ( <i>n</i> = 3).	28
<b>Figure 2.9.</b> Scanning electron micrograph PLGA nanoparticles.	31
<b>Figure 3.1.</b> Schematic of MB loaded PLGA nanoparticle preparation. Single (A), double (B) and combined (C) emulsification techniques.	38
<b>Figure 3.2.</b> Characteristics of MB-PNP prepared by different emulsification techniques. (A) Particle diameters and PDI. (B) Zeta potentials. Blank nanoparticles and MB-PNP prepared with an O/W emulsification technique for 2.0 and 4.0 % TDL (■). MB-PNP prepared with a W/O/W emulsification technique for 4.0, 8.0 and 16.0 % TDL (■). MB-PNP prepared by a combined W/O/W emulsion method for 12 % TDL (■). Data represent mean ± SD ( <i>n</i> = 3).	43
<b>Figure 3.3.</b> Drug loading (△) and encapsulation efficiency (■) for the MB-PNP with different theoretical drug loading experiments prepared by the different emulsification techniques. Data represent mean ( <i>n</i> = 3).	44
<b>Figure 3.4.</b> Scanning electron micrograph of blank-PNP. The insert represents the particle size distribution histogram of blank-PNP.	46
<b>Figure 3.5.</b> In vitro MB release profiles from 4.0 % (■) TDL MB-PNP prepared with an O/W emulsification technique, 8.0 % (◆) TDL prepared by W/O/W emulsion method; and 12 % (▲) prepared by a combined W/O/W emulsion method. Data represent mean ± SD ( <i>n</i> = 3).	47
<b>Figure 3.6.</b> MB release initial burst model (****), diffusion model (----) and a combined initial burst and diffusion model (---) profiles from (A) 4.0 % (■) TDL MB-PNP	

## LIST OF FIGURES - Continued

prepared with an O/W emulsification technique, (B) 8.0 % (◆) TDL prepared by W/O/W emulsion method; and (C) 12 % (▲) prepared by a combined W/O/W emulsion method. Data represent mean ± SD ( $n = 3$ ).	49
<b>Figure 4.1.</b> Schematic of the synthesis of the polymer PLGA-PEG-FA. First, PLGA carboxylic acid is activated and coupled to a primary amine of PEG (PLGA-PEG). Then, a carboxylic acid from FA is activated and conjugated to the primary amine of PLGA-PEG to finally obtain PLGA-PEG-FA.	58
<b>Figure 4.2.</b> FT-IR absorption peaks of PLGA-PEG-FA polymer. Characteristic bands for aromatic ring present in the folic acid at 1452 and 1608 $\text{cm}^{-1}$ and PLGA-PEG-FA representative absorption peaks at 1623 and 1571 $\text{cm}^{-1}$ due to the presence of – CONH– linkage.	62
<b>Figure 4.3.</b> Characteristics of pDNA-NP prepared at different pVAX1-NH36 TDL. (A) Particle diameter and PDI; (B) zeta potentials; (C) EE and DL for different pVAX1-NH36 with TDL of 0.2 % (■), 0.5 % (■) and 0.8 % (■) were evaluated. Data represent	64
<b>Figure 4.4.</b> (A) SEM images of pDNA-NP with 0.8% TDL. AFM images of pDNA-NP with (B) 0.2% TDL, and (C) 0.5% TDL.	66
<b>Figure 4.5.</b> <i>In vitro</i> pVAX1-NH36 release profiles from pDNA-NP for TDL of 0.2 % (◆), 0.5 % (■) and 0.8 % (▲). Data represent mean ( $n = 3$ ).	68
<b>Figure 4.6.</b> Agarose gel electrophoresis for pVAX1-NH36 before and after nanoparticle preparation. (1) Size marker for supercoiled plasmid form over the range 2 972 – 12 138 bp. (2) Initial pVAX1-NH36 solution used to formulate the pDNA-NP. (3) Sample acquired from 0.5 % TDL solution after pDNA-NP purification. (4) Sample obtained from 0.8 % TDL solution after pDNA-NP purification.	70
<b>Figure A.5.1.</b> DPBF decay after irradiation in the presence of 6.25 $\mu\text{M}$ MB (A) or 31.26 $\mu\text{M}$ MB (C). Proportionality between DPBF absorbance decay and irradiation time in the presence of 6.25 $\mu\text{M}$ of MB (B) and 31.26 $\mu\text{M}$ of MB (D).	76

## LIST OF FIGURES - Continued

<b>Figure A.5.2.</b> (A) ROS production in cells detected by the chemical probe HDFC-DA and (B) cell viability after treatment with MB concentrations ranging from 0 to 156 $\mu$ M in combination with energy fluences of 0J/cm <sup>2</sup> (■), 6J/cm <sup>2</sup> (■), 18J/cm <sup>2</sup> (■), and 36J/cm <sup>2</sup> (■). Data represent the mean with standard deviation for --- replicates?? (n = 3).....	77
<b>Figure B.1.</b> <i>In vitro</i> release kinetics of pGFP-PNP.....	81
<b>Figure B.2.</b> Comparison of internalization between naked and encapsulated plasmid.....	81

## LIST OF TABLES

<b>Table 2.1.</b> PNP preparation scheme and range of study.....	14
<b>Table 2.2.</b> Characteristics of PLGA nanoparticles when modifying parameters for the emulsification method. Data represent mean $\pm$ SD ( $n = 3$ ).....	23
<b>Table 2.3.</b> Characteristics of PLGA nanoparticles when modifying the centrifugation speed during purification. Data represent mean $\pm$ SD ( $n = 3$ ).....	27
<b>Table 2.4.</b> Characteristics of PLGA nanoparticles when adding cryoprotectants during dry-freezing process. Data represent mean $\pm$ SD ( $n = 3$ ).....	29
<b>Table 3.1.</b> Characteristics of MB-PNP as a function of TDL. Data represent mean $\pm$ SD ( $n = 3$ ). .....	45
<b>Table 3.2.</b> Parameters of MB release from MB-PNP. The parameters were determined and used in the mathematical development of the release model. ....	50
<b>Table 4.1.</b> Characteristics of pDNA-NP as a function of pVAX1-NH36 TDL. Data represent mean $\pm$ SD ( $n = 3$ ). .....	63
<b>Table 4.2.</b> Parameters of plasmid pVax1-NH36 release from pDNA-NP. The parameters were determined and used in the mathematical development of the release model. ....	69

## ABSTRACT

In this research, the process of preparation of biodegradable polymeric nanoparticles was evaluated. The emulsification and nanoprecipitation techniques were used to prepare drug and gene loaded nanoparticles of poly-dl-lactic-co-glycolic acid (PLGA). A comparison of the main parameters controlling the preparation of nanoparticles by both techniques was completed. These parameters included: the polymer concentration; surfactant concentration; organic to aqueous rate; sonication amplitude or injection speed; and the agitation speed during solvent evaporation. The centrifugation speeds during purification of nanoparticles and the use of cryoprotectants in the emulsification and nanoprecipitation techniques were also investigated.

Polymeric nanoparticles of PLGA (PNP) loaded with methylene blue (MB) were prepared by a combination of the single and double emulsification techniques, and compared with the individual techniques. PNP loaded with MB (MB-PNP) sizes obtained from the combined technique are similar to the single emulsion technique, while the diameter of particles prepared by double emulsion increased in proportion to the mass of MB used in the preparation. Experimental release of MB from MB-PNP nanoparticles was evaluated obtaining a monophasic release profile. A mathematical model of release that simultaneously combines the mechanisms of initial burst and drug diffusion was used to successfully describe the experimental release. This drug release mathematical analysis could be extended to other drugs with partial solubility.

The relationship between ROS produced by photoactivation of MB and BEAS-2B cell survival was evaluated. Increments of ROS produced by MB photoactivation are directly related to BEAS-2B cell survival. Even though BEAS-2B cells presented oxidative stress when exposed to MB alone, results suggest that BEAS-2B cells are more resistant to ROS than some cancerous cell lines reported in literature. Therefore, in lung cancer photodynamic treatments using MB, selective cell damage could be achieved.

PLGA was modified with polyethylene glycol (PEG) and functionalized with folic acid (FA) following basic carbodiimide chemistry to obtain the copolymer PLGA-PEG-FA. This synthesis was verified by FT-IR and spectrophotometry methods. Nanoparticles of PLGA-PEG-FA loaded with pVAX1-NH36 (pDNA-PNP) were prepared by using the double emulsification-solvent evaporation technique. Plasmid pVAX1-NH36 was replicated in *E. coli* cell cultures and purified using a commercial kit. Experimental drug release presented a multiphase release profile for the duration of more than 30-days. Plasmid release was effectively analyzed with a mathematical model that considers a simultaneous contribution of initial burst and the degradation-relaxation of nanoparticle. This mathematical analysis presents a novel approach to describe and predict the release of plasmid DNA from biodegradable nanoparticles.

A plasmid containing green fluorescent protein (pGFP) was encapsulated into PLGA-Rhodamine nanoparticles (PLGA-Rh) to study plasmid expression and cellular uptake. PLGA-Rh nanoparticles loaded with pGFP (pGFP-PNP) were prepared by using double emulsification-solvent evaporation technique. PLGA-Rh synthesis was verified by FT-IR. The difference in size and zeta potential between blank nanoparticles and pGFP-PNP suggest the successful encapsulation of the pGFP and the *in vitro* release studies showed a single-stage release profile with 10-days of duration. Cellular uptake and plasmid expression were confirmed by fluorescence microscopy visualization of the nanoparticles and the GFP protein on H441 cells.

# CHAPTER 1. INTRODUCTION

## 1.1 Nanomedicine

During the last few years, the term nanotechnology has become popular among researchers in the academic and commercial sectors. According to the US National Nanotechnology Initiative, nanotechnology is the “understanding and control of matter at the nanoscale, at dimensions between approximately 1 and 100 nanometers, where unique phenomena enable novel applications” (National Nanotechnology Initiative, 2017a). In this scale, materials display unusual properties that are absent at larger (bulk materials) or smaller (atoms or molecules) length scales (Noury & López, 2017). These properties include magnetism, heat or electricity conduction, chemical reactivity, light reflection, among others; and can be attributed to quantum mechanical and surface science effects (National Nanotechnology Initiative, 2017b; Noury & López, 2017). Nanomedicine is therefore identified as the application of nanotechnology to medicine. The European Technology Platform on Nanomedicine defines nanomedicine as the application of nanotechnology to health and focus on the potential impact on the prevention, early and reliable diagnosis and treatment of diseases by exploiting the physical, chemical, and biological properties of materials at the nanometric scale (European Technology Platform on NanoMedicine, 2005).

In literature, authors describe nanomedicine as the comprehensive monitor, control, construction, repair, defense and improvement of all human biological system with the purpose of achieving medical benefits (Boisseau & Loubaton, 2011a).

Nanomedicine is expected to drastically change the practice of health care thoroughly from diagnostics to therapeutics, promising that diagnosis and treatments would be personalized, meaning that they would be tailored to individual needs of the patient (Noury & López, 2017). Another promise of nanomedicine is the pre-symptomatic diagnosis and the treatment of diseases before severe damage occurs, resulting in better outcome for patients and lower cost of treatment (Leary, 2010). In order to fulfill these

tasks, engineered devices and nanostructures must be used, systems that include active components or objects in the size range from one to hundreds of nanometers (Boisseau & Loubaton, 2011b). Regenerative medicine, implanted devices, in vitro and in vivo diagnostics that involve imaging; and delivery of pharmaceuticals are some of the most important areas of application of nanomedicine (Boisseau & Loubaton, 2011b)(Würmseher & Firmin, 2017).

## **1.2 Nanosystems in drug and gene delivery**

Delivery of pharmaceuticals or therapeutic agents to cells, tissues or tumours is more effective when drug delivery vehicles or nanocarriers are design. The aim of these systems is to deliver a specific amount of the compound or gene of interest to a specific place in a timely and controlled manner. These systems must be biodegradable and biocompatible, and should also be able to improve stability of the active substances; protect the integrity of the gene of interest; reduce drug toxicity; reach higher intracellular uptake than other particulate system; and also, recognize specific tissues (Mu & Feng, 2003; Kreuter, 2007a; Peer *et al.*, 2007; Mora-Huertas *et al.*, 2010; Shi *et al.*, 2010; Makadia & Siegel, 2011; Danhier *et al.*, 2012; Nava-Arzaluz *et al.*, 2012). Size of the nanocarrier is an important factor, as they should be big enough to prevent fast incorporation into blood vessels but small enough to prevent elimination from the immune system (Cho *et al.*, 2008).

Immunization methods based on plasmid DNA (pDNA) consist on gene transfection to human cells to encode the synthesis of a protein, which carries an immunizing or therapeutic action. Gene delivery using nanocarriers aims to overcome limitations and restrictions in transport of pDNA through traditional routes (Wang *et al.*, 1999).

A variety of materials have been used for nanocarriers, including inorganic materials such as metallic and magnetic nanoparticles, ceramic based and silica-based nanostructures, quantum dots and carbon materials; and also organic materials including liposomes, micelles, polysaccharides, dendrimers and polymers (Paszko *et al.*, 2011; Vivero-Escoto & Elnagheeb, 2015).

The poly (ester) poly-dl-lactic-co-glycolic acid (PLGA) has been extensively used in research as a nanocarrier as it has an immense potential as drug delivery vehicle as well as a platform for tissue engineering (Makadia & Siegel, 2011; Danhier *et al.*, 2012).

PLGA has important properties that are desired for drug delivery

- It is biodegradable as it hydrolyzes into lactic acid and glycolic acid monomers, which subsequently degrades into carbon dioxide and water (Jain, 2000; Kumari *et al.*, 2010; Danhier *et al.*, 2012)
- Degradation rate can be controlled by adjusting its molecular weight and copolymer composition (Jain, 2000)
- It has been approved by the Food and Drug Administration (FDA) to be used in therapeutic devices (Parveen & Sahoo, 2008; Danhier *et al.*, 2012).
- Contains a carboxylic acid that can be easily functionalized with other molecules before or after nanoparticles preparation (Gutiérrez-Valenzuela *et al.*, 2016)

The purpose of functionalizing PLGA is to modify its properties and therefore the biological response to the nanocarrier. The coupling of polymer polyethylene glycol (PEG) can improve circulation in blood, prevent recognition by mononuclear phagocytic system and also facilitate the control of drug release rate (Peracchia *et al.*, 1997). Coupling of folic acid can attribute selective gene delivery to folate receptor overexpressing tissues (Esmaeili *et al.*, 2008; Liang *et al.*, 2011; Benfer *et al.*, 2012) and coupling of fluorescent dyes as rhodamine can be used to perform in vitro microscopic visualization (Yang *et al.*, 2006).

In literature, varieties of techniques to prepare PLGA nanoparticles (PNP) have been reported. Some of the most common techniques are: diffusion or reverse salting-out, polymerization, emulsification followed by either solvent evaporation, nanoprecipitation, among others (Murakami *et al.*, 2000; Chorny *et al.*, 2002; Dhar *et al.*, 2008; Sahana *et al.*, 2008; Cohen-Sela *et al.*, 2009; Park *et al.*, 2009; Vauthier & Bouchemal, 2009; Mora-Huertas *et al.*, 2010).

The emulsion process is used to encapsulate hydrophobic or hydrophilic component by performing a single or double emulsion, respectively. Authors have study the process variables extensively, modifying variables like solvents, stabilizers, organic to aqueous

ratio, different polymers, and others (Sahoo *et al.*, 2002; Astete & Sabliov, 2006; Budhian *et al.*, 2007; Iqbal *et al.*, 2015).

One of the major challenges that all of the encapsulation techniques present is low drug loading and encapsulation efficiency. Authors have presented a wide variety of adaptations to the methods such as variations of pH, temperature, variation of surfactants and the addition of excipients as fatty acids, stabilizers or cross-linkers. (Zambaux *et al.*, 1998; Govender *et al.*, 1999; Tewes *et al.*, 2007; Klepac-Ceraj *et al.*, 2011; Nava-Arzaluz *et al.*, 2012; Cannavà *et al.*, 2016; Song *et al.*, 2016).

Authors have explained a variety of phenomenon occurring in the drug release from polymeric nanoparticles. These mechanisms include initial burst, polymer-dug and drug-drug interactions, polymer relaxation, hydrolysis, polymer erosion, drug dissolution, formation of cracks and deformation, transport through water-filled pores and transport through the polymer (Fitzgerald & Corrigan, 1993; Corrigan & Li, 2009; Fredenberg *et al.*, 2011). Mathematical modelling involving one or more mechanisms of release are reported in literature; the most representative mechanisms are the initial burst, drug diffusion and the degradation of PLGA (Batycky *et al.*, 1997; Lao *et al.*, 2011; Lucero-Acuña & Guzmán, 2015; Cannavà *et al.*, 2016).

### **1.3 Photodynamic therapy**

Since early 1900s, it has been known that the use of dyes for staining cellular components could inactivate microorganisms such as viruses and bacteria even under the conditions of microscope illumination (Tuite & Kelly, 1993). Nowadays, photodynamic therapy (PDT) has become of great interest in many areas of clinical medicine as an alternative and promising non-invasive treatment for cancer and non-cancer diseases. PDT consists of the application of a photosensitizer (PS) agents in area of interest, a light of specific wavelength activates the PS which in the presence of oxygen produces reactive species of oxygen (ROS) that create oxidative damage to the targeted cells (Zhang *et al.*, 2007; Kolarova *et al.*, 2008).

ROS are naturally involved in biological functions, however, when ROS are overproduced, or when levels of antioxidants become severely depleted, these species become dangerous and produce oxidation of molecules which leads to oxidative stress, therefore cellular damage (Gomes *et al.*, 2005).

Methylene blue (MB) has been used in PDT as it satisfies several requirements of an ideal photosensitizer: it absorbs light intensively within the therapeutic window and it has a simple chemical structure that allows it to easily penetrate biological membranes and the facility of oxidation-reduction in situ (Wainwright & Crossley, 2002; Tardivo *et al.*, 2005; Fioramonti Calixto *et al.*, 2016). MB absorbs at 665 nm in its monomer form, and as other dyes has a tendency to form large aggregates in the form of dimers, that have a visible absorption band about 60 nm shorter than the monomer (Lai *et al.*, 1984; Tuite & Kelly, 1993). Authors have research MB for treating from neurological disorders to cancer chemotherapy (Wainwright & Crossley, 2002; Cannavà *et al.*, 2016). It has also been encapsulated in different matrices as silica, chitosan, and polymer (He *et al.*, 2009; Klepac-Ceraj *et al.*, 2011; Cannavà *et al.*, 2016; Darabpour *et al.*, 2016; Deprá de Souza *et al.*, 2016)

#### **1.4 Dissertation description**

The focus of this dissertation is the process of preparation of biodegradable polymeric nanoparticles. Hence, Chapter 2 includes the preparation of PNP by emulsification and by nanoprecipitation technique. An evaluation of the nanoparticles obtained when modifying parameters in the formulation of both techniques is reported. These parameters include the polymer concentration; surfactant concentration; organic to aqueous rate; sonication amplitude or injection speed; agitation speed during evaporation; centrifugation speed during purification; and the use of cryoprotectants.

Chapter 3 describes the encapsulation of MB in PLGA nanoparticles (MB-PNP) were prepared a new approach of combining the single and double emulsification techniques is studied. A comparison of the MB-PNP obtained with the combined and the individual techniques are presented. The sizes of MB-PNP obtained from the single emulsion

technique are similar to the combined technique, while the diameter of particles prepared by double emulsion increased as the theoretical drug loading (TDL) increased. *In-vitro* release studies show a monophasic release profile that was analyzed by considering the mechanisms of initial burst, drug diffusion and a combination of them. Experimental results could be better described using a mathematical model of release that simultaneously combines the mechanisms of initial burst and drug diffusion. The approach presented to encapsulate MB and to analyze the drug release could be extended to other drugs with partial solubility. Appendix A includes an evaluation of the relationship between ROS produced by photoactivation of MB and BEAS-2B cell survival. In this project, the production of ROS from laser stimulation of MB was evaluated in aqueous -dimethyl sulfoxide solutions using 1,3-diphenylisobenzofuran as probe and 2',7'-dichlorodihydrofluorescein diacetate as probe for BEAS-2B cells. Even though BEAS-2B cells presented oxidative stress when exposed to MB alone, results suggest that BEAS-2B cells are more resistant to ROS than some cancerous cell lines reported in literature.

In Chapter 4, plasmid pVAX1-NH36 was encapsulated in nanoparticles of PLGA functionalized with PEG and folic acid (PLGA-PEG-FA) without losing integrity. PLGA-PEG-FA nanoparticles loaded with pVAX1-NH36 (pDNA-PNP) were prepared by using double emulsification-solvent evaporation technique. PLGA-PEG-FA synthesis was verified by FT-IR and spectrophotometry methods. pVAX1-NH36 was replicated in *E. coli* cell cultures. *In vitro* release studies confirmed a multiphase release profile for the duration of more than 30-days. Plasmid release kinetics were analyzed with a release model that considered simultaneous contributions of initial burst and degradation-relaxation of nanoparticles. Fitting of release model against experimental data presented excellent correlation. This mathematical analysis presents a novel approach to describe and predict the release of plasmid DNA from biodegradable nanoparticles.

In order to prove plasmid functionality after the encapsulation process, Appendix B shows the nanoparticles characteristics and *in vitro* release profile for a plasmid containing the GFP gene (pGFP). After transfection, a fluorescent protein is expressed and can be visualized microscopically. pGFP was successfully expressed in H441 cells.

## 1.5 Objective

To prepare and characterize polymeric nanoparticles for the controlled and specific administration of drugs and genes.

### 1.5.1 Specific aims:

- To synthesize and characterize copolymers with applications in the preparation of functionalized, biocompatible and biodegradable nanoparticles.
- To prepare polymeric nanoparticles encapsulating different drugs or genes.
- Functionalize nanoparticles with ligands on the surface for cancerous cell recognition
- To characterize the nanoparticles by using characterization techniques such as DLS, SEM, laser Doppler electrophoresis, HPLC-HIC, drug loading and encapsulation efficiency.
- To analyze *in vitro* release kinetics of different actives.

## **CHAPTER 2. COMPARISON OF PLGA NANOPARTICLES PREPARED BY THE TECHNIQUES OF SOLVENT EVAPORATION AND NANOPRECIPIATION**

### **2.1 Abstract**

In this study, the preparation of PNP using the techniques of emulsification and nanoprecipitation is presented. A comparison of the nanoparticles obtained when modifying parameters in the formulation of both techniques is reported, including parameters such as the polymer concentration; surfactant concentration; organic to aqueous rate; sonication amplitude or injection speed; agitation speed during evaporation; centrifugation speed during purification; and the use of cryoprotectants. Characterization of nanoparticles was done by DLS, laser Doppler electrophoresis and SEM. Results indicate that nanoparticles characteristics can be adjusted by modifying this parameters. To obtain smaller, monodisperse and repeatable nanoparticles with negative zeta potential, the following parameters have been selected: polymer concentration of 5mg/mL solvent; organic to aqueous rate 1 to 5; and agitation speed during evaporation of 400 rpm. For the emulsification techniques a surfactant concentration of 5% and sonication amplitude of 75%, and for nanoprecipitation, surfactant concentration of 3% and injection speed of 2.4 mL/min. For purification of nanoparticles, a centrifugation speed of 20,000 rpm resulted in smaller PNP size and standard deviation, and in more negative zeta potentials and better yield compared to the other considered speeds. When glucose was used as a cryoprotectant in a 1 to 1 ratio compared to the initial amount of PLGA, PNP size and zeta potentials' change was negligible. These parameters would result in monodisperse, sub 200nm in size nanoparticles and reproducible experiments.

## 2.2. Introduction

The use of nanodevices for medical applications is one of the most promising technologies of the last 50 years, when the first nanoparticles were developed for drug delivery and vaccination purposes (Kreuter, 2007b). Over time, the objectives of these systems remain the same: to achieve drug release in a control manner from particles that are biocompatible with tissue and cells; to reach higher intracellular uptake than other particulate systems; to improve stability of active substances, to be able to target specific tissue (Kreuter, 2007b; Mora-Huertas *et al.*, 2010). (Peer *et al.*, 2007; Shi *et al.*, 2010). An important factor in the design of this systems is the size, it should be big enough to prevent fast incorporation into blood vessels but small enough to prevent elimination from the immune system (Cho *et al.*, 2008). Among all the materials used as nanocarriers, polymeric nanoparticles have shown higher structural integrity and stability than other nanocarriers; they are also capable of controlling the drug release profile and can be easily synthesized and functionalize (Ghitman *et al.*, 2017).

Authors report that PLGA has shown to have this important properties (Jain, 2000; Kumari *et al.*, 2010; Danhier *et al.*, 2012). Different methods of preparation of polymeric nanoparticles have been used, depending on the characteristics of the drug to encapsulate. During nanoparticle preparation, it is important to obtain uniform size nanoparticles, reproducible experiments and being able to adjust the particle size as needed. When encapsulating hydrophobic compounds, two of the most commonly used techniques are the emulsification-solvent evaporation and the nanoprecipitation technique (Astete & Sabliov, 2006; Mora-Huertas *et al.*, 2011). Emulsification consist of the use of a volatile non-miscible solvent and water and the application of high shear force by ultrasonication, which results in the formation of an emulsion. Its advantage is that it can be used for hydrophobic and hydrophilic compounds and also presents good reproducibility, and even though it has a high consumption of energy, the evaporation process time can be reduced. Another consideration reported is that sonication could affect the stability of certain drugs (Astete *et al.*, 2007; Nava-Arzaluz *et al.*, 2012). Nanoprecipitation is also known as solvent-displacement, in this method, nanoparticle formation takes place in one-step, is instantaneous (Bilati *et al.*, 2005). Involves the use

of miscible solvents and its advantages include simplicity, good reproducibility, low energy input and importantly, ease of scalability (Miladi *et al.*, 2016).

After nanoparticle formulation, potentially toxic impurities such as organic solvents, surfactant, residual monomers and large polymer aggregates must be eliminated. Some of the most commonly used methods for laboratory scale particle purification include dialysis, gel filtration, evaporation under reduced pressure and ultracentrifugation (Limayem *et al.*, 2004).

In this work, biodegradable nanoparticles by emulsification-solvent evaporation and nanoprecipitation technique were prepared. Several factors that intervene in the nanoparticle preparation process were compared, including polymer concentration, molecular weight, stabilizer concentration, organic to stabilizer ratio, sonication amplitude and injection speed, and evaporation mixing speed. Centrifugation speed during concentration and cryoprotectant use was also evaluated. Nanoparticles were characterized by DLS, laser Doppler electrophoresis and SEM.

## **2.3 Materials and Methods**

### *2.3.1 Materials*

PLGA acid terminated (PLGAa) (50/50 DL-lactide/glycolide copolymer) with molecular weight of 17 kg/mol and PLGA (50/50 DL-lactide/glycolide copolymer) with molecular weight of 153 kg/mol were received as gift sample from Corbion Purac, Gorinchem, The Netherlands. Polyvinyl alcohol (86-89% hydrolysis, low molecular weight, PVA) was obtained from Alfa Aesar, Ward Hill, Massachusetts, USA. Dichloromethane (DCM) was obtained from Fisher Scientific Inc., Fair Lawn, New Jersey, USA. Acetonitrile (AC) was obtained from Sigma Aldrich, Inc., St. Louis, MO, USA.

### *2.3.2 Preparation of PNP*

PNP were prepared by using the single emulsification and the nanoprecipitation techniques. Fig. 2.1 illustrates a preparation scheme for both techniques and the parameters that were evaluated within the study. Table 2.1 outlines the parameters

considered in each experiment; these parameters were varied individually while maintaining the rest of them constant. Overall, in the single emulsification technique (Fig. 2.1A), an organic solution (DCM) containing 10 mg/mL PLGA was added to an aqueous solution (5% PVA) in a 1 to 5 ratio. The mixture was then emulsified during 1 min at 75% amplitude (90  $\mu$ m) under an ice bath by using a QSonica 500 sonicator (QSonica LLC, Newtown, Connecticut, USA). In the nanoprecipitation technique (Fig. 2.1B), an organic solution (AC) solution containing 10 mg/mL PLGA was injected to an aqueous solution (PVA 3%) in a 1 to 5 ratio using a NE-300 Just Infusion™ Syringe Pump (New Era Pump Systems Inc, Farmingdale, New York, USA). After emulsification or organic phase injection, respectively, the solvent was evaporated under magnetic stirring at 400 rpm, at room temperature. Then, PNP were washed by three centrifugation cycles by using a Sigma 3-30KS centrifuge (Sigma Laborzentrifugen GmbH, Osterode am Harz, Germany) operated at 37,565\*g (20,000 rpm) for 20 minutes, discarding supernatant and resuspending pellet nanoparticles in deionized water. A cryoprotectant solution was added to the PNP solution and then placed in a -80°C freezer. Finally, PNP were freeze-dried in lyophilizer freezone 4.5 (Labconco, Kansas City, Missouri, USA). Experiments were performed by triplicate.

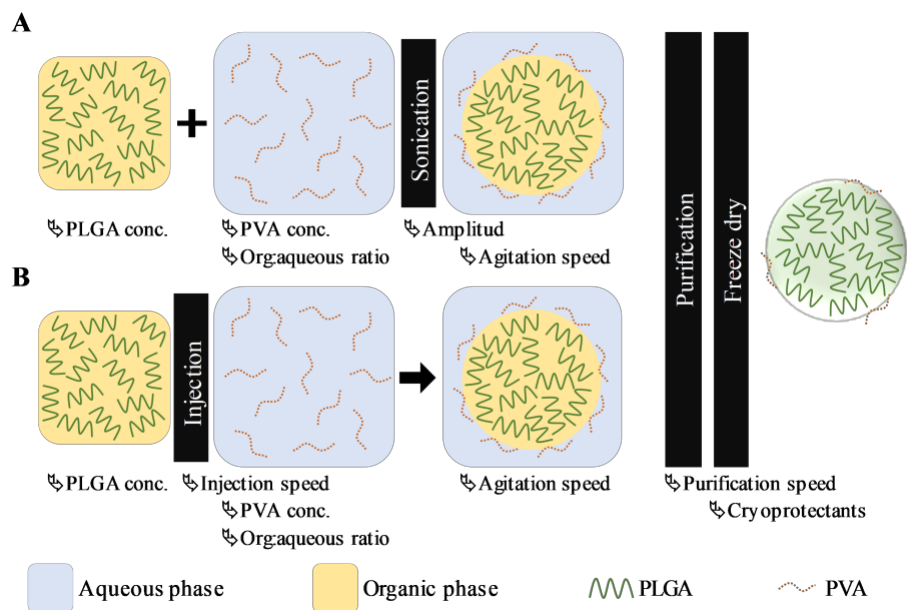


**Figure 2.1.** Nanoparticle preparation scheme by (A) simple emulsification and (B) nanoprecipitation techniques

**Table 2.1.** PNP preparation scheme and range of study.

<b>Emulsification technique</b>			
PLGA concentration (mg/mL)	5	10	15
PVA concentration (mg/mL)	1	3	5
Organic:aqueous phase ratio	1:1	1:2	1:5
Sonication amplitude (%)	25	50	75
Agitation speed (rpm)	200	300	400
<b>Nanoprecipitation technique</b>			
PLGA concentration (mg/mL)	5	10	20
PVA concentration (mg/mL)	1	3	5
Organic:aqueous phase ratio	1:1	1:5	1:10
Injection speed (mL/min)	0.6	1.2	2.4
Agitation speed (rpm)	200	400	600
Purification (*g)	9,092	27,216	48,384
Cryoprotectant	sucrose	lactose	glucose

### 2.5 Nanoparticle characterization

Nanoparticle size distribution and zeta potentials were measured using a zetasizer Nano ZS equipment (Malvern Instruments Ltd., Worcestershire, United Kingdom). Measurements of PNP sizes were performed by DLS. Each sample was measured three times with 10 runs respectively. Additionally, each sample for zeta potential was measured by duplicated with at least 10 runs at constant temperature (25°C) by laser Doppler electrophoresis. Z-averages and zeta potentials were obtained from three independent experiments.

Surface morphology of PNP were analyzed by SEM through a field emission scanning electron microscope (Hitachi S-4800 FE-SEM, Hitachi Corporation, Tokyo, Japan). Samples were prepared by placing a small quantity of lyophilized nanoparticles on a double-sided carbon tape previously placed on a SEM stub. Compressed air was used to remove loose nanoparticles. Platinum coating was applied using with an Anatech

Hummer 6.2 sputter system (Anatech USA, Hayward, California, USA). A total of 60 seconds under 10 mA under argon plasma were applied. A beam strength of 1.0 kV and a working distance in the range of 8-9 mm were used to visualize nanoparticles.

### **2.3. Results and discussions**

Nanoparticles were characterized by measuring their particle size, polydispersity index (PDI), and zeta potential on all experiments. Some parameters were evaluated for the process:

#### *2.3.1 PLGA Concentration*

For the PNP prepared by the emulsification technique, PLGA concentration was evaluated by using 5 mg/mL, 10 mg/mL and 15 mg/mL of solvent. As it can be appreciated in Fig 2.2, for all formulations, sizes obtained were 175 nm. However, PDI decreased from 0.144 to 0.078 as the PLGA concentration increased. Meaning that when PLGA was more concentrated, PNP sizes were less uniform in size. In addition, zeta potential was maintained between -26.8 and -30.0 mV. For the PNP prepared by nanoprecipitation technique, PLGA concentration was also considered, in this case, 5 mg/mL, 10 mg/mL and 20 mg/mL were evaluated. PNP size increased from 202.5 nm to 214.8 nm to 246.3 nm respectively. The PDI was maintained within 0.058 to 0.083 and zeta potential between -5.0 and -5.9 mV. The difference in size between both techniques can be attributed to the difference in molecular weight of the PLGA used (Astete & Sabliov, 2006). The considerable change in zeta potential between the emulsification and the nanoprecipitation technique could be attributed to the use of acid terminated PLGA in the emulsification technique, meaning that it has a carboxylic group at the end of the polymer, giving it the negative surface charge (Ghitman *et al.*, 2017). PLGA concentration affected the resulting size for the nanoprecipitation technique and resulted in a wider range of sizes for the emulsification technique. According to literature, an increase in the viscosity of the organic phase, means a higher content of polymer per volume of solution, therefore, more polymer in the droplets formed during the process of

nanoprecipitation, therefore a larger size of PNP (Astete & Sabliov, 2006; Feczko *et al.*, 2011).

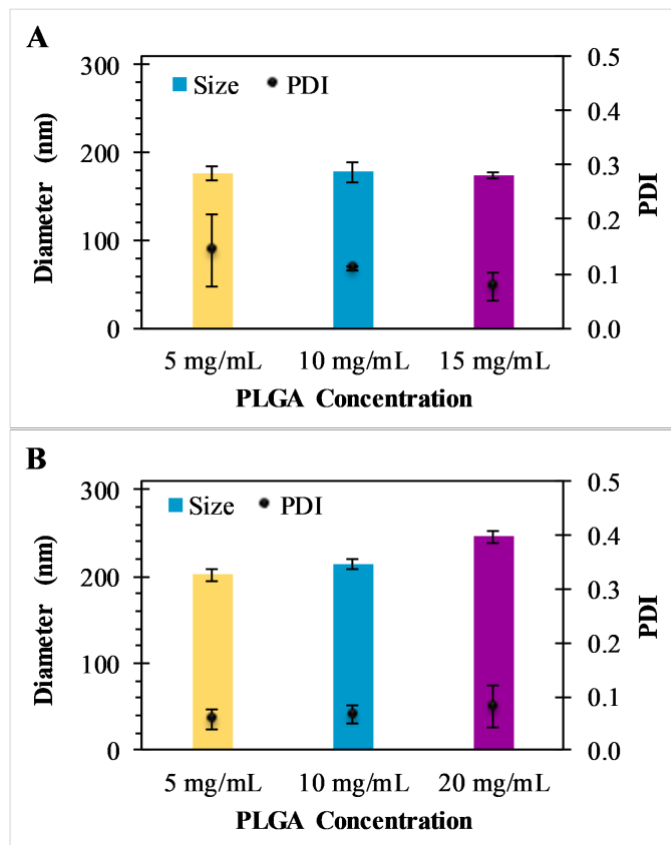


**Figure 2.2.** Characteristics of PLGA nanoparticles prepared by emulsification and nanoprecipitation techniques. Particle diameter and PDI of nanoparticles prepared by: (A) emulsification technique with 5 mg/mL (■), 10 mg/mL (■) and 15 mg/mL (■) PLGA concentration, and (B) nanoprecipitation technique with 5 mg/mL (■), 10 mg/mL (■) and 20 mg/mL (■) PLGA concentration. Data represent mean  $\pm$  SD ( $n = 3$ ).

### 2.3.2 PVA Concentration

Another parameter considered during preparation was the aqueous phase PVA concentration. A 1, 3 and 5% PVA solutions were used for the preparation of PNP using both techniques. As shown in Fig. 2.3A, for the emulsification technique, PNP sizes decreased from 187 nm to 178 nm to 159 nm as concentration of PVA increased from 1% to 3% to 5% respectively, The PDI values obtained for these formulations ranged

from 0.074 to 0.111. Whereas in nanoprecipitation technique (Fig. 2.3B), the effect was contrary, PNP sizes increased from 210 nm to 215 nm to 237 nm as PVA concentration increased as well; however, PDI values were around 0.070 for all formulations. Zeta potential obtained for emulsification technique were -29 mV for 1% PVA and -27 mV for 3 and 5% PVA. Nanoprecipitation values ranged from -3.7 to -6.0 mV. As described before, PLGA used to prepare PNP by emulsification technique has an acid termination that cause the surface negativity. The difference in sizes is consistent with the difference in molecular weight as previously discussed.

When the emulsification method is used, higher concentration of PVA produce smaller PNP. According to Sahoo et al. in 2002, when PVA concentration is greater than 2.5% w/v, PVA molecules are found in aggregated form, this enhance the its surfactant activity (Sahoo *et al.*, 2002). Therefore, droplets formed during emulsification would be more stable and would not have a tendency to aggregate. In the case of nanoprecipitation, lower concentrations of PVA produce smaller PNP, this could be caused by the mechanism of formation of PNP itself. In nanoprecipitation, PNP are formed by a rapid solvent diffusion to the aqueous phase, the mixing process plays an important role, when PVA has greater concentration, the mixing process is compromised by the increase of viscosity (Arica & Lamprecht, 2005; Budhian *et al.*, 2007).

### 2.3.3 Organic to aqueous phase ratio

The organic to aqueous phase ratio was one of the parameter evaluated in the formulation of PNP. In Fig. 2.4, it can be appreciated that for the emulsification technique, the organic to aqueous phase ratio plays an important role. When this ratio is 1 to 1, PNP obtained were 243 nm with a PDI of 0.272, when the ratio increased to 1 to 2 and 1 to 5, PNP sizes decreased to 178 nm and 167 nm respectively, with PDI numbers between 0.111 and 0.138. This could be caused by the insufficient surfactant to cover the surface area of the nanoparticles, therefore causing droplets form in the emulsification process to aggregate; this is similar to having low concentration of PVA as discussed in 2.3.2 (Budhian *et al.*, 2007).

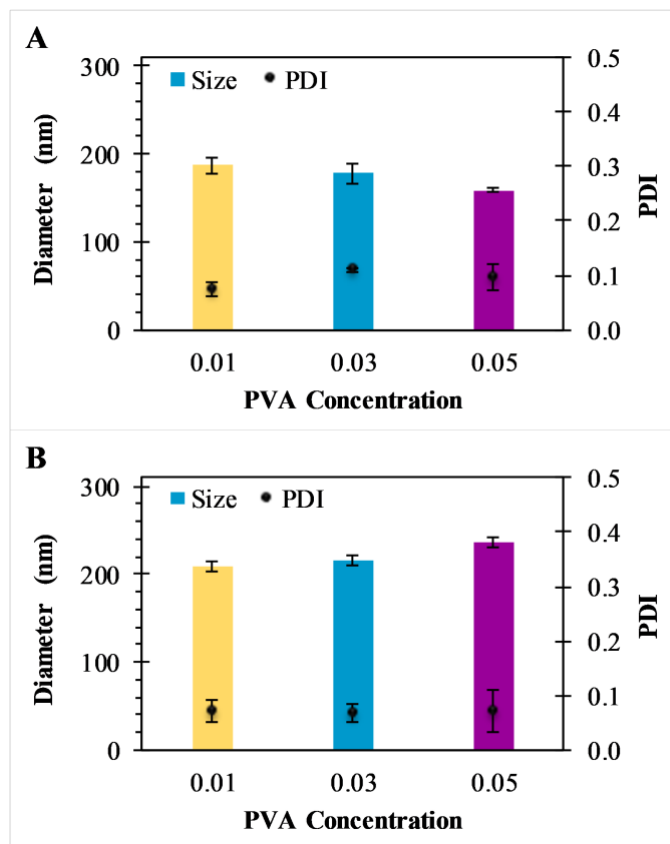


**Figure 2.3.** Characteristics of PLGA nanoparticles prepared by (A) emulsification and (B) nanoprecipitation techniques. Particle diameter and PDI of nanoparticles prepared with 1% (■), 3% (■) and 5 % (■) PVA. Data represent mean  $\pm$  SD ( $n = 3$ ).

For the nanoprecipitation technique, this parameter was not of great impact, as PNP sizes remained at 215 nm for a 1 to 2 and a 1 to 5 ratio and 223 nm for a 1 to 10 ratio. PDI values ranged between 0.050 and 0.070 for all formulations. Zeta potential values remained in the same range as when previous parameters were tested, between -26.5 mV and -31.0 mV for the emulsification technique, and between -4.4 mV and -5.9 mV for nanoprecipitation technique. This is a result of the PNP formation mechanism, where as discussed before, PNP are formed by rapid solvent diffusion to the aqueous phase, when the volume of the aqueous phase is larger, the solvent diffusion would be larger and resulting PNP would be smaller (Budhian *et al.*, 2007). It is possible that in this case, the

system was far from saturation, therefore solvent can easily diffuse over the aqueous phase.

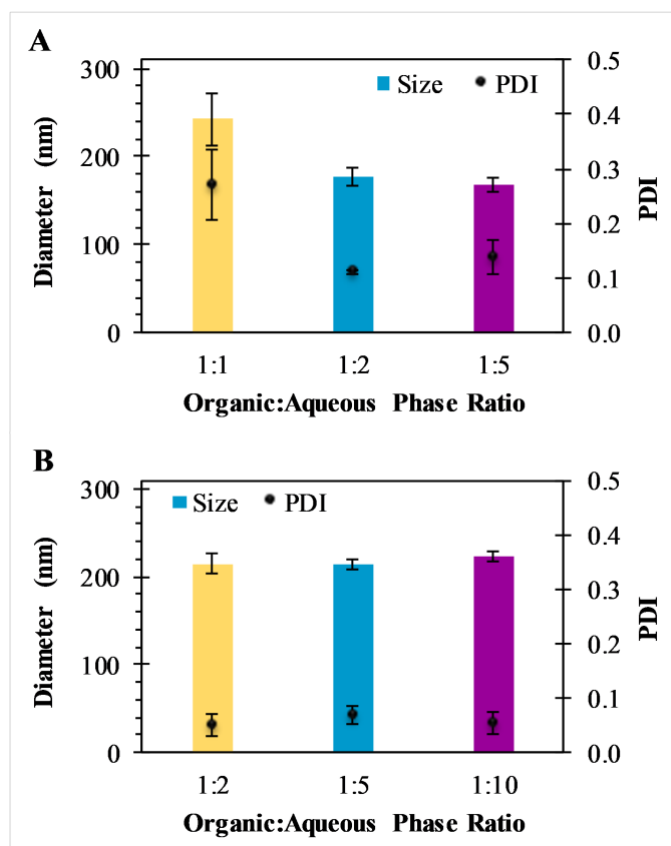


**Figure 2.4.** Characteristics of PLGA nanoparticles prepared by emulsification and nanoprecipitation techniques. Particle diameter and PDI of nanoparticles prepared by: (A) emulsification technique with 1:1 (■), 1:2 (■) and 1:5 (■) organic:aqueous ratio and (B) nanoprecipitation technique with 1:2 (■), 1:5 (■) and 1:10 (■) organic:aqueous ratio. Data represent mean  $\pm$  SD ( $n = 3$ ).

#### 2.3.4 Sonicator amplitude and injection rate.

One of the differences in the preparation of PNP with these two techniques is the use of either a sonicator or an injection system. The sonication amplitude was evaluated for the emulsification technique, where three different sonication amplitudes were utilized: 25%, 50% and 75% that correspond to 30  $\mu$ m, 60  $\mu$ m and 90  $\mu$ m of amplitude respectively (Fig. 2.5A). The PNP sizes obtained when an amplitude of 25% were 193 nm, and when

amplitude is increased to 60  $\mu\text{m}$  and 90  $\mu\text{m}$ , size decreases to 177 nm for both cases. However, PDI values for 25% and 50% amplitude correspond to 0.108 and 0.111 and it decreases to 0.055 when sonication is at 75%, meaning that PNP are more uniform in size.

According to literature, the magnitude of shear stress is inversely proportional to the droplet size formed in the emulsification process (Budhian *et al.*, 2007; Sharma *et al.*, 2016). Therefore, increasing the amplitude of sonication would produce higher shear stress on the solution. This is consistent with the results obtained.

For the nanoprecipitation technique, the injection speed can be adjusted during the formulation of PNP. The injection speeds used in this experiment were 0.6 mL/min, 1.2 mL/min and 2.4 mL/min, sizes obtained ranged between 136 nm and 139 nm, with PDI ranging between 0.010 and 0.080 respectively (Fig. 2.5B). Therefore no significant variation is appreciated within the range of study. For this comparison, PNP were prepared using acid terminated PLGA in both techniques. This can be noticed by comparing the zeta potential of both methods. Surface charge values of -23 mV to -27 mV and -21 mV and -23 mV were obtained for emulsification and nanoprecipitation technique respectively.

### 2.3.5 Agitation speed

Once PNP are formulated with either of the techniques, solvent is set to evaporate under magnetic stirring. Even for the nanoprecipitation technique, the evaporation of the solvent would allow the hardening of the surface of the nanoparticle (Freitas *et al.*, 2004). Agitation speed during this stage of the process can influence in the size of nanoparticles. The PNP prepared by the emulsification technique were agitated at 200 rpm, 300 rpm and 400 rpm. Fig. 2.6 presents the sizes obtained when the agitation speed was 200 rpm and 300 rpm, sizes measured were 198 nm and 195 nm respectively. But when the agitation speed increased to 400 rpm, PNP size decrease to 179 nm. PDI value for all three formulations ranged between 0.026 and 0.041. When PNP were prepared by nanoprecipitation, the sizes obtained were 229 nm when agitated at 200 rpm, also, 215

nm and 207 nm when the stirring speed was 400 rpm and 600 rpm. PDI values ranged 0.068

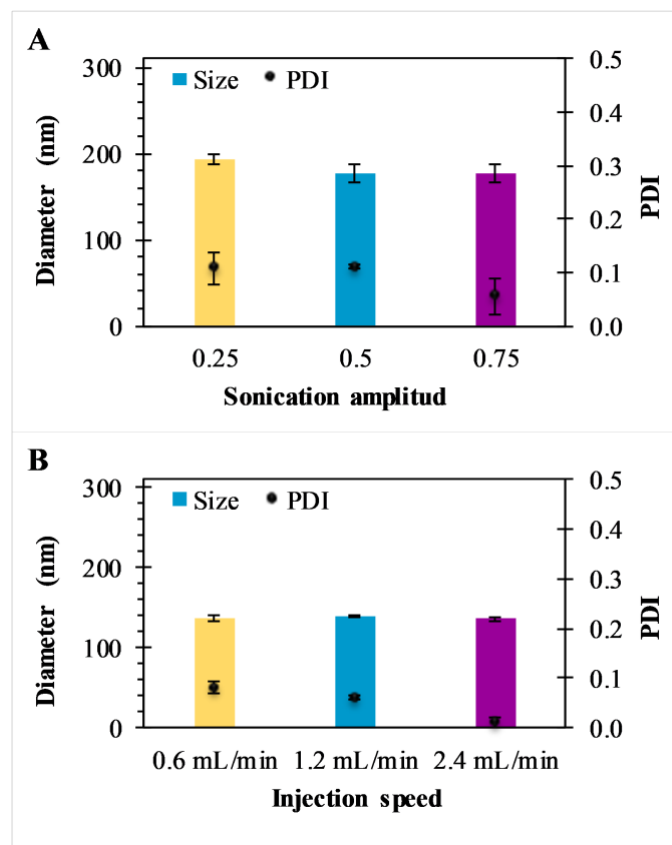


**Figure 2.5.** Characteristics of PLGA nanoparticles prepared by emulsification and nanoprecipitation techniques. Particle diameter and PDI of nanoparticles prepared by: (A) emulsification technique with 25% (■), 50% (■) and 75% (■) sonication amplitude and (B) nanoprecipitation technique with 0.6 mL/min (■), 1.2 mL/min (■) and 2.4 mL/min (■) injection speed. Data represent mean  $\pm$  SD ( $n = 3$ ).

and 0.082 for all cases. Zeta potential values obtained ranged -22 mV and -25 mV for emulsification technique prepared with acid terminated PLGA and -5.2 mV and -5.9 mV for the nanoprecipitation technique prepared with non-acid terminated PLGA.

A summary of all results obtained for the various experiments preparing PNP by emulsification and nanoprecipitation techniques are shown in Table 2.2.

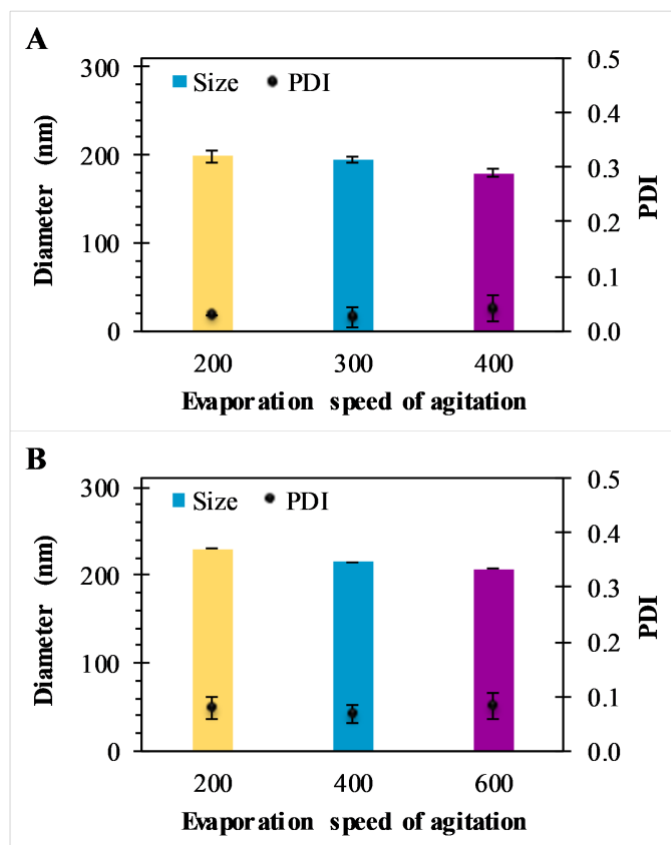


**Figure 2.6.** Characteristics of PLGA nanoparticles prepared by emulsification and nanoprecipitation techniques. Particle diameter and PDI of nanoparticles prepared by: (A) emulsification technique with a speed of agitation of 200 rpm (■), 300 rpm (■) and 400 rpm (■) and (B) nanoprecipitation technique with a speed of agitation of 200 rpm (■), 400 rpm (■) and 600 rpm (■) during solvent evaporation. Data represent mean  $\pm$  SD ( $n = 3$ ).

**Table 2.2.** Characteristics of PLGA nanoparticles when modifying parameters for the emulsification method. Data represent mean  $\pm$  SD ( $n = 3$ ).

<b>PLGA Concentration</b>			
<b>Parameter</b>	<b>Size (nm)</b>	<b>PDI</b>	<b><math>\zeta</math> (mV)</b>
5 mg/mL	176.20 $\pm$ 8.20	0.144 $\pm$ 0.066	-30.05 $\pm$ 6.13
10 mg/mL	177.70 $\pm$ 10.60	0.111 $\pm$ 0.004	-26.80 $\pm$ 4.95
15 mg/mL	174.70 $\pm$ 3.40	0.078 $\pm$ 0.026	-27.65 $\pm$ 6.77
<b>PVA Concentration</b>			
<b>Parameter</b>	<b>Size (nm)</b>	<b>PDI</b>	<b><math>\zeta</math> (mV)</b>
1%	187.00 $\pm$ 8.50	0.074 $\pm$ 0.013	-29.40 $\pm$ 6.78
3%	177.70 $\pm$ 10.60	0.111 $\pm$ 0.004	-26.80 $\pm$ 4.95
5%	159.10 $\pm$ 2.00	0.097 $\pm$ 0.024	-26.60 $\pm$ 5.45
<b>Organic:aqueous phase ratio</b>			
<b>Parameter</b>	<b>Size (nm)</b>	<b>PDI</b>	<b><math>\zeta</math> (mV)</b>
1:1	242.80 $\pm$ 30.00	0.272 $\pm$ 0.064	-31.00 $\pm$ 5.88
1:2	177.70 $\pm$ 10.60	0.111 $\pm$ 0.004	-26.80 $\pm$ 4.95
1:5	167.50 $\pm$ 7.80	0.138 $\pm$ 0.031	-26.55 $\pm$ 5.97
<b>Sonication amplitude</b>			
<b>Parameter</b>	<b>Size (nm)</b>	<b>PDI</b>	<b><math>\zeta</math> (mV)</b>
25%	193.40 $\pm$ 5.40	0.108 $\pm$ 0.030	-23.25 $\pm$ 6.03
50%	177.70 $\pm$ 10.60	0.111 $\pm$ 0.004	-26.80 $\pm$ 4.95
75%	177.40 $\pm$ 10.00	0.055 $\pm$ 0.033	-26.10 $\pm$ 6.18
<b>Agitation speed</b>			
<b>Parameter</b>	<b>Size (nm)</b>	<b>PDI</b>	<b><math>\zeta</math> (mV)</b>
200 rpm	198.23 $\pm$ 6.11	0.030 $\pm$ 0.001	-21.69 $\pm$ 0.43
300 rpm	195.00 $\pm$ 4.11	0.026 $\pm$ 0.018	-24.14 $\pm$ 3.20
400 rpm	179.45 $\pm$ 5.19	0.041 $\pm$ 0.024	-25.06 $\pm$ 3.09

**Table 2.2.** Characteristics of PLGA nanoparticles when modifying parameters for the nanoprecipitation method. Data represent mean  $\pm$  SD ( $n = 3$ ).

<b>PLGA Concentration</b>			
<b>Parameter</b>	<b>Size (nm)</b>	<b>PDI</b>	<b><math>\zeta</math> (mV)</b>
5 mg/mL	202.48 $\pm$ 6.84	0.058 $\pm$ 0.018	-5.01 $\pm$ 0.42
10 mg/mL	214.84 $\pm$ 5.60	0.068 $\pm$ 0.017	-5.90 $\pm$ 0.51
20 mg/mL	246.28 $\pm$ 7.51	0.083 $\pm$ 0.039	-5.18 $\pm$ 0.55
<b>PVA Concentration</b>			
<b>Parameter</b>	<b>Size (nm)</b>	<b>PDI</b>	<b><math>\zeta</math> (mV)</b>
1%	209.90 $\pm$ 5.56	0.073 $\pm$ 0.020	-3.68 $\pm$ 0.94
3%	214.84 $\pm$ 5.60	0.068 $\pm$ 0.017	-5.90 $\pm$ 0.51
5%	237.24 $\pm$ 5.46	0.072 $\pm$ 0.038	-4.57 $\pm$ 0.34
<b>Organic:aqueous phase ratio</b>			
<b>Parameter</b>	<b>Size (nm)</b>	<b>PDI</b>	<b><math>\zeta</math> (mV)</b>
1:2	214.64 $\pm$ 11.20	0.050 $\pm$ 0.020	-5.24 $\pm$ 0.37
1:5	214.84 $\pm$ 5.60	0.068 $\pm$ 0.017	-5.90 $\pm$ 0.51
1:10	222.67 $\pm$ 6.12	0.055 $\pm$ 0.021	-4.35 $\pm$ 0.91
<b>Injection speed</b>			
<b>Parameter</b>	<b>Size (nm)</b>	<b>PDI</b>	<b><math>\zeta</math> (mV)</b>
0.6 mL/min	137.18 $\pm$ 3.36	0.080 $\pm$ 0.012	-21.38 $\pm$ 4.88
1.2 mL/min	139.17 $\pm$ 2.40	0.060 $\pm$ 0.004	-21.77 $\pm$ 2.40
2.4 mL/min	135.53 $\pm$ 2.08	0.010 $\pm$ 0.009	-23.15 $\pm$ 3.46
<b>Agitation speed</b>			
<b>Parameter</b>	<b>Size (nm)</b>	<b>PDI</b>	<b><math>\zeta</math> (mV)</b>
200 rpm	229.47 $\pm$ 8.26	0.080 $\pm$ 0.020	-5.16 $\pm$ 0.38
400 rpm	214.84 $\pm$ 5.60	0.068 $\pm$ 0.017	-5.90 $\pm$ 0.51
600 rpm	207.00 $\pm$ 15.59	0.082 $\pm$ 0.023	-5.34 $\pm$ 0.86

### 2.3.5 Purification process

The following step after solvent evaporation is purification. In order to remove the excess of surfactant. Several methods of purification can be used, but centrifugation is practical to perform on small scale experiments (Vauthier & Bouchemal, 2009).

Three different centrifugation speeds were tested, 10,000 rpm, 15,000 rpm and 20,000 rpm, which correspond to 12,096\*g, 27,216\*g and 48,384\*g. Samples were taken at each point in the purification process, sizes and zeta potential was measured at each point. During the purification process, an increase in size was consistent (Fig. 2.7). When the purification was performed at a centrifugation speed of 10,000 rpm, an increase of 56 nm was measured, when purification was performed at 15,000 rpm, an increase of 30 nm was measured and an increase in 16 nm when purifying at 20,000 rpm. These values represent an increase of 54%, 29% and 15% in size respectively. Variations on the PDI thought the purification process indicate the presence of non-uniform population of PNP. For the experiments performed at 10,000 rpm and 15,000 rpm, PDI values start at 0.150 on the prewash measurement, along the process, they decrease and at the end, the PDI value is 0.221 and 0.266 respectively. However, when purification was performed at 20,000 rpm, the PDI value decreased from 0.147 to 0.042, representing a more uniformed population of PNP. Zeta potential during the purification process decreased in all of preparations. From -16 mv to -28 mV when purifying at 10,000 rpm, from -15 mV to -31 mV when purifying at 15,000 rpm and from -15 mV to -34 mV when purifying at 20,000 rpm. This effect could be attributed to the removal of the PVA layer on the surface of the nanoparticles as the purifying process is being done. By removing the PVA layer, the carboxylic groups from the PLGA become exposed and the surface charge changes (Sahoo *et al.*, 2002). Other available methods for PNP purification are dialysis, cross-flow filtration and gel filtration (Vauthier & Bouchemal, 2009). Table 2.3 presents the values for size, PDI and zeta potential for the nanoparticles at each point of the purification process.

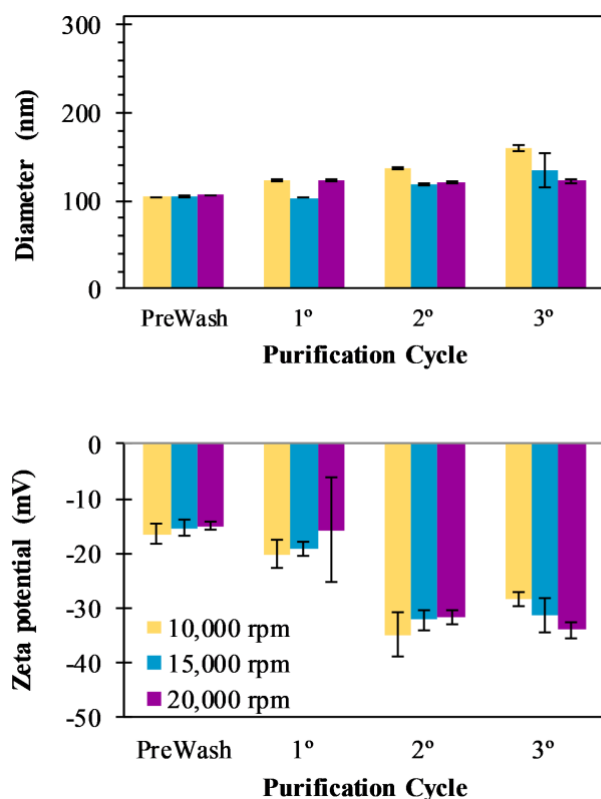


**Figure 2.7.** Characteristics of PLGA nanoparticles during the purification process. Particle diameter (A), PDI (A) and zeta potential (B) of nanoparticles at different points of the purification process with centrifugation speed of 10,000 rpm (■), 15,000 rpm (■) and 20,000 rpm (■). Data represent mean  $\pm$  SD ( $n = 3$ ).

### 2.3.6 Cryoprotectants

The last part of the PNP preparation is freeze drying. During this stage, the use of cryoprotectants is commonly used to prevent nanoparticles from aggregation. Before lyophilizing, cryoprotectants were added to the PNP solutions in different ratios (0, 0.25, 0.50 and 1.0), size and zeta potential were measured at this point. For the three cases, the size of the nanoparticles were not affected by the addition of the cryoprotectants, however, the zeta potential did change. For sucrose, from -25 mV to -18 mV, glucose changed from -25 mV to -22 mV and lactose from -25 mV to -19 mV (Fig. 2.8). This effect is explained in literature as the result of the nanoparticle being covered by the cryoprotectant as a result of the hydrogen bonding between the OH groups of the

cryoprotectant and the surface of the nanoparticle (Abdelwahed *et al.*, 2006). After lyophilization, samples were resuspended and the size and zeta potential was measured again.

**Table 2.3.** Characteristics of PLGA nanoparticles when modifying the centrifugation speed during purification. Data represent mean  $\pm$  SD ( $n = 3$ ).

10,000 rpm			
Parameter	Size (nm)	PDI	$\zeta$ (mV)
PreWash	103.63 $\pm$ 0.38	0.160 $\pm$ 0.008	-16.47 $\pm$ 1.94
1°	123.83 $\pm$ 0.92	0.101 $\pm$ 0.011	-20.13 $\pm$ 2.65
2°	135.80 $\pm$ 1.27	0.090 $\pm$ 0.030	-34.90 $\pm$ 3.94
3°	159.47 $\pm$ 3.51	0.221 $\pm$ 0.050	-28.33 $\pm$ 1.28
15,000 rpm			
Parameter	Size (nm)	PDI	$\zeta$ (mV)
PreWash	103.63 $\pm$ 1.08	0.150 $\pm$ 0.008	-15.37 $\pm$ 1.59
1°	103.03 $\pm$ 0.21	0.160 $\pm$ 0.014	-19.30 $\pm$ 1.34
2°	118.03 $\pm$ 1.23	0.093 $\pm$ 0.016	-32.23 $\pm$ 1.94
3°	133.93 $\pm$ 20.00	0.266 $\pm$ 0.092	-31.37 $\pm$ 3.14
20,000 rpm			
Parameter	Size (nm)	PDI	$\zeta$ (mV)
PreWash	106.10 $\pm$ 0.28	0.147 $\pm$ 0.005	-15.07 $\pm$ 0.68
1°	123.13 $\pm$ 1.70	0.034 $\pm$ 0.011	-15.70 $\pm$ 9.57
2°	120.57 $\pm$ 0.85	0.039 $\pm$ 0.017	-31.60 $\pm$ 1.34
3°	121.83 $\pm$ 1.19	1.032 $\pm$ 1.392	-33.97 $\pm$ 1.49

When no cryoprotectant was added, over the freeze drying process, the zeta potential remained constant, but size increased 35% to 242 nm and PDI value of 0.214, meaning a wide range of PNP sizes. When sucrose was added in 0.25 and 0.5 ratio, size increased from 179 nm to 190 nm and 183 nm, however, when sucrose was added in a 1:1 ratio,

size decrease 1 nm. Zeta potential increased to -18 mV, -11 mV and -14 mV for each of the preparations. Glucose had a similar outcome, were for the 0.25, 0.5 and 1 ratio, an increase to 193 nm, 184 nm and 182 nm for each formulation. Where the zeta potential was maintained between -18 mV and -20 mV. For lactose as cryoprotectant, as the ratio of lactose added incremented, the size obtained were 200 nm, 193 nm and 189 nm for the 0.5, 0.5 and 1 ratio respectively, and all formulations with zeta potentials ranging between of -18 mV and -20 mV. A summary of the characteristics of all the nanoparticles analyzed with and without cryoprotectant treatment is shown in Table 2.4.

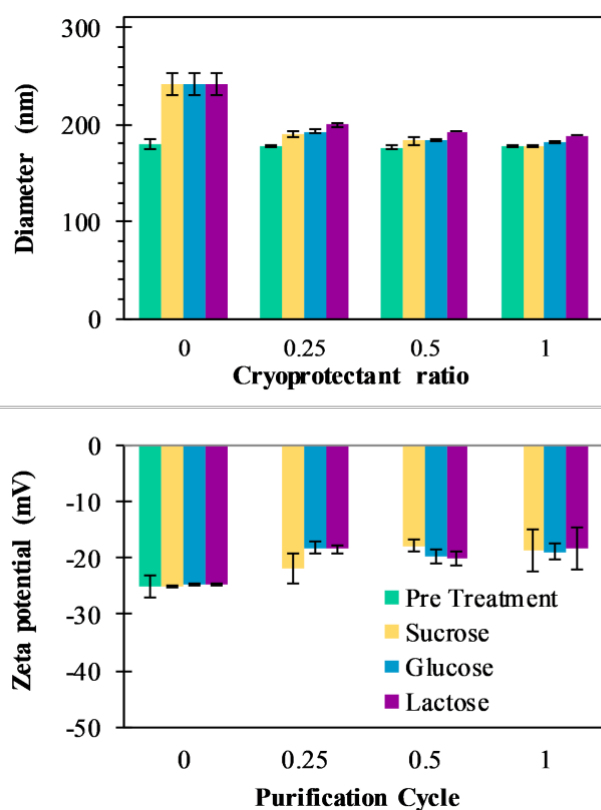


**Figure 2.8.** Characteristics of PLGA nanoparticles when adding different ratios of cryoprotectants with respect to initial PLGA mass during dry-freezing process before lyophilization (■), sucrose (■), glucose (■) and lactose (■). Data represent mean  $\pm$  SD ( $n = 3$ ).

**Table 2.4.** Characteristics of PLGA nanoparticles when adding cryoprotectants during dry-freezing process. Data represent mean  $\pm$  SD ( $n = 3$ ).

<b>Sucrose - Before</b>			
<b>Ratio</b>	<b>Size (nm)</b>	<b>PDI</b>	<b><math>\zeta</math> (mV)</b>
0	179.45 $\pm$ 5.19	0.041 $\pm$ 0.024	-25.06 $\pm$ 3.09
0.25	177.70 $\pm$ 0.20	0.034 $\pm$ 0.009	-21.88 $\pm$ 3.25
0.5	176.70 $\pm$ 1.20	0.041 $\pm$ 0.007	-17.81 $\pm$ 2.55
1	178.45 $\pm$ 0.95	0.021 $\pm$ 0.009	-18.80 $\pm$ 0.17
<b>Sucrose</b>			
<b>Ratio</b>	<b>Size (nm)</b>	<b>PDI</b>	<b><math>\zeta</math> (mV)</b>
0	242.05 $\pm$ 10.75	0.214 $\pm$ 0.037	-24.80 $\pm$ 0.20
0.25	190.45 $\pm$ 2.45	0.109 $\pm$ 0.015	-17.91 $\pm$ 2.65
0.5	183.30 $\pm$ 3.70	0.067 $\pm$ 0.014	-11.21 $\pm$ 1.09
1	178.35 $\pm$ 0.75	0.044 $\pm$ 0.006	-14.30 $\pm$ 3.73
<b>Glucose - Before</b>			
<b>Ratio</b>	<b>Size (nm)</b>	<b>PDI</b>	<b><math>\zeta</math> (mV)</b>
0	179.45 $\pm$ 5.19	0.041 $\pm$ 0.024	-25.06 $\pm$ 3.09
0.25	177.50 $\pm$ 0.80	0.022 $\pm$ 0.001	-21.02 $\pm$ 1.82
0.5	177.80 $\pm$ 0.40	0.024 $\pm$ 0.002	-21.95 $\pm$ 1.72
1	177.90 $\pm$ 0.00	0.025 $\pm$ 0.005	-21.82 $\pm$ 2.28
<b>Glucose</b>			
<b>Ratio</b>	<b>Size (nm)</b>	<b>PDI</b>	<b><math>\zeta</math> (mV)</b>
0	242.05 $\pm$ 10.75	0.214 $\pm$ 0.037	-24.80 $\pm$ 0.20
0.25	192.55 $\pm$ 1.95	0.085 $\pm$ 0.032	-18.20 $\pm$ 1.10
0.5	184.25 $\pm$ 1.75	0.061 $\pm$ 0.004	-19.75 $\pm$ 1.35
1	182.05 $\pm$ 1.05	0.043 $\pm$ 0.001	-18.95 $\pm$ 1.35

**Table 2.4.** Characteristics of PLGA nanoparticles when adding cryoprotectants during dry-freezing process. Data represent mean  $\pm$  SD ( $n = 3$ ). *Continued*

<b>Lactose - Before</b>			
<b>Ratio</b>	<b>Size (nm)</b>	<b>PDI</b>	<b><math>\zeta</math> (mV)</b>
0	179.45 $\pm$ 5.19	0.041 $\pm$ 0.024	-25.06 $\pm$ 3.09
0.25	177.30 $\pm$ 0.90	0.038 $\pm$ 0.004	-23.50 $\pm$ 2.37
0.5	178.10 $\pm$ 1.20	0.025 $\pm$ 0.006	-22.97 $\pm$ 0.36
1	178.35 $\pm$ 0.65	0.027 $\pm$ 0.007	-19.48 $\pm$ 1.42
<b>Lactose</b>			
<b>Ratio</b>	<b>Size (nm)</b>	<b>PDI</b>	<b><math>\zeta</math> (mV)</b>
0	242.05 $\pm$ 10.75	0.214 $\pm$ 0.037	-24.80 $\pm$ 0.20
0.25	200.00 $\pm$ 2.10	0.122 $\pm$ 0.014	-18.45 $\pm$ 0.75
0.5	192.50 $\pm$ 0.00	0.075 $\pm$ 0.014	-20.10 $\pm$ 1.20
1	188.55 $\pm$ 0.15	0.065 $\pm$ 0.014	-18.40 $\pm$ 3.70

### 2.3.7 Surface morphology

Surface morphology of PLGA blanks obtained by the O/W emulsification process can be observed in Figure 2.9. PLGA nanoparticles were spherical with smooth surface with average sizes of less than 200 nm, which correspond to the values obtained by DLS. Modification of the methods or parameters did not affect particle size as determined by SEM.

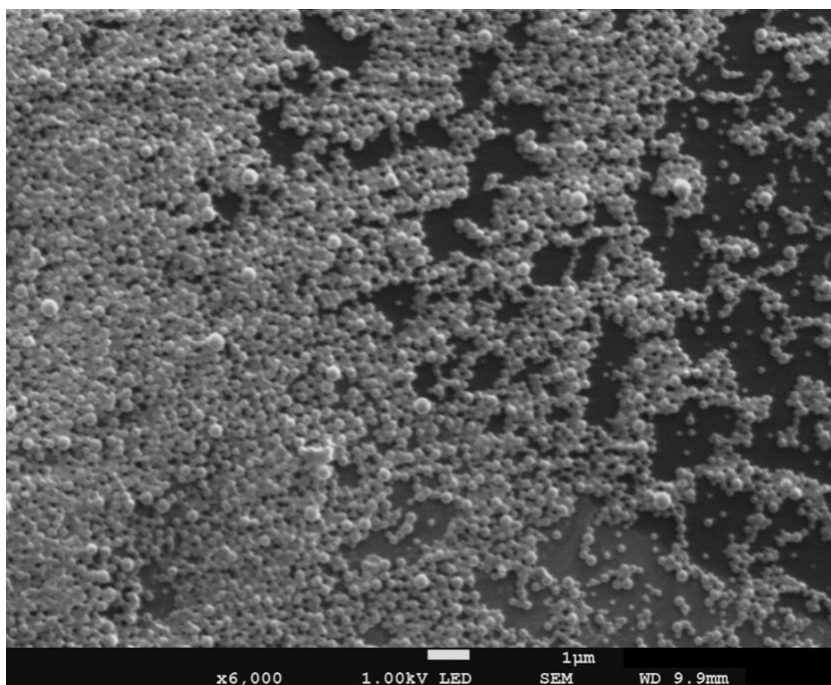


**Figure 2.9.** Scanning electron micrograph PLGA nanoparticles.

#### **2.4. Conclusion**

PNP were successfully prepared by the emulsification and the nanoprecipitation techniques modifying a variety of parameters. A comparison among the results obtained was based on size, PDI and zeta potential. It was found that polymer concentration is important for both techniques, the greater the concentration, the greater size on nanoparticles. Surfactant concentration effect was contrary for both techniques, for the emulsification technique, higher concentrations would carry smaller particle size, were as in the nanoprecipitation technique, smaller concentrations of PVA would result in smaller particle size. The organic to aqueous ratio was important for the emulsification technique, where it was important to maintain a higher ratio to obtain smaller sizes of PNP. Both a higher surfactant concentration and higher organic to aqueous ratio make PVA more available for organic phase droplets stabilization during the formulation. Sonication amplitude is an important parameter for the emulsification technique as it is proportional to the shear stress produced in the process and therefore inversely proportional to the size of the PNP. The centrifugation speed during purification and the

use of cryoprotectants for storage of nanoparticles was also evaluated. Throughout the purification study, zeta potential decrease significantly, this could be explained by the removal of a PVA coating around the nanoparticles, leaving carboxylic groups exposed. This effect was noted in the opposite way, when cryoprotectants were added to the purified PNP solution and zeta potential increased, meaning a surrounding coat of cryoprotectant on PNP. As it was studied, PNP process is sensitive to modifications in almost every step of the formulation, purification and storage process.

## **CHAPTER 3. EVALUATION OF COMBINED EMULSION PROCESS TO ENCAPSULATE METHYLENE BLUE INTO PLGA NANOPARTICLES**

### **3.1 Abstract**

The delivery of photosensitizer compounds using biodegradable nanoparticles could improve dosage, control release and its bioavailability. In this study, MB loaded PLGA nanoparticles (MB-PNP) are prepared by a new approach combining the single and double emulsification techniques. Comparisons of MB-PNP obtained with the combined and the individual techniques are presented. Nanoparticles are characterized by dynamic light scattering, laser Doppler electrophoresis and scanning electron microscopy. Particles prepared by the combined technique presented hydrodynamic diameters of 186nm. The sizes of MB-PNP obtained from the single emulsion technique are similar to the combined technique, while the diameter of particles prepared by double emulsion increased from 201nm to 287nm as the TDL increased. MB-PNP displayed an average zeta potential between -21mV and -28mV for all formulations. MB loading ranges between 0.3%-1.4%, while the encapsulation efficiency ranges from 8%-14%, both depending on the TDL and the preparation technique. In-vitro release studies show a monophasic release profile that was analyzed by considering the mechanisms of initial burst, drug diffusion and a combination of them. Experimental results could be better described using a mathematical model of release that simultaneously combines the mechanisms of initial burst and drug diffusion. The approach presented to encapsulate MB and also to analyze the drug release could be extended to other drugs with partial solubility.

### 3.2. Introduction

Drug delivery has become an ideal strategy to overcome problems associated with the degradation of drugs, dosage, targeting, among others. Drug delivery approaches have been receiving continuous efforts to develop and optimize the methods of drug entrapment. Within these approaches, nanocarriers are getting more attention due to the great potential to comply with the requirements of an ideal drug delivery system, as they may increase drug bioavailability, reduce toxicity, improve efficiency, provide controlled drug release, recognize specific tissues and protect drugs from undesirable interaction with other tissues (Mu & Feng, 2003; Peer *et al.*, 2007; Makadia & Siegel, 2011; Danhier *et al.*, 2012; Nava-Arzaluz *et al.*, 2012). Within the materials used in the preparation of nanocarriers are polymers; inorganic materials such as ceramic based and silica-based nanostructures; metallic and magnetic nanoparticles; quantum dots and carbon materials; as well as organic materials that include liposomes, micelles, polysaccharides and dendrimers (Paszko *et al.*, 2011; Vivero-Escoto & Elnagheeb, 2015). From these materials, PLGA is extensively used in research as a nanocarrier. PLGA is a biodegradable and biocompatible poly(ester) that can be easily functionalized with different ligands prior (Gutiérrez-Valenzuela *et al.*, 2016) and after nanoparticle preparations. PLGA degradation rates depends on its molecular weight and copolymer composition (Jain, 2000). PLGA is also a polymer approved by the Food and Drug Administration (FDA) for drug delivery nanosystems (Jain, 2000; Danhier *et al.*, 2012). Several techniques for PLGA nanoparticle preparation have been reported in literature: emulsification followed by either solvent evaporation, diffusion or reverse salting-out, polymerization, nanoprecipitation, among others (Murakami *et al.*, 2000; Chorny *et al.*, 2002; Dhar *et al.*, 2008; Sahana *et al.*, 2008; Cohen-Sela *et al.*, 2009; Park *et al.*, 2009; Vauthier & Bouchemal, 2009; Mora-Huertas *et al.*, 2010). Within these techniques, the most common is the emulsion process, which could be used to practically encapsulate any hydrophobic or hydrophilic component. The emulsion process could be carried out by single and double emulsion. An extensive review using the double emulsion technique by analysing the process variables like solvents, stabilizers, different polymers in the encapsulation of hydrophobic and hydrophilic drugs was reported in literature

(Iqbal *et al.*, 2015). However, this technique occasionally present low drug loading and encapsulation efficiency for hydrophilic compounds and could be difficult to scale up (Park *et al.*, 2009; Danhier *et al.*, 2012). In order to overcome the low drug loading issue, authors have proposed a wide variety of modifications to the commonly used methods, some of these modifications include: (1) adjustments on the pH of the aqueous phase with the purpose of modifying lipophilicity of the drug to encapsulate in the single or double emulsification method (Tewes *et al.*, 2007; Nava-Arzaluz *et al.*, 2012); (2) variations on temperature while encapsulating iron oxide nanoparticles in PLGA in a double emulsion method (Song *et al.*, 2016); (3) the use of different surfactants such as polyvinyl alcohol (PVA), human serum albumin (HSA) (Zambaux *et al.*, 1998), or Pluronic F-108 when a solvent displacement method is used (Pagonis *et al.*, 2010); (4) addition of excipients such as poly(DL-lactide) oligomers or fatty acids into the formulation (Govender *et al.*, 1999) or stabilizer agents and cyclodextrins (Cannavà *et al.*, 2016); (5) the use of cross-linkers such as anionic surfactant Aerosol (OTTM) and polysaccharide polymer alginate to improve the encapsulation efficiency and to delay the release of water soluble drugs such as MB, doxorubicin, rhodamine, verapamil, and clonidine (Chavanpatil *et al.*, 2007); among others.

MB has been of great interest in many areas of clinical medicine, from neurological disorders to cancer chemotherapy (Wainwright & Crossley, 2002; Cannavà *et al.*, 2016). It can be used in photodynamic therapy (PDT), which consists on the application of the photosensitizer (PS) agent in the area of interest, and then activated by light of specific wavelength producing reactive oxygen species, that leads to the death of the target cell via oxidative damage (Zhang *et al.*, 2007; Bechet *et al.*, 2008; Huang *et al.*, 2011; Fioramonti Calixto *et al.*, 2016). MB has been encapsulated using phosphonate-terminated silica particles (He *et al.*, 2009), silica-coated magnetic particles (Tada *et al.*, 2007), chitosan nanoparticles (Darabpour *et al.*, 2016; Deprá de Souza *et al.*, 2016), molecular imprinted polymeric nanoparticles (Long *et al.*, 2016), a combination of gold nanoparticles in a polystyrene-alt-maleic acid layer (Yu *et al.*, 2015), and also in PLGA nanoparticles (Klepac-Ceraj *et al.*, 2011; Cannavà *et al.*, 2016).

Drug release from polymeric systems can be attributed to different mechanisms such as initial burst, polymer-drug and drug-drug interactions, polymer relaxation, hydrolysis, polymer erosion, drug dissolution, formation of cracks and deformation, transport through water-filled pores and transport through the polymer (Fitzgerald & Corrigan, 1993; Corrigan & Li, 2009; Fredenberg *et al.*, 2011). In the case of MB release from PLGA nanoparticles, a zero order, first order and a Higuchi models have been used to analyse the kinetics of release (Cannavà *et al.*, 2016). However, the release analysis from biodegradable nanoparticles usually involves more than one mechanism of release (Lao *et al.*, 2011). In this regard, Batycky *et al.* presented a model that combines initial burst and drug diffusion, solving first for the initial burst and after an induction time they consider the drug diffusion (Batycky *et al.*, 1997). In similar way, a model that combines the mechanisms of initial burst, drug diffusion and also the degradation of PLGA has been reported, but considering that all mechanisms occur simultaneously (Lucero-Acuña & Guzmán, 2015).

In this work, the preparation of MB-loaded PLGA nanoparticles (MB-PNP) by a combination of single and double emulsion techniques is reported. A comparison of the nanoparticles obtained with the combined and the individual techniques is presented. MB-PNP were prepared using different theoretical drug loadings (TDL) depending of the encapsulation technique. Nanoparticles were characterized by dynamic light scattering (DLS), laser Doppler electrophoresis and scanning electron micrographs (SEM). In vitro MB release from MB-PNP was evaluated under physiological conditions and analysed with three models of release. The first model considers the mechanism of initial burst, the second one considers the release of MB by diffusion and the third model considers a simultaneous contribution of both. Initial burst was evaluated using a first order equation and the diffusion of MB from MB-PNP was evaluated with a fickian diffusion.

### 3.3. Materials and methods

#### 3.3.1 Materials

PLGA acid terminated (50/50 DL-lactide/glycolide copolymer, IV midpoint 0.2 dL/g) was received as gift sample from Corbion Purac, Gorinchem, The Netherlands. MB was obtained from Química Suastes SA de CV, Tlahuac, Estado de Mexico, Mexico. Polyvinyl alcohol (86-89% hydrolysis, low molecular weight, PVA) was obtained from Alfa Aesar, Ward Hill, Massachusetts, USA. Dichloromethane (DCM) was obtained from Fisher Scientific Inc., Fair Lawn, New Jersey, USA. Phosphate buffered saline tablets were obtained from Sigma-Aldrich, St. Louis, Missouri, USA.

#### 3.3.2 Preparation of MB-PNP

PLGA nanoparticles loaded with MB (MB-PNP) were prepared by using a combination of the single and double emulsification techniques (Gutiérrez-Valenzuela *et al.*, 2017). Nanoparticles prepared by the individual techniques were used to evaluate the method. A representation of the nanoparticle preparations is presented in Figure 3.1. Briefly, in the single emulsification technique, 25 mL of an aqueous solution of 5% w/v PVA are added into a 5 mL DCM solution containing 50 mg of PLGA. The mixture is emulsified during 1 min at 75% amplitude (90  $\mu\text{m}$ ) under an ice bath by using the equipment QSonica 500 sonicator (QSonica LLC, Newtown, Connecticut, USA). In the double emulsification technique, a specific amount of MB (depending on TDL) is dissolved in 0.5 mL of deionized water and then added into a 5 mL DCM solution containing 50 mg of PLGA. Then, the mixture is emulsified by sonication during 1 min at 22% of amplitude (26.5  $\mu\text{m}$ ) under an ice bath. Next, 25 mL of an aqueous solution of 5% w/v PVA are added into the mixture and a second emulsification is carried by sonication during 1 min at 75% amplitude (90  $\mu\text{m}$ ) under an ice bath. In the combined emulsification technique, 2 mg of MB are dissolved in 0.5 mL of deionized water and then added into a 5 mL DCM solution containing 4 mg of MB and 50 mg of PLGA. Then, the mixture is emulsified two times following the same procedure than the one for the double emulsification technique. After the emulsifications in all the preparations, the

solvent is evaporated under magnetic stirring, at room temperature. Then, MB-PNP are washed by three centrifugation cycles by using a Sigma 3-30KS centrifuge (Sigma Laborzentrifugen GmbH, Osterode am Harz, Germany) operated at 37,565\*g for 20 minutes, discarding supernatant and resuspending pellet nanoparticles in deionized water. Finally, MB-PNP are freeze-dried in lyophilizer freezezone 4.5 (Labconco, Kansas City, Missouri, USA). All experiments were performed by triplicate.

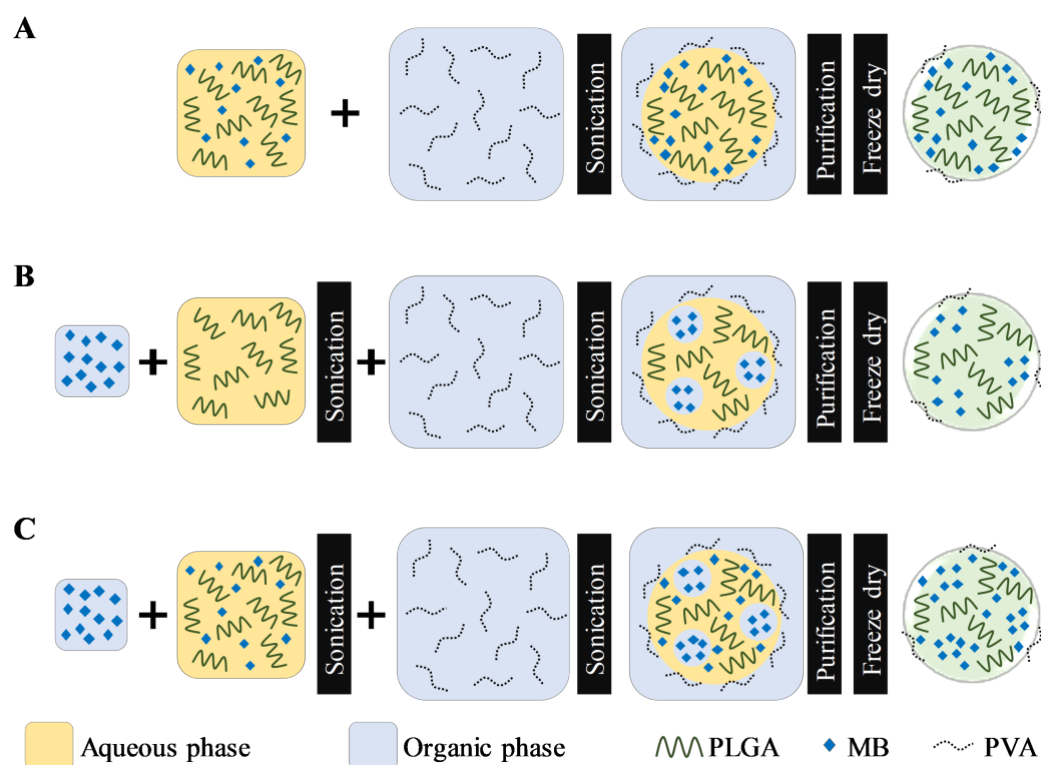


**Figure 3.1.** Schematic of MB loaded PLGA nanoparticle preparation. Single (A), double (B) and combined (C) emulsification techniques.

### 3.3.3 Nanoparticle characterization

Nanoparticle size distribution and zeta potentials were measured using a zetasizer Nano ZS equipment (Malvern Instruments Ltd., Worcestershire, United Kingdom). Measurements of MB-PNP sizes were performed by dynamic light scattering (DLS). Each sample was measured three times with 10 runs respectively. Additionally, each sample for zeta potential was measured by duplicated with at least 10 runs at constant

temperature (25°C) by laser Doppler electrophoresis. Z-averages and zeta potentials were obtained from three independent experiments.

MB concentrations were quantified by spectrometry at 665 nm using a calibration curve obtained with a standard model MB solutions prepared in 10 mM phosphate buffer pH 7.4 ( $\epsilon = 5.246 \times 10^4 \text{ M}^{-1} \text{ cm}^{-1}$ ). TDL is the ratio of initial amount of MB used in the process with respect to initial amount of polymers used in preparation. Drug loading (DL) was defined as the actual amount of MB encapsulated per mass of nanoparticles, while the encapsulation efficiency (EE) was described as percent of MB encapsulated in MB-PNP with respect to initially added amount of MB.

Surface morphology of MB-PNP was analysed by scanning electron microscopy (SEM) through the field emission scanning electron microscope Hitachi S-4800 FE-SEM (Hitachi Corporation, Tokyo, Japan). Samples were prepared by placing a small quantity of lyophilized nanoparticles on a double-sided carbon tape previously placed on a SEM stub. Compressed air was used to remove loose nanoparticles. Platinum coating was applied during 60 seconds using with an Anatech Hummer 6.2 sputter system (Anatech USA, Hayward, California, USA) at 10 mA under argon plasma. For visualization of nanoparticles a working distance in the range from 6-9 mm and a beam strength of 1.0 – 1.5 kV were used.

#### 3.3.4 *In vitro release study*

*In vitro* MB release from MB-PNP was evaluated by the dialysis method (Lucero-Acuña & Guzmán, 2015; Cannavà *et al.*, 2016). Briefly, a specific amount of MB-PNP is dispersed in PBS buffer and placed into a Spectra/Por membrane dialysis of 12,000-14,000 MWCO (Spectrum Laboratories, Rancho Dominguez, California, USA). MB-PNP-loaded membrane is immersed in a tube containing phosphate buffer solution (10 mM, pH 7.4) and incubated at 37°C. At fixed time intervals, a sample from the dialysis medium is collected and replaced by fresh phosphate buffer. The collected samples are analysed by UV-vis spectroscopy at 665 nm and compared to the MB calibration curve to obtain concentrations. Then, a mass balance is followed to obtain the release profile curves. The experiments were performed by triplicate.

### 3.3.5 Mathematical analysis of MB release

Drug release from biodegradable nanoparticles can be contributed to a variety of mechanisms. One of the most relevant mechanism of release, especially for hydrophilic drugs is the initial burst, which is attributed to a process of interfacial diffusion between the solid sphere surface and the liquid media. According to literature, the rate of drug dissolution is proportional to the effect of a variety of factors such as concentration of drug on the surface, surface area, interphase properties, solubility of the drug, and the electrostatic interactions between the drug and the carrier, these factors are combined into a proportionality constant (Batycky *et al.*, 1997; Lucero-Acuña & Guzmán, 2015). This mechanism analysis results into a first order equation considering that at the beginning, MB is completely incorporated in the MB-PNP. The solution of the first order equation presents an exponential profile, as presented in the following equation:

$$\frac{M_t}{M_\infty} = 1 - \exp(-k_b t) \quad (3.1)$$

where  $M_t$  is the cumulative amount of MB released at time  $t$ ,  $M_\infty$  is the cumulative amount of MB released at infinite time and  $k_b$  is the initial burst constant, incorporating factors such as concentration of MB on MB-PNP surface, surface area, interphase properties, MB solubility and electrostatic interactions between MB and the MB-PNP (Corrigan & Li, 2009).

Following the literature, other mechanism that can be considered in a release kinetics analysis is the drug release by fickian diffusion. A general mass balance in the radial direction and under transient conditions can be evaluated using spherical coordinates. Considerations to these analysis include: symmetry conditions; uniform concentration of drug at fixed radius; and effective diffusion coefficient constant with no chemical alteration of the drug in the system (Lucero-Acuña & Guzmán 2015). The resulting equation is:

$$\frac{\partial C(r, t)}{\partial t} = D_e \left( \frac{\partial^2 C(r, t)}{\partial r^2} + \frac{2}{r} \frac{\partial C(r, t)}{\partial r} \right) \quad (3.2)$$

where the concentration (C) is a function of time and radial position in the nanoparticle. The symmetry condition at the centre of the particle described by Equation (3.3) is

considered as a boundary condition. Also, MB concentration on the surface of the sphere for times larger than zero, is considered negligible due to its hydrophilic nature and high solubility, as presented in Equation (3.4), where  $r_1$  represents the nanoparticle radius. The assumption that initially all the encapsulated MB is homogeneously distributed over the entire volume of the sphere ( $v_s$ ), as expressed in Equation (3.5) is considered.

$$\frac{\partial C(0, t)}{\partial t} = 0 \quad t > 0 \quad (3.3)$$

$$C(r_1, t) = 0 \quad t > 0 \quad (3.4)$$

$$C(r, 0) = \frac{M_0}{v_s} \quad 0 < r < r_1 \quad (3.5)$$

An analytical solution for this system could be obtained by using separation of variables, resulting in the following equation:

$$\frac{M_t}{M_\infty} = 1 - \frac{6}{\pi^2} \sum_{n=1}^{\infty} \frac{1}{n^2} \cdot \exp\left(-\frac{\pi^2 n^2 D_e t}{r_1^2}\right) \quad (3.6)$$

Depending on the drug release system, one or more mechanisms could be considered and each one of them can contribute in different proportions to the system. In this case, a linear combination of initial burst (Eq. (3.1)) and fickian diffusion (Eq. (3.6)), is considered, resulting in:

$$\frac{M_t}{M_\infty} = \theta_b \{1 - \exp(-k_b t)\} + (1 - \theta_b) \left\{ 1 - \frac{6}{\pi^2} \sum_{n=1}^{\infty} \frac{1}{n^2} \cdot \exp\left(-\frac{\pi^2 n^2 D_e t}{r_1^2}\right) \right\} \quad (3.7)$$

where  $\theta_b$  is the initial burst mechanism contribution fraction over the total mass drug release. The additional equation:  $\theta_b + \theta_d = 1$  is included to add mathematical consistency, where  $\theta_d$  is referred to the diffusion contribution fraction over the total mass drug release. The release model presented in Eq. (3.7) considers the simultaneous contributions of initial burst and MB diffusion.

The release models condensed in Eq. (3.1), Eq. (3.6), and Eq. (3.7) contain unknown parameters, which can be determined by adjusting the equation to experimental data of MB release by using nonlinear least-squares algorithm in MATLAB<sup>®</sup> (MathWorks, USA). Due to the difference in the number of parameters between the burst release, the

diffusion model, and the combination of both, an adjusted coefficient of determination ( $R^2_{adjusted}$ ) was incorporated in the analysis. The  $R^2_{adjusted}$  is given by:

$$R^2_{adjusted} = 1 - \frac{(n_{dp} - 1)}{(n_{dp} - p)}(1 - R^2) \quad (3.8)$$

where  $n_{dp}$  is the number of data points ( $M_t/M_\infty$ ) and  $p$  is the number of parameters in the model. The use of this parameter is an indication of the effect of new parameters in the model, resulting in more effective comparison between them (Costa & Sousa Lobo, 2001).

### 3.4. Results and discussions

#### 3.4.1 Nanoparticles characterization

Different sets of experiments were performed by changing the initial amount of MB used in preparations while the amount of polymer was maintained constant. MB-PNP average diameter and average PDI for all preparations are presented in Fig. 3.2 part a. It is noted that average diameters for blank nanoparticles were around 180 nm. Results for the O/W and the combined W/O/W emulsification techniques are in similar size of blank nanoparticles, around 183 nm. Results of the well-known W/O/W emulsification technique indicate that MB-PNP size increase from 201 to 287 nm depending on TDL. The average PDI obtained for MB-PNP prepared by the O/W emulsification technique was around 0.78 and 0.109 for the TDL of 2% and 4%. When MB-PNP were prepared with the well-known W/O/W emulsification technique, the average PDI obtained increased from 0.080 to 0.249 as the TDL increased, indicating saturation in the system. The combined W/O/W emulsification method present low values of PDI similar to the blank nanoparticles indicating a uniform nanoparticle size, compared with the other methods of preparation. Zeta potential for all the different preparations varied between -21 mV and -31 mV, indicating fair to good stability of the nanoparticles, respectively (Fig. 3.2 part b). In general, the zeta potential values were influenced by TDL, indicating some interactions between MB and the surface of the nanoparticles. In literature MB have been encapsulated in sol-gel silica nanoparticles obtaining sizes ranging the 160

nm to 190 nm and silica-based nanoparticles in the range of 20-30 nm diameter (Tang *et al.*, 2005). Other silica nanoparticles entrapping MB have been obtained in sizes of 105 nm with zeta potential charges ranging between -44 mV and -29 mV (He *et al.*, 2009). When MB is encapsulated in PLGA, authors have found sizes ranging the 190 nm to 220 nm with surface charges of -38 mV for MB charged PLGA nanoparticles and -17.5 mV for blank PLGA nanoparticles (Klepac-Ceraj *et al.*, 2011). Recently, Cannavà *et al.* reported a study where MB was also encapsulated in PLGA at a 2.5% TDL by single and double emulsification techniques. Sizes obtained by them ranged between 220 nm and 266 nm diameter, with PDI values of 0.19 and 0.4 for single and double emulsification technique respectively (Cannavà *et al.*, 2016).

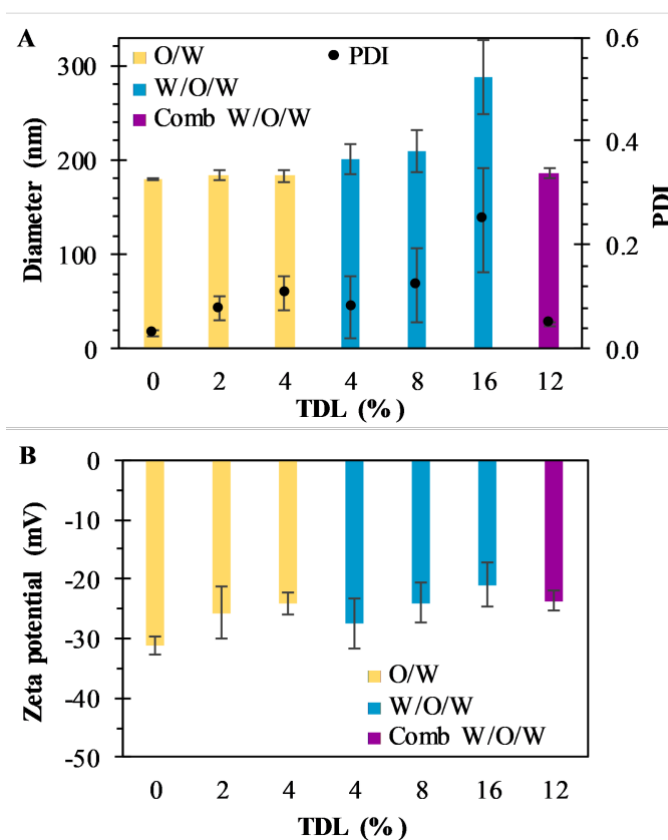


**Figure 3.2.** Characteristics of MB-PNP prepared by different emulsification techniques. (A) Particle diameters and PDI. (B) Zeta potentials. Blank nanoparticles and MB-PNP prepared with an O/W emulsification technique for 2.0 and 4.0 % TDL (■). MB-PNP prepared with a W/O/W emulsification technique for 4.0, 8.0 and 16.0 % TDL (■). MB-PNP prepared by a combined W/O/W emulsion method for 12 % TDL (■). Data represent mean  $\pm$  SD (n = 3).

In Fig. 3.3 are presented the DL and EE for all the preparations. DL ranged between 0.4% and 1.06% for all the formulations. The respective EE values obtained were between 8.0% and 13.3%. The DL of particles prepared by the combined method are similar to the ones obtained by the double emulsion but the diameters of particle and PDI are reduced significantly. Cannavà et al. prepared MB loaded PLGA nanoparticles by the single emulsification technique with values of 0.52% and 3.13% for the DL and EE, respectively. Also, they prepared the same kind of nanoparticles by the double emulsification technique reporting values of 1.13% and 6.75% for the DL and EE, respectively (Cannavà *et al.*, 2016). These reported values for DL are comparable to the ones obtained in this work. The results obtained in the present work when the combined emulsification technique was used have values of 1.04% and 8.06% for the DL and EE, respectively, which are also comparable to literature. A summary with the average values of particle size, PDI, zeta-potential, DL and EE for the different preparations of MB-PNP is presented in Table 3.1.

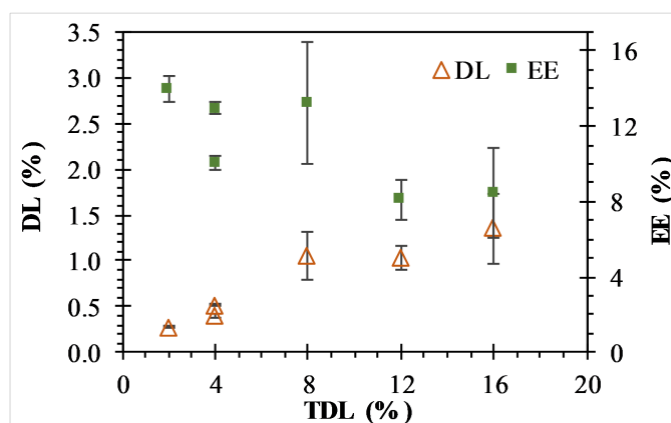


**Figure 3.3.** Drug loading ( $\triangle$ ) and encapsulation efficiency ( $\blacksquare$ ) for the MB-PNP with different theoretical drug loading experiments prepared by the different emulsification techniques. Data represent mean ( $n = 3$ ).

**Table 3.1.** Characteristics of MB-PNP as a function of TDL. Data represent mean  $\pm$  SD ( $n = 3$ ).

	Nanoparticle Preparation	TDL (%)	Size (d. nm)	PDI	$\zeta$ (mV)	DL (%)	EE (%)
MB-PNP	PNP O/W	0	179.6 $\pm$ 1.0	0.030 $\pm$ 0.007	-31.2 $\pm$ 1.4		
	O/W	2	184.5 $\pm$ 5.0	0.078 $\pm$ 0.025	-25.7 $\pm$ 4.3	0.28 $\pm$ 0.01	13.95 $\pm$ 0.66
	O/W	4	183.0 $\pm$ 5.8	0.109 $\pm$ 0.032	-24.1 $\pm$ 1.7	0.40 $\pm$ 0.01	10.06 $\pm$ 0.37
	W/O/W	4	201.4 $\pm$ 16.2	0.080 $\pm$ 0.061	-27.6 $\pm$ 4.2	0.52 $\pm$ 0.01	12.95 $\pm$ 0.28
	W/O/W	8	209.2 $\pm$ 22.7	0.123 $\pm$ 0.072	-24.0 $\pm$ 3.4	1.06 $\pm$ 0.26	13.23 $\pm$ 3.19
	W/O/W	16	287.2 $\pm$ 39.3	0.249 $\pm$ 0.100	-21.0 $\pm$ 3.6	1.36 $\pm$ 0.39	8.47 $\pm$ 2.41
	Combined W/O/W	12	186.0 $\pm$ 4.6	0.048 $\pm$ 0.005	-23.6 $\pm$ 1.6	1.03 $\pm$ 0.13	8.12 $\pm$ 1.05

Blank PLGA nanoparticles prepared by the O/W emulsification process are presented in Fig. 3.4. As depicted in this figure, PLGA nanoparticles are spherical with smooth surface. PLGA nanoparticles presented diameters of 113.86 $\pm$ 39 nm when evaluated by the particle size distribution histogram shown in the insert of Fig. 3.4. This diameter obtained with the histogram is in accordance to the measurements of DLS by considering the hydrodynamic radius in the DLS analysis. SEM of MB-PNP for the different preparations did not affect particle size as determined by SEM (results not shown).

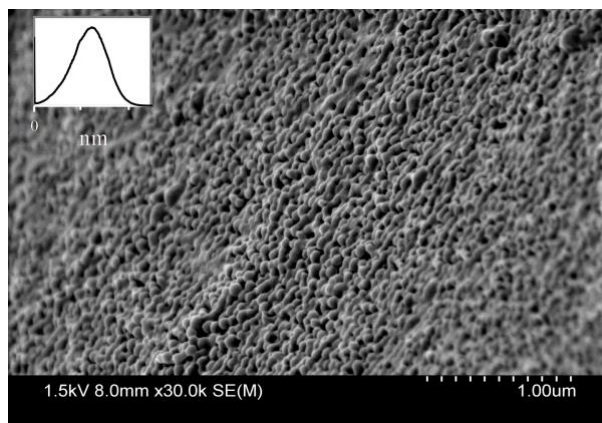


**Figure 3.4.** Scanning electron micrograph of blank-PNP. The insert represents the particle size distribution histogram of blank-PNP.

#### 3.4.2 MB release analysis

*In vitro* release studies of MB from MB-PNP were performed with different TDL and formulation techniques. Similar MB release profiles were obtained for all preparations. The preparations of O/W emulsification with a TDL of 4% and W/O/W emulsification with a TDL of 8% are presented in Fig. 3.5 in order to compare with the release profiles of the combined method prepared with a TDL of 12%. The percent of MB released in the initial times could be attributed to the initial burst mechanism. Within the first 4 hours of release above of 80% of MB was release for all the formulations. This fast release is related to the high solubility nature of MB. Also, based in this solubility is considered that most of the MB is encapsulated close to the surface of nanoparticles. In terms of mass, during the first 4 hours of release, 3.0  $\mu\text{g}$ , 8.5  $\mu\text{g}$  and 7.22  $\mu\text{g}$  of MB per mg of nanoparticle were released by the particles prepared at TDL of 4% (O/W), TDL of 8% (W/O/W) and TDL of 12% (combined W/O/W), respectively. After the initial burst stage, a slower release was observed until a plateau was reached indicating that all MB was released from the nanoparticles. This slower release stage can be explained by the diffusion of MB through the polymer matrix. Analogous behaviour was reported in literature for similar systems, where 80% of encapsulated MB was release after 5-12 hours, reaching a 100% at approximately in 24 hours (Klepac-Ceraj *et al.*, 2011; Cannavà *et al.*, 2016).

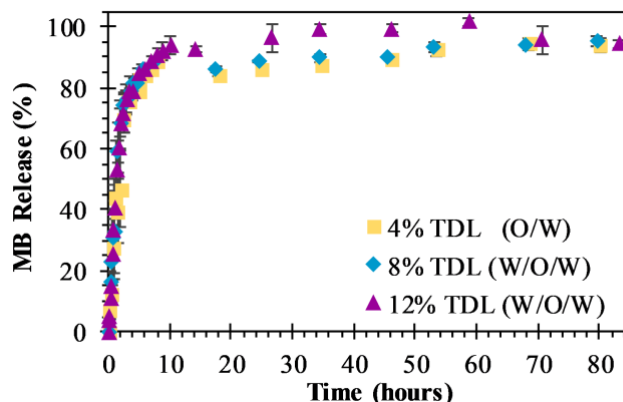


**Figure 3.5.** In vitro MB release profiles from 4.0 % (■) TDL MB-PNP prepared with an O/W emulsification technique, 8.0 % (◆) TDL prepared by W/O/W emulsion method; and 12 % (▲) prepared by a combined W/O/W emulsion method. Data represent mean  $\pm$  SD ( $n = 3$ ).

Experimental MB release data was analysed by three different models represented in Ec. (3.1), Ec. (3.6), and Ec. (3.7) for initial burst, MB diffusion and a combination of both mechanisms, respectively. In general, a good fit of the three models with the experimental data was obtained, as presented in Fig. 3.6. The parameters obtained for each model are presented in Table 3.2. The fit of the initial burst model (Eq. (3.1)) to the experimental data are fair. As expected, this model is good to describe the experimental data at smaller times, but it's not able to describe the middle part of the release profile. The initial burst constant values obtained with this model are  $0.377 \text{ h}^{-1}$ ,  $0.453 \text{ h}^{-1}$ , and  $0.464 \text{ h}^{-1}$ , for particles prepared at TDL of 4% (O/W), TDL of 8% (W/O/W) and TDL of 12% (combined W/O/W), respectively. The initial burst constant increases proportionally to the DL. In other words, since more mass of drug was released in the same amount of time, the initial burst changes in proportion. These effect was previously described in literature indicating that more drug could be trapped on the surface of the polymer matrix during the manufacturing process especially in the case of high drug loading (Huang & Brazel, 2001). The fickian diffusion model (Eq. (3.6)) was able to fairly describe experimental data, especially at shorter times, as could be observed in Fig. 3.6. Although, the fit of this model to the middle part of the release profile curve

was not ideal. The effective diffusion coefficient values obtained by the model were in the range of  $10^{-16}$  cm<sup>2</sup>/s for all formulations. However, the effective diffusion coefficient could be also associated to the DL in the same terms than initial burst constant analysis presented for Eq. (3.1). When using fickian model, the coefficients of determination obtained are considerably lower, compared with the initial burst model, as could be observed in Table 3.2.

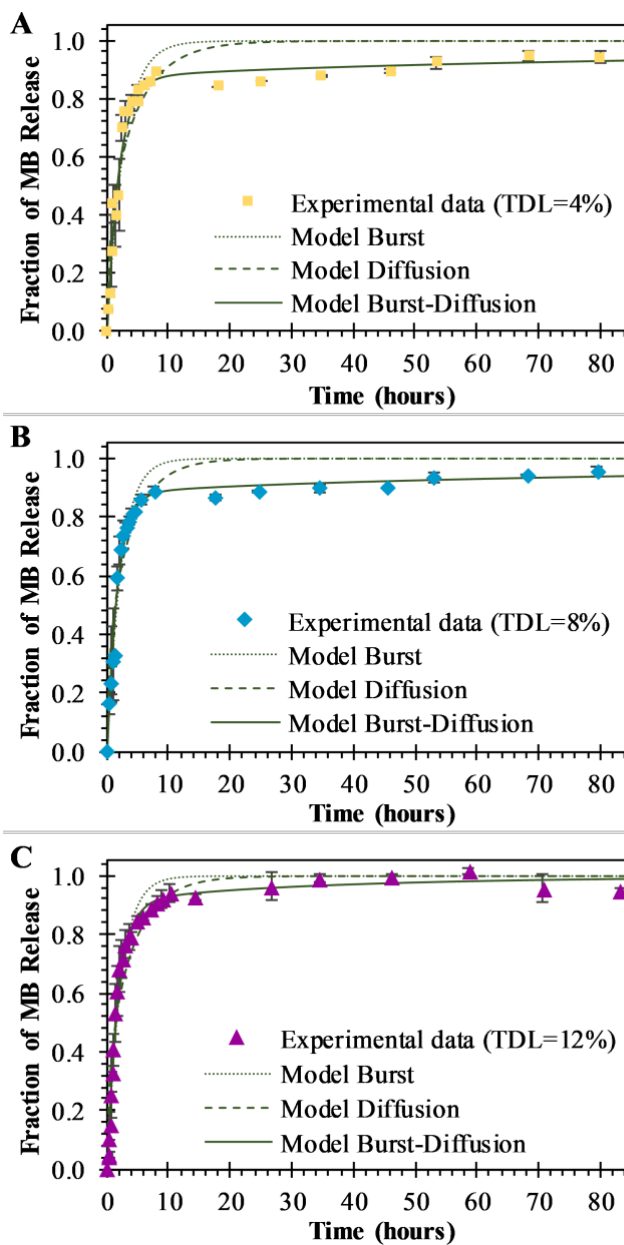


**Figure 3.6.** MB release initial burst model (.....), diffusion model (----) and a combined initial burst and diffusion model (—) profiles from (A) 4.0 % (■) TDL MB-PNP prepared with an O/W emulsification technique, (B) 8.0 % (◆) TDL prepared by W/O/W emulsion method; and (C) 12 % (▲) prepared by a combined W/O/W emulsion method. Data represent mean  $\pm$  SD ( $n = 3$ ).

**Table 3.2.** Parameters of MB release from MB-PNP. The parameters were determined and used in the mathematical development of the release model.

Parameters	Description	Unit	O/W Single emulsion TDL = 4%	W/O/W Double emulsion TDL = 8%	W/O/W Combined emulsion TDL = 12%
Model of Initial Burst					
$k_b$	Burst constant	$hours^{-1}$	0.377	0.453	0.464
$R^2$	Coefficient of determination		0.934	0.948	0.979
Model of Diffusion					
$D$	Diffusion constant	$cm^2/s$	4.454E-16	5.450E-16	5.100E-16
$R^2$	Coefficient of determination		0.907	0.921	0.936
Model of Initial Burst and Diffusion					
$\theta_b$	Fraction of burst release	-	0.851	0.862	0.876
$k_b$	Burst constant	$hours^{-1}$	0.516	0.600	0.556
$\theta_d$	Fraction of diffusion	-	0.149	0.138	0.124
$D$	Diffusion constant	$cm^2/s$	9.179E-18	1.086E-17	5.941E-17
$R^2$	Coefficient of determination		0.978	0.988	0.988
$R^2_{adjusted}$	Adjusted coefficient of determination		0.976	0.986	0.987

By combining both models, the initial burst and the fickian diffusion into a linear equation that considers the simultaneous contribution of both models (Eq. (3.7)) a better fit to the experimental data is obtained, compared to the individual models. In the combined model, initial burst constant values increased compared to the ones obtained by the initial burst model by itself. In contrast, the effective diffusion coefficient decreases in comparison with the values obtained by the model of Eq. (3.6). The combined model is able to describe more accurately the release phenomena since simultaneously consider the influence of two mechanisms of release, as could be observed in the coefficients of determination presented in Table 3.2. Cannavà et al. used three individual models of release to describe MB release from PLGA nanoparticles when encapsulated with cyclodextrin: a zero order, a first order and a Higuchi model

that resulted in release rate constants of  $0.5358 \text{ h}^{-1}$ ,  $0.0346 \text{ h}^{-1}$  and  $6.7967 \text{ h}^{-1/2}$ , respectively. These models resulted with coefficients of determination of 0.8794, 0.9361 and 0.9799 respectively. According to this author, the release of MB can be described as the squared root of a time-dependent process based on fickian diffusion (Cannavà *et al.*, 2016). Also, authors have found that diffusion is the controlling mechanism of release when encapsulating other photosensitizers with low solubility.

### **3.5. Conclusion**

MB-PNP were successfully prepared by the proposed combined emulsification technique consisting in a combination of the single and double emulsification. Size, PDI, zeta potential, MB loading and the encapsulation efficiency of nanoparticles were determined. These results suggest that the particles prepared by the combined technique resulted with uniform particle size and repeatability compared with the individual techniques. The combine technique could be applied to several compounds that have partial solubility to improve the drug loading and also the physicochemical characteristics of nanoparticles. The release profile curve of MB from PLGA nanoparticles indicate that most of the MB was encapsulated close to the surface of nanoparticles. This release profile was analysed by considering an initial burst model, a MB diffusion model and also by simultaneously combining both mechanisms of release into a linear model. It was found that initial burst constant and the effective diffusion coefficient are associated to the DL. The combined model describes more accurately the release phenomena than the individual mechanisms indicating that both mechanisms are significant. This mathematical analysis could be used to describe and predict the release of compounds with intermediate to high solubility from biodegradable nanoparticles.

## **CHAPTER 4. FOLATE FUNCTIONALIZED PLGA NANOPARTICLES LOADED WITH PLASMID pVAX1-NH36: MATHEMATICAL ANALYSIS OF RELEASE**

### **4.1 Abstract**

Plasmid DNA (pVAX1-NH36) was encapsulated in nanoparticles of PLGA functionalized with PEG and folic acid (PLGA-PEG-FA) without losing integrity. PLGA-PEG-FA nanoparticles loaded with pVAX1-NH36 (pDNA-PNP) were prepared by using double emulsification-solvent evaporation technique. PLGA-PEG-FA synthesis was verified by FT-IR and spectrophotometry methods. pVAX1-NH36 was replicated in *E. coli* cell cultures. AFM analysis confirmed pDNA-PNP size with an average diameter of 177-229 nm, depending on pVAX1-NH36 loading and zeta potentials were below -24 mV for all preparations. In vitro release studies confirmed a multiphase release profile for the duration of more than 30-days. Plasmid release kinetics were analyzed with a release model that considered simultaneous contributions of initial burst and degradation-relaxation of nanoparticles. Fitting of release model against experimental data presented excellent correlation. This mathematical analysis presents a novel approach to describe and predict the release of plasmid DNA from biodegradable nanoparticles.

### **4.2. Introduction**

Research related to the use of nano-systems in drugs and genes has increased in last decades due to number of innovative applications of nano-systems in health-related issues. The global market for drug delivery systems and genes is projected to reach \$175.6 billion by 2016, which represents an increase of \$44 billion from 2010 (Santini, 2013). The main focus of such nano-systems administrated drugs and genes research is to deliver a specific amount of component of interest in right place at right time and nano-formulation has received the most attention out of others. The exposure of cells/tissues/tumors to therapeutic agents increases when nano-formulations are designed as drug delivery vehicles. Various therapeutic and immunization agents such as anticancer drugs and plasmid DNA (pDNA) could be encapsulated and

administered simultaneously to enhance the effectiveness of such therapy and/or immunization (Peer *et al.*, 2007; Shi *et al.*, 2010).

Among different materials used for drug delivery, one of the most successful is poly (ester): PLGA, which has immense potential as drug delivery vehicle as well as a platform for tissue engineering (Makadia & Siegel, 2011; Danhier *et al.*, 2012). PLGA is biodegradable polymer mostly used for developing nano-medicines. It hydrolyzed in body to produce lactic acid and glycolic acid monomers, which subsequently degraded to carbon dioxide and water (Jain, 2000; Kumari *et al.*, 2010; Danhier *et al.*, 2012). Degradation rates and structural/mechanical properties of PLGA depend on proportion of monomers formed (Jain, 2000; Danhier *et al.*, 2012). PLGA contains carboxylic acid, which can also be functionalized with other molecules before or after the preparation of PNP. One of the possible modifications of PLGA is coupling with polymer polyethylene glycol (PEG). It has been shown that PEG-coated carriers have increased circulation half-life in blood, reduced rate of uptake by liver and prevent its recognition by mononuclear phagocytic system (Peracchia *et al.*, 1997). In addition, they can facilitate a full control of drug release rates (Paun *et al.*, 2012). Furthermore, PLGA and PEG are already approved by Food and Drug Administration (FDA) and European Medicine Agency (EMA) and used in therapeutic devices (Parveen & Sahoo, 2008; Danhier *et al.*, 2012).

Another desirable characteristic of these nano-systems is possible functionalization to target specific cells. Selective gene delivery to folate receptor overexpressing tissues by decorating PNP with folic acid (FA) as targeting ligand is of great interest (Esmaeili *et al.*, 2008; Liang *et al.*, 2011; Benfer *et al.*, 2012). Chemical coupling of PLGA, PEG and FA will enable us to produce PNP with blood compatibility, drug release rate control and targeting characteristics. Polymer PNP have been prepared using different methods and the most common of them is emulsification - solvent evaporation technique (Jain, 2000; Grazia Cascone *et al.*, 2002; Yang *et al.*, 2007; Danhier *et al.*, 2012). Other available methods are emulsification - diffusion of solvent (Murakami *et al.*, 2000; Sahana *et al.*, 2008), nanoprecipitation (Chorny *et al.*, 2002; Dhar *et al.*, 2008) and others.

Leishmaniasis is the third most important vector-borne disease worldwide, caused by protozoan *Leishmania* parasites that are transmitted by the bite of infected sandflies. There is consensus that vaccines ought to become a major tool in the control of such group of diseases (Iborra *et al.*, 2004). In the specific case of leishmaniasis, a recent review confirms that up to this

date there is no drug therapy or human vaccine available (Jain & Jain, 2015). pDNA has inherent features that make them promising vaccine candidates in a variety of diseases like leishmaniasis (Dumonteil, 2003; Gamboa-León *et al.*, 2006; Chalé-balboa *et al.*, 2009; Ismail *et al.*, 2012). pDNA based therapeutic and immunization methods relay on genes transfer to human cells to encode the synthesis of a protein, which when expressed, carries an immunizing or therapeutic action. In this regard, NH36 gene is one of the candidates for DNA vaccines against leishmaniasis and has already been tested in several animal models (Palatnik-de-Sousa, 2008; Nagill & Kaur, 2011). On the other hand, reports have shown limitations and restrictions in transport of pDNA through intramuscular, cutaneous and intracutaneous routes (Wang *et al.*, 1999). Therefore, an improved system for transferring pDNA to a specific site are necessary to address these limitations. Wang *et al.* (Wang *et al.*, 1999) tried to solve this problem by encapsulating pDNA into micro-particles of biodegradable polymers. In this way, they protect the plasmid from being digested by ribonucleases and also assist transport and control release rate. Recent reports on pDNA encapsulation into PNP are focused in cancer gene therapy and vaccination applications (Schaffert & Wagner, 2008; Jayakumar *et al.*, 2010; Gaspar *et al.*, 2011; Kunugi & Yamaoka, 2012; Basto, 2013) where the authors have address encapsulation of pDNA into PNP by using different approaches. In general, the process of pDNA encapsulation into PNP involves several steps and preparation parameters that should be modulated according to desired PNP characteristics. Experimental pDNA release from biodegradable matrices have been reported for different plasmids (Perez *et al.*, 2001; Saljoughian *et al.*, 2013; Zhao *et al.*, 2014) and to the best of our knowledge, only few efforts to mathematically describe the pDNA release kinetics have been reported, where the entire plasmid release process has been attributed to the diffusion mechanism (Megeed *et al.*, n.d.). Contrary to pDNA release kinetics, mathematical analysis of drug release from biodegradable matrices have been extensively reported in literature by considering one or more mechanisms of release (Fredenberg *et al.*, 2011; Lao *et al.*, 2011). In this present research, a preparation process of biodegradable nanoparticles loaded with plasmid pVAX1-NH36 was developed. pVAX1-NH36 was replicated using *E. coli* bacteria and purified to obtain a pure plasmid followed by capsuling into PNP prepared with PLGA-PEG-FA by using different theoretical DNA loadings. Several techniques were used to characterize PNP such as dynamic light scattering, laser doppler electrophoresis, AFM, HPLC-HIC and agarose electrophoresis. pVAX1-NH36 release was evaluated *in vitro* under physiological conditions and

release kinetics were analyzed by using an effective mathematical release model that simultaneously considers the mechanism of initial burst as well as mechanism of degradation-relaxation of PNP (Corrigan & Li, 2009). Mechanism of initial burst was calculated using first order rate burst release and the mechanism of release due to bulk degradation of polymer or PNP relaxation was evaluated in analogous way to thermal decomposition of potassium permanganate crystals (Prout & Tompkins, 1944; Fitzgerald & Corrigan, 1993). These two mechanisms were linearly coupled to effectively describe the entire plasmid release process.

### **4.3 Materials and Methods**

#### **4.3.1 Materials**

PLGA acid terminated (50/50 DL-lactide/glycolide copolymer, IV midpoint 0.2 dL/g) was obtained from Corbion Purac, Gorinchem, The Netherlands. Glycerol, yeast extract, tryptone, potassium sulfate dibasic and monobasic, kanamycin, N-Hydroxysuccinimide (NHS), dimethyl sulfoxide (DMSO), methanol and diethyl ether were obtained from Sigma-Aldrich, Inc., Milwaukee, Wisconsin, USA. Supercoiled DNA ladder was obtained from Invitrogen, Corp., Carlsbad, California, USA. O,O'-Bis(2-aminopropyl) polypropylene glycol - block - polyethylene glycol-block - polypropylene glycol (PEG) of 1,900 amu was obtained from Fluka, Buchs, Switzerland. Folic acid (FA) and polyvinyl alcohol (Mowiol® 4-88 Mw ~31,000 amu, PVA) was obtained from Sigma Aldrich, Inc., St. Louis, Missouri, USA. N,N'-Dicyclohexylcarbodiimide (DCC) was obtained from Alfa Aesar, Ward Hill, Massachusetts, USA. Dichloromethane (DCM) was obtained from Fisher Scientific Inc., Fair Lawn, New Jersey, USA.

#### **4.3.2 Cell culture and pVAX1-NH36 recovery**

Plasmid pVAX1-NH36 was produced by cultivation of recombinant *Escherichia coli DH5α*. Cell package was supplied by the Department of Scientific and Technological Research at the University of Sonora, Hermosillo, Sonora, Mexico. Size of the plasmid was 4.0 kbp and contains an antibiotic resistance gene against kanamycin for selection purposes. Host strain was maintained in 30% (v/v) glycerol at -80°C. Culture medium consisted of terrific broth supplemented with glycerol and kanamycin with following composition: 13.0 g/L glycerol, 24.0

g/L yeast extract, 12.0 g/L tryptone, 12.54 g/L potassium phosphate dibasic, 2.31 g/L potassium phosphate monobasic and 50.0 µg/mL kanamycin. Cultures were started from glycerol stocks inoculated into medium and grown in shake flasks at 37°C on an orbital shaker at 250 rpm for 8 hours. Cell culture concentration was obtained by using a Perkin Elmer UV/VIS spectrometer lambda 2S (Perkin-Elmer de Mexico, Monterrey, Nuevo Leon, Mexico) measuring optical density (OD) at 600 nm. After fermentation, culture was centrifuged and pellet was used for plasmid recovery. pVAX1-NH36 was purified using GenElute™ plasmid Maxiprep Kit (Sigma Aldrich Co., St. Louis, Missouri, USA) according to manufacturer's instructions. Plasmid solution was concentrated using a stirred ultrafiltration cell system Millipore 8050 (Millipore Corporation, Bedford, MA, USA) with regenerated cellulose ultrafiltration membrane with MWCO of 100,000 Da (Millipore Corporation, Billerica, MA, USA). Quantification of pVAX1-NH36 was carried out by measuring OD at 260 nm in a NanoDrop 1000 spectrophotometer (Thermo Fisher Scientific Inc., Waltham, MA, USA).

#### 4.3.3 Polymer modification

Synthesis of PLGA-PEG-FA was carried in two steps: PLGA activation and coupling of PEG followed by FA conjugation (Yoo & Park, 2004a; Nie *et al.*, 2009), as shown schematically in Figure 4.1. Briefly, PLGA was activated by DCC and NHS in DCM with molar ratio of PLGA:DCC:NHS = 1:5:5 where reaction was carried out overnight at room temperature under nitrogen atmosphere. The resultant solution was filtered (Watman#1 filter) to remove dicyclohexylurea. For PEG coupling, activated PLGA solution was treated with PEG at a molar ratio of 1:5 and left to react overnight under nitrogen atmosphere. Polymer was washed by three cycles of precipitation using 3 volumes of cold organic mixture of methanol-diethyl ether (50/50) followed by centrifugation, discarding supernatant and resuspending in DCM. In last cycle, after centrifugation and removal of supernatant, polymer was dried under vacuum. To attach FA to polymer, PLGA-PEG was dissolved in DMSO and treated with FA in DMSO at a molar ratio of 1:5 with overnight stirring at room temperature under nitrogen atmosphere. Then, solution was filtrated (Watman #1 filter) and set to dialyze in a Spectra/Por®Membrane MWCO 3,500 in 5 mM sodium carbonate (pH 8.0) buffer for 4 hours. Next, buffer was replaced and sample was dialyzed for 4 more hours, followed by overnight dialysis in deionized water. Finally, PLGA-PEG-FA was lyophilized to remove water and trace amount of organic solvent in lyophilizer

Freezone 4.5 (Labconco, Kansas City, Missouri, USA). Structure of the copolymer was confirmed by FT-IR spectrometer spectrum (Perkin Elmer, Llantrisant, United Kingdom). For FT-IR measurements, polymer was set directly onto ATR crystal and spectrum was collected in a range between 4,000 and 550  $\text{cm}^{-1}$  with a resolution of 4  $\text{cm}^{-1}$  (16 scans per sample).

#### 4.3.4 Preparation of pDNA-PNP

Folic acid functionalized PLGA PNP loaded with pVAX1-NH36 (pDNA-PNP) were prepared by using a double emulsification technique followed by solvent evaporation (Hans & Lowman, 2002; Boddu & Vaishya, 2012; Danhier *et al.*, 2012; Lucero-Acuna, 2013). Three different theoretical pVAX1-NH36 loadings (TDL), *ratio of initial amount of pVAX1-NH36 used in the process with respect to initial amount of polymers*, were used in the preparations. Briefly, a mixture with 1 mL of pVAX1-NH36 in aqueous phase (0.2%, 0.5%, and 0.8% TDL) and polymers was dissolved in 4 mL of DCM (25 mg of PLGA and 25 mg of PLGA-PEG-FA) and emulsified using an ice bath with a QSonica 500 sonicator (QSonica LLC, Newtown, Connecticut, USA) operating at 26.5  $\mu\text{m}$  of amplitude for 1 minute. Then, 8 mL of 3% PVA were added and a second emulsification at 90  $\mu\text{m}$  of amplitude in an ice bath was performed for 1 minute. Organic solvent was then evaporated under magnetic stirring at room temperature overnight. Next, a 2 minutes centrifugation cycle at 2,000 rpm (376 \*g) using a Sigma 3-30KS centrifuge (Sigma Laborzentrifugen GmbH, Osterode am Harz, Germany) was employed and supernatant was collected. Supernatant was washed by three centrifugation cycles at 19,000 rpm (33,902 \*g) for 10 minutes, discarding supernatant and re-suspending pellet pDNA-PNP in 8 mL of deionized water. On final centrifugation cycle, pDNA-PNP were re-suspended in 4 mL of deionized water and freeze-dried in lyophilizer freezone 4.5 (Labconco, Kansas City, Missouri, USA). All experiments were triplicate.

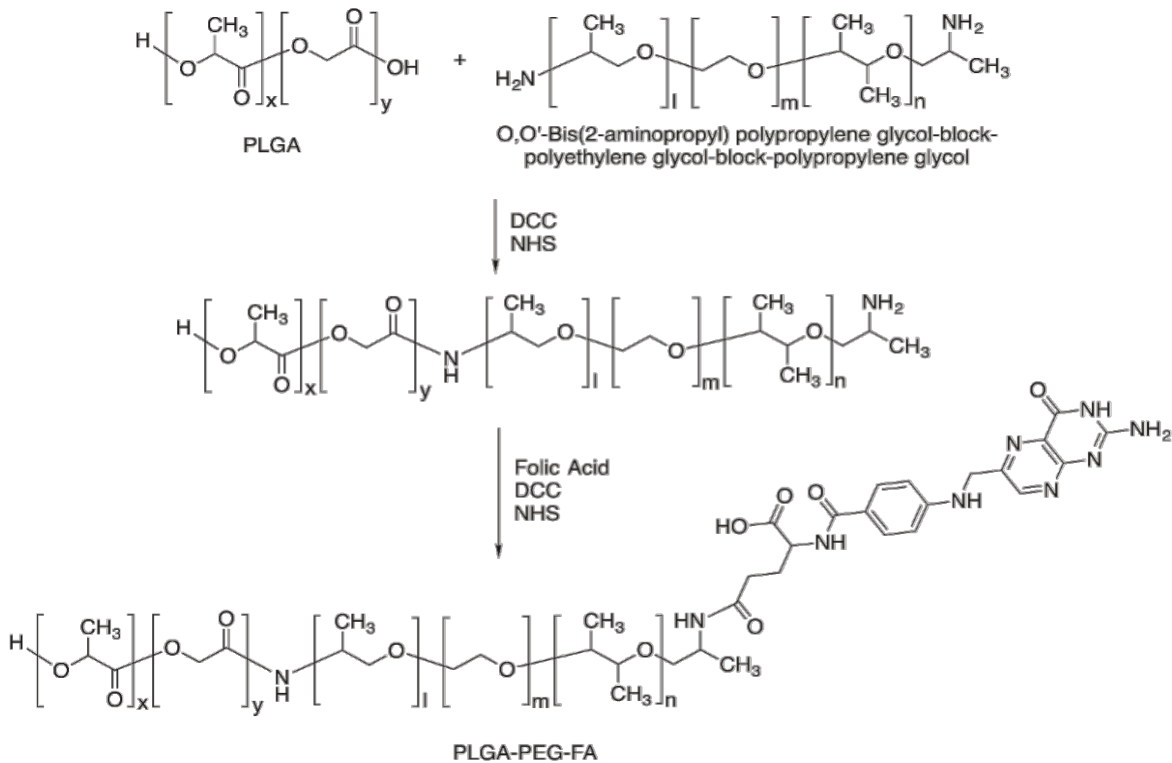


**Figure 4.1.** Schematic of the synthesis of the polymer PLGA-PEG-FA. First, PLGA carboxylic acid is activated and coupled to a primary amine of PEG (PLGA-PEG). Then, a carboxylic acid from FA is activated and conjugated to the primary amine of PLGA-PEG to finally obtain PLGA-PEG-FA.

#### 4.3.5 Nanoparticle characterization

Nanoparticle size distribution and zeta potentials were measured using a zetasizer Nano ZS equipment (Malvern Instruments Ltd., Worcestershire, United Kingdom). Measurements of pDNA-PNP sizes were performed by dynamic light scattering. Each sample was measured three times with 10 runs respectively. Additionally, each sample for zeta potential was measured by duplicated with at least 10 runs at constant temperature (25°C) by laser doppler electrophoresis. Z-averages and zeta potentials were obtained from three independent experiments.

Surface morphology of pDNA-PNP was analyzed by scanning electron microscopy (SEM) through a field emission scanning electron microscope (JSM-7800F, JEOL, US). Nanoparticle samples were prepared using formvar carbon film and air-dried for several minutes. Surface morphology was confirmed by atomic force microscopy (AFM JSP-4210, JEOL, Japan) in noncontact mode by using a NSC15 silicon cantilever (MikroMasch, Oregon, USA). For surface

analysis, a drop of pDNA-PNP solution was deposited onto freshly cleaved mica and air-dried for several minutes. AFM images were analyzed with WSxM software (Horcas *et al.*, 2007).

pVAX1-NH36 loading in pDNA-PNP (DL) was determined by subtracting the amount of pVAX1-NH36 recovered in wash solutions from initial amount of pDNA added (Perez *et al.*, 2001; Son & Kim, 2010; Menon *et al.*, 2014). Free pVAX1-NH36 concentration in all solutions was measured by HPLC-HIC (Diogo *et al.*, 2003) with a source 15PHE (Phenil-Polystyrene) column of 0.46x10 cm on an Akta purifier 10 UPC (GE Healthcare, USA). Briefly, the column was equilibrated with 1.5 M ammonium sulphate in Tris-HCl 10 mM with pH of 8.0 at a flow rate of 1 mL/min and sample (30  $\mu$ L) was injected at same flow rate. Column was eluted for 0.8 min with same buffer used for equilibration and an isocratic elution was performed using Tris-HCl buffer for 0.7 min. After this period, ammonium sulphate concentration was increased to its initial value. This condition was maintained during next 5.5 min to re-equilibrate column. Absorbance at 260 nm and conductivity of eluate were recorded continuously. Plasmid amount was quantified using a calibration curve obtained with a standard model plasmid prepared in 0-60  $\mu$ g/mL concentration range. Encapsulation efficiency (EE) was defined as percent of pVAX1-NH36 encapsulated in pDNA-PNP with respect to initially added amount of pVAX1-NH36.

#### 4.3.6 *In vitro release study*

To evaluate *in vitro* pVAX1-NH36 release from pDNA-PNP, an ultracentrifugation method was used (Soppimath *et al.*, 2001). Initially, 10 mg of freeze dried pDNA-PNP were re-suspended in 1 mL of PBS buffer (pH 7.4) and incubated at 37°C. Samples were taken periodically and centrifuged using a centrifuge (Thermo Sisher Scientific, Asheville, North Carolina, USA) at 19,000 rpm (32,186 \*g) for 10 min at 37°C to obtain pellet pDNA-PNP. The supernatants were removed and replaced with fresh buffer and pDNA-PNP were re-suspended by vortex. The supernatant solution was analyzed for pVAX1-NH36 by HPLC-HIC, as described above.

#### 4.3.7 *Mathematical analysis of pDNA release*

Release analysis of active components from biodegradable systems is a combination of a number of factors. These factors determine the contribution of mechanisms of release involved, such as initial burst, PNP degradation-relaxation and diffusion. Fredenberg *et al.* reported a comprehensive review that considers several physical factors such as temperature and pH of the

system, size and shape of PNP, drug solubility, and others (Fredenberg *et al.*, 2011). pDNA release analysis from biodegradable PNP usually considers those factors, resulting in more than one mechanism of release to describe the entire release process. One of the most relevant mechanisms of release is initial burst, which is attributed to a process of interfacial diffusion between solid sphere surface and liquid media. By considering initially all pVAX1-NH36 is incorporated in PNP, kinetics of initial burst follow an exponential relationship as reported in literature (Batycky *et al.*, 1997; Lucero-Acuña & Guzmán, 2015).

$$\frac{M_t}{M_\infty} = 1 - \exp(-k_b t) \quad (4.1)$$

where  $M_t$  is the cumulative amount of pVAX1-NH36 released at time  $t$ ,  $M_\infty$  is the cumulative amount of pDNA released at infinite time and  $k_b$  is the initial burst constant, incorporating factors such as concentration of pVAX1-NH36 on PNP surface, surface area, interphase properties, solubility of pVAX1-NH36 and electrostatic interactions between pDNA and carrier (Corrigan & Li, 2009).

Other mechanism associates the amount of pDNA released with polymeric matrix degradation, which depends on factors such as pH of the media, incubation temperature and larger particles degrade at faster rates than smaller ones (Dunne *et al.*, 2000). Degradation of PLGA in aqueous solutions was carried by hydrolysis, resulting in relaxation of PNP as evident in literature (Lao *et al.*, 2009). PLGA PNP degradation – relaxation effects has been explained by using Prout-Tompkins equation (Fitzgerald & Corrigan, 1993; Dunne *et al.*, 2000; Corrigan & Li, 2009; Lucero-Acuña & Guzmán, 2015). This equation can be used also to describe pDNA release and could be rewritten in the following form:

$$\frac{M_t}{M_\infty} = \frac{\exp[k_r(t - t_{max})]}{1 + \exp[k_r(t - t_{max})]} \quad (4.2)$$

where  $k_r$  is the rate of degradation - relaxation constant and  $t_{max}$  is the time to achieve a maximum rate of pDNA release or the time to achieve 50% of release.

Hence, a linear combination of Eq. (4.1) and Eq. (4.2), that simultaneously considers the stages of initial burst and PNP degradation-relaxation, was used to describe the entire pDNA release process from biodegradable PNP according to Ec. (4.3):

$$\frac{M_t}{M_\infty} = \theta_b \{1 - \exp(-k_b t)\} + (1 - \theta_b) \left\{ \frac{\exp[k_r(t - t_{max})]}{1 + \exp[k_r(t - t_{max})]} \right\} \quad (4.3)$$

where the initial burst contribution fraction over entire pDNA release process is  $\theta_b$ . Eq. (4.3) contains four unknown parameters, which were determined by adjusting the equation to experimental data of pVAX1-NH36 release by using nonlinear least-squares algorithm in MATLAB® (MathWorks, USA).

#### *4.3.8 Purity and integrity of plasmid*

Electrophoresis was used to determine the purity of plasmid with the purpose of verifying quality of supercoiled pVAX1-NH36. Agarose gels (1%) were prepared in Tris–Acetic acid–EDTA (TAE) buffer (40 mM Tris, 20 mM acetic acid, 1 mM EDTA pH 8.0). Gels were run at 80 V (40 A) for 100 min on a PowerPac™ power supply unit (Bio-Rad Laboratories, Inc., Hercules, CA, USA). DNA in gels was visualized by staining in ethidium bromide (EtBr, Sigma 0.5 µg/ml) for 30 min. Stained gels were scanned using a UVP MultiDoc-It digital imaging systems.

### **4.4. Results and discussions**

#### *4.4.1 Cell culture and pDNA recovery*

Cell culture was inoculated from a previous culture at exponential growth phase. A cell culture OD of 5.47 was reached after 8 hours of culture. pVAX1-NH36 recovery and purification was done according to kit protocol. pVAX1-NH36 was concentrated in ultrafiltration system described above to obtain a plasmid stock solution with concentration of 774.6 mg/L. A ratio of  $A_{260}/A_{280}=1.9$  was obtained. This measurement is used to assess the purity of DNA. A ratio of  $\sim 1.8$  is generally accepted as “pure” for DNA. If the ratio is appreciably lower, it may indicate the presence of protein, phenol or other contaminants that absorb strongly at or near 280 nm.

#### *4.4.2 Polymer modification*

PLGA-PEG-FA was successfully synthesized in two conjugation steps. FT-IR studies were carried out to confirm the presence of amide linkage in polymer (Figure 4.2). Characteristic bands for folic acid at 1,452 and 1,608  $\text{cm}^{-1}$  are presented in functionalized copolymer and could be due to stretching vibrations of C=C in backbone of aromatic ring present in folic acid (Choy *et al.*, 2004; Yang *et al.*, 2010). Most significant FT-IR absorption peak in PLGA-PEG-FA polymer was caused by the presence of -CONH- linkage. The carbonyl (C=O) and amine (N–H)

groups present in amide linkage exhibited bands at 1,623 and 1,571  $\text{cm}^{-1}$  respectively (Yang *et al.*, 2010; Boddu & Vaishya, 2012). Previous works with similar polymer modifications reported characteristic FT-IR absorption peaks obtained in present work. For example, Choy *et al.* (Choy *et al.*, 2004) hybridized folic acid with layered double hydroxide by ion-exchange reaction. In the same way, Yang *et al.* (Yang *et al.*, 2010) reported FA-chitosan conjugates and Boddu *et al.* (Boddu & Vaishya, 2012) synthesized PLGA-PEG-FA. Boddu *et al.* work on FT-IR spectrum results matches the spectrum obtained with copolymer prepared in present work.

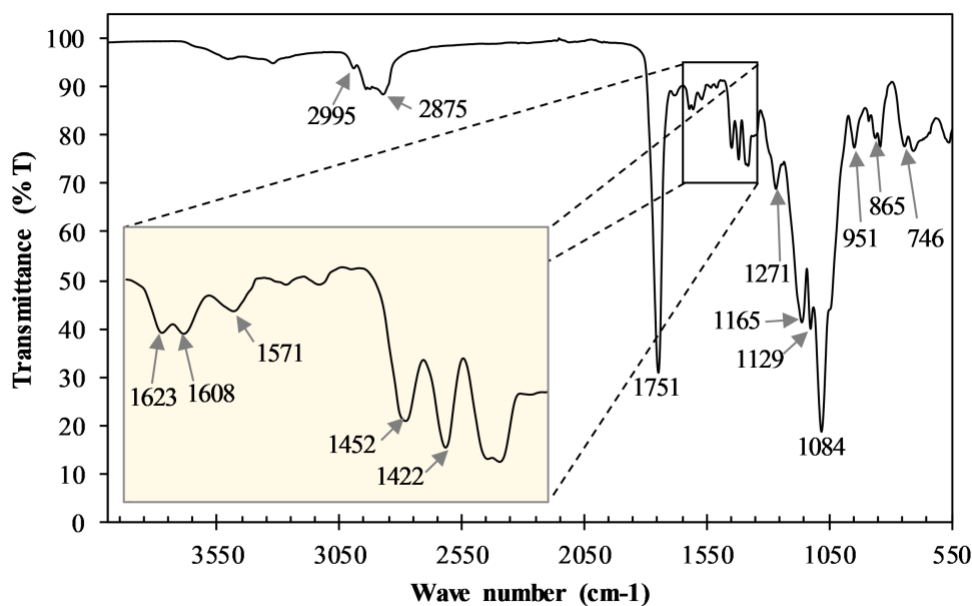


**Figure 4.2.** FT-IR absorption peaks of PLGA-PEG-FA polymer. Characteristic bands for aromatic ring present in the folic acid at 1452 and 1608  $\text{cm}^{-1}$  and PLGA-PEG-FA representative absorption peaks at 1623 and 1571  $\text{cm}^{-1}$  due to the presence of  $-\text{CONH}-$  linkage.

#### 4.4.3 Nanoparticles characterization

Average values of particle size, PDI, zeta-potential, DL and EE for different preparations of pDNA-PNP are shown in Table 4.1. Three different sets of experiments were performed by changing initial amount of pVAX1-NH36 used in preparations, while the number of polymers was maintained constant and related in the form of TDL. pDNA-PNP average diameter and average PDI could be observed in Figure 4.3A, where it is noted that average diameters of three

formulations are in range of 170–230 nm and also a correlation with TDL was observed. In the range of study, diameter of pDNA-PNP increases with an increase in TDL.

**Table 4.1.** Characteristics of pDNA-NP as a function of pVAX1-NH36 TDL. Data represent mean  $\pm$  SD ( $n = 3$ ).

pDNA-NP TDL (%)	Size (d. nm)	PDI	Zeta Potential (mV)	DL (%)	EE (%)
0.2	177.2 $\pm$ 18.2	0.131 $\pm$ 0.020	-26.6 $\pm$ 4.7	0.0309 $\pm$ 0.003	15.437 $\pm$ 1.56
0.5	202.1 $\pm$ 12.1	0.144 $\pm$ 0.047	-24.0 $\pm$ 4.1	0.0794 $\pm$ 0.004	15.881 $\pm$ 0.74
0.8	229.3 $\pm$ 20.0	0.142 $\pm$ 0.053	-29.5 $\pm$ 2.8	0.1874 $\pm$ 0.024	23.429 $\pm$ 2.96

In previous works, Wang et al. performed plasmid encapsulation using PLGA with different molecular mass and obtained spherical microspheres in range of 0.4 to 2.0  $\mu$ m (Wang *et al.*, 1999). Similarly, Gaspar et al. encapsulated plasmid for gene therapy using chitosan and obtained particles in range of 157-198 nm (Gaspar *et al.*, 2011). Liang et al. and Esmaili et al. have encapsulated different cancer chemotherapeutics using modified polymer PLGA-PEG-FA, obtaining particles in range of 216-220 nm with PDI of 0.225-0.113 (Esmaili *et al.*, 2008; Liang *et al.*, 2011). Yoo et al. also encapsulated anticancer drug by conjugating drug to PEG-FA, resulting in nano-aggregates with average size of 200 nm (Yoo & Park, 2004a). Therefore, size range obtained in present research is appropriate for the type of particles being synthesized. Figure 4.3a also exhibits average PDI for pDNA-PNP ranges from 0.130 to 0.145.

Surface charge is an important indication for stability of colloidal nanoparticle system suspended in medium. Electrostatic repulsion among nanoparticles with same type of surface charge provides an extra stability (Liu *et al.*, 2010). Figure 4.3B show zeta potential obtained for diverse sets of experiments which vary between -26 to -30 mV, indicating good stability. In present work, variations in zeta potential with respect to different TDL do not present a significant statistical difference. Nanoparticle zeta potentials from previous works with similar polymer results in same kind of values (-28.0 mV) are reported (Liang *et al.*, 2011). Other similar works when positively charged polymers such as PEI 25 K or chitosan were being used, reported zeta potentials in range of 20 to 50 mV (Gaspar *et al.*, 2011; Benfer *et al.*, 2012).

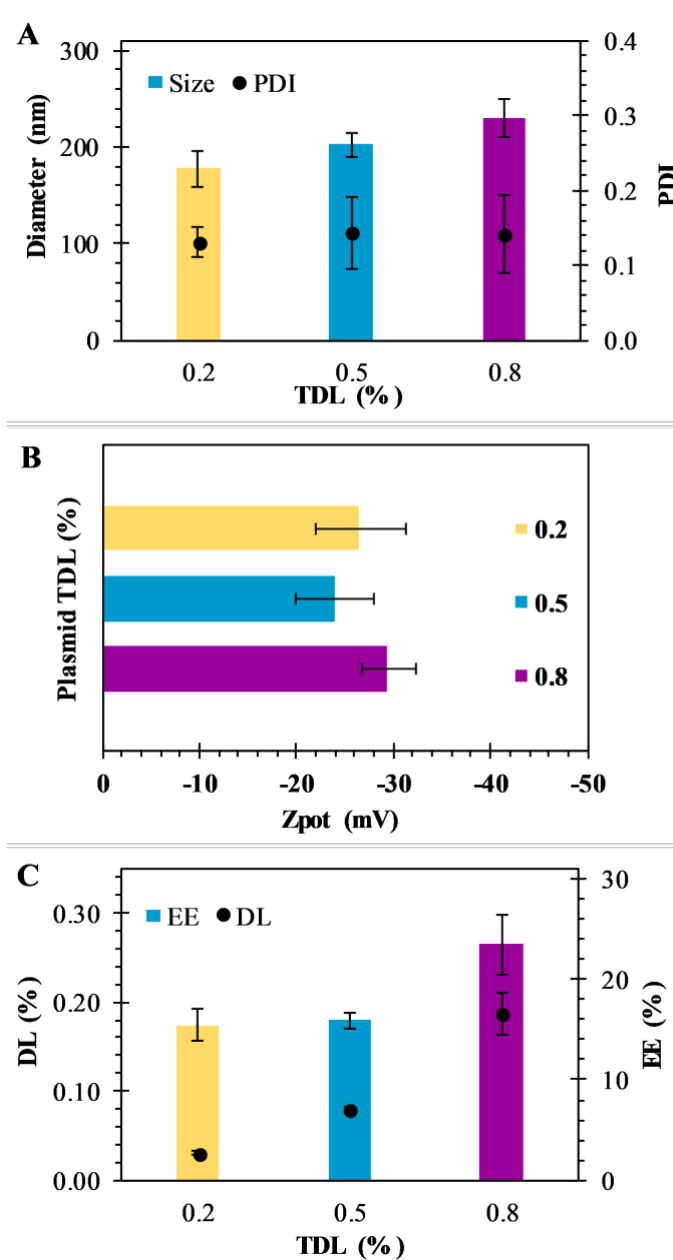


**Figure 4.3.** Characteristics of pDNA-NP prepared at different pVAX1-NH36 TDL. (A) Particle diameter and PDI; (B) zeta potentials; (C) EE and DL for different pVAX1-NH36 with TDL of 0.2 % (■), 0.5 % (■) and 0.8 % (■) were evaluated. Data represent

EE and DL are represented in Figure 4.3C. DL ranged between 0.03 to 0.19% as TDL increase. EE was 15.437%, 15.881% and 23.429% for corresponding TDL of 0.2%, 0.5% and 0.8%. This trend could be explained if the double emulsification process employed (W/O/W) in the preparation of nanoparticles is considered. After the first emulsification, plasmid is mostly in the

discontinuous phase (aqueous phase). In the second emulsification, some plasmid could migrate to the continuous water phase, decreasing the amount of plasmid that could be encapsulated. If the initial amount of plasmid used in the preparation is increased, then more plasmid could be retained in the water discontinuous phase, resulting in more plasmid physically entrapped into the nanoparticles, until some saturation point is reached. Comparing to other research reports, Wang et al. obtained an encapsulation efficiency of 53% in their experiments, but as previously noted, these experiments lead to larger particle size (Wang *et al.*, 1999). When encapsulating drugs such as cancer treatment medication, higher efficiencies can be achieved, as Esmaeili et al. reported an efficiency of 87.3% (Esmaeili *et al.*, 2008). Yoo et al. encapsulated an anticancer drug conjugated with PEG-FA with a drug loading efficiency of 97.2% (Yoo & Park, 2004b). Gaspar et al. performed plasmid encapsulation in chitosan and obtained a particle loading capacity of 51.2% with an encapsulation efficiency of over 75% (Gaspar *et al.*, 2011). Benfer et al. reported encapsulating plasmid using PEG-PEI polyplexes with PLGA with encapsulation efficiencies of 26.4-27.8% (Benfer *et al.*, 2012). Shi et al. obtained a drug load in range of 0.71-0.77% which led to 88-92% encapsulation efficiency when encapsulating a combination of cancer medication and plasmid DNA in porous PLGA nanoparticles and as of plasmid only, load was 0.036-0.041% with plasmid encapsulation efficiency of 36-40% (Shi *et al.*, 2014). It is noticeable that, higher efficiencies can be achieved during encapsulating medication in comparison with plasmid DNA, as negative charge of plasmid increase its encapsulation efficiency in PEI 25K (Benfer *et al.*, 2012; Shi *et al.*, 2014). However, PEI is non-degradable and molecular weight affects cytotoxicity and gene transfer activity; as high molecular weight PEI (PEI 25K) showed high transfection efficiency with significant cytotoxicity (Wen *et al.*, 2009). Although encapsulation efficiency obtained using PEI is larger, in this project polymers used in formulation of nanoparticles are degradable and/or not present cytotoxicity issues. The morphology of pDNA-PNP is smooth and spherical as confirmed by SEM and AFM images as shown in Figure 4.4, with particles size in range of 200-250 nm. Spherical morphology is congruent by other observations reported in literature for a similar system (Wang *et al.*, 1999; Liang *et al.*, 2011; Shi *et al.*, 2014).

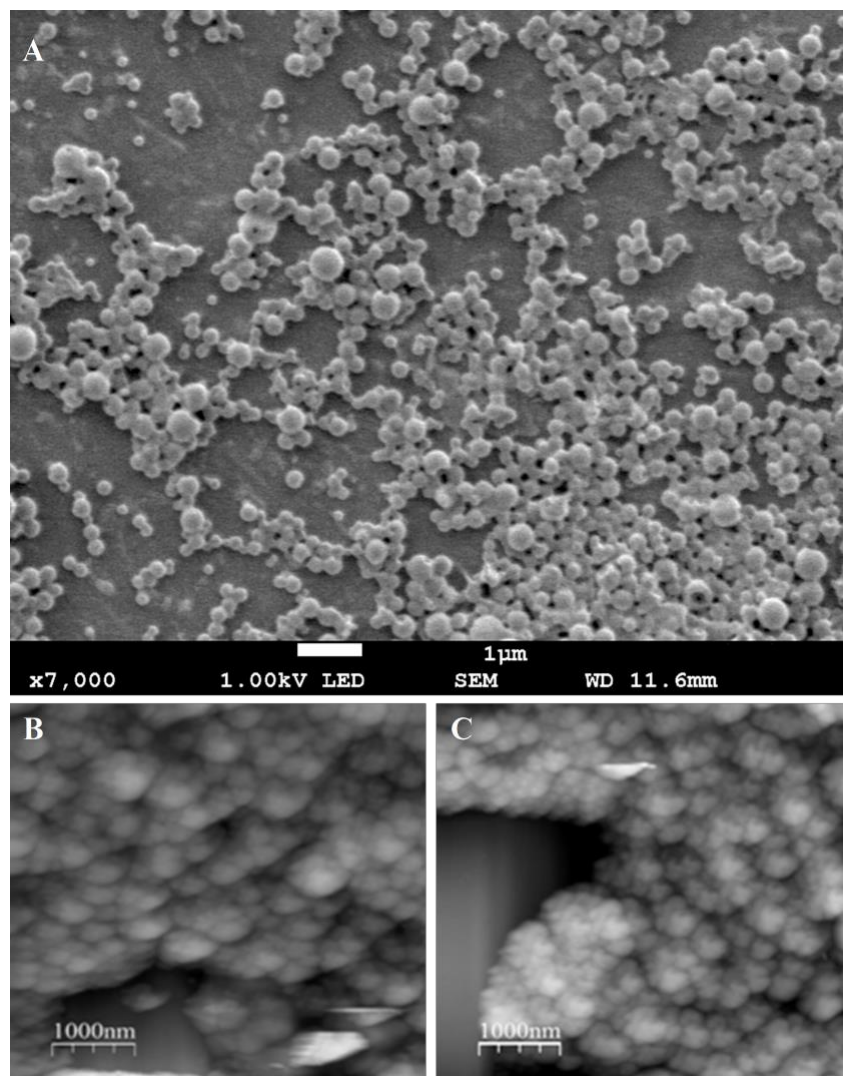


**Figure 4.4.** (A) SEM images of pDNA-NP with 0.8% TDL. AFM images of pDNA-NP with (B) 0.2% TDL, and (C) 0.5% TDL.

#### 4.4.4 Plasmid release analysis

In vitro release studies of pVAX1-NH36 from pDNA-PNP were performed with three different TDL used in preparations and are presented in Figure 4.5. During first days of study, initial burst rate was proportionally related to DL of pVAX1-NH36. Amounts of pVAX1-NH36 released in these initial burst stages were around 0.44, 1.88 and 10.39  $\mu\text{g}$  corresponding to 13, 22 and 55% for TDL of 0.2, 0.5 and 0.8% respectively. Since pVAX1-NH36 is hydrophilic in nature, we hypothesize that most of plasmid was encapsulated close to surface of nanoparticles, which could explain initial high rate of release by rapid dissolution of pVAX1-NH36 in release media. After initial burst stage, a slow release was observed for three TDL evaluated until a plateau was

reached indicating that all pVAX1-NH36 was released from pDNA-PNP. This retardation in release after initial burst could be explained by physical entrapment of pVAX1-NH36 and low rate of water penetration into nanoparticle. Plasmid is then slowly released by degradation-relaxation of PNP. In addition, PLGA PNP hydrolyzes promote water permeation and transport of plasmid in to media. Similar results have been presented by Shi et al. with an initial burst of 40% within first 4 hours of the study, followed by a slower release rate period of 7 days with a cumulative release of 60% after day 1 and 70% after day 3 (Shi *et al.*, 2014). The difference in release times could be attributed to porosity of particles. Likewise, Liang et al. observed same profile behavior with release of a drug from PLGA-PEG-FA nanoparticles with an initial burst release of 20% in first 2 hours followed by a cumulative release of 40% by next 12 hours and then a slow linear release until reach 80% at day 7 (Liang *et al.*, 2011).

Experimental pVAX1-NH36 release data was analyzed by a coupled model that incorporates initial burst as well as PNP degradation-relaxation (Eq. (3)). In general, an excellent fit of the proposed model with experimental profiles was obtained. Figure 4.5A, 4.5B and 4.5C show the release profiles of pVAX1-NH36 for TDL of 0.2%, 0.5% and 0.8%, where experimental data is represented by diamonds, squares and triangles in figures, respectively. For all cases, fitting of the model to experimental release was denoted by a solid line. Model parameters obtained by fitting are presented in Table 4.2. Burst constant decreases from 4.4513 to 3.6538 days<sup>-1</sup> when TDL increases from 0.2 to 0.5% and maintained in same range even though TDL increases up to 0.8%. Fraction of burst release increase proportionally with TDL, from 1.0587x10<sup>-8</sup> to 0.1914 and finally to 0.4977 for TDL of 0.2, 0.5 and 0.8% respectively. Degradation-relaxation constant increases from 0.2060 to 0.2792 days<sup>-1</sup> for 0.2 and 0.5% TDL followed by a decrease to 0.2439 days<sup>-1</sup> for 0.8% TDL. Time to achieve 50% of release was maintained in range of 12 to 15 days for all cases. As expected, fraction of PNP relaxation release behave in opposite way to fraction of burst release, decreasing from 0.9999 to 0.8086 to 0.5023 for TDL of 0.2, 0.5 and 0.8% respectively. The proposed model of release, presented in eq. (3), simultaneously considers the stages of initial burst and PNP degradation-relaxation. Therefore, depending on experimental data, the fraction values of burst ( $\theta_b$ ) or NP relaxation ( $\theta_r$ ) reflected contributions of each mechanism over the complete release profile. Values obtained with the model are within same range of others reported in literature for release of small molecules (ketoprofen, indomethacin, and coumarin-6) and macromolecules (human serum albumin, ovalbumin) (Corrigan & Li,

2009). Finally, resulted coefficients of determination for all fittings were greater than 0.99 and thus ensure the validity of present model.

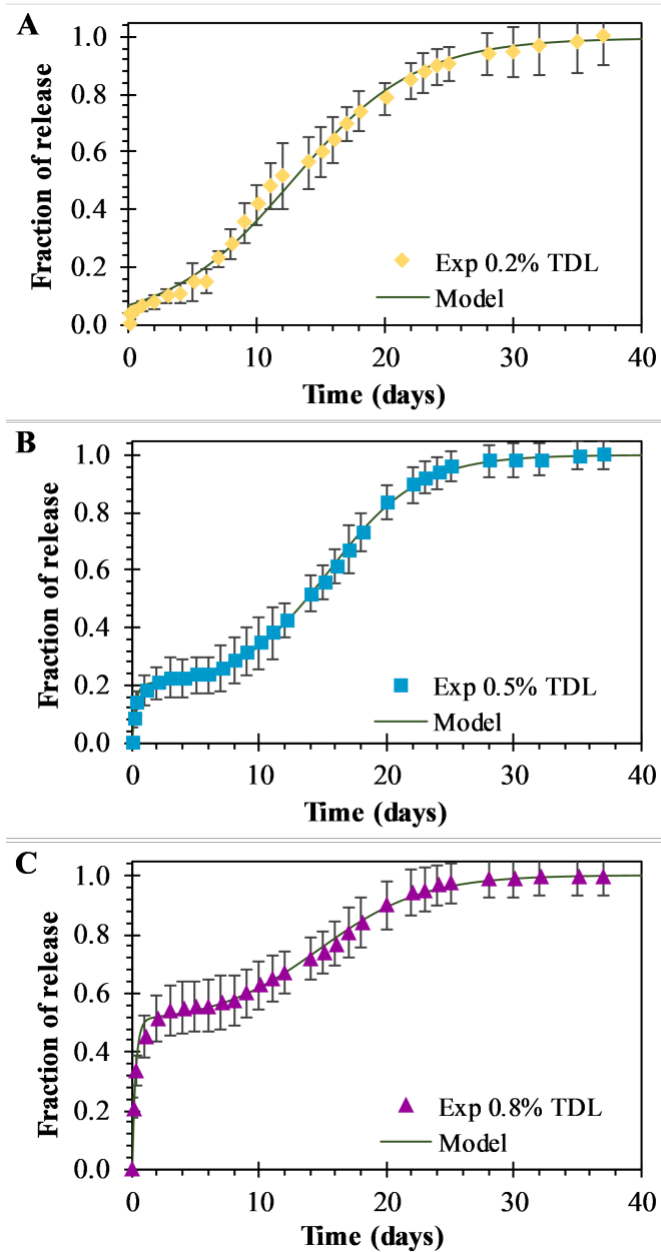


**Figure 4.5.** *In vitro* pVAX1-NH36 release profiles from pDNA-NP for TDL of 0.2 % (◆), 0.5 % (■) and 0.8 % (▲). Data represent mean ( $n = 3$ ).

**Table 4.2.** Parameters of plasmid pVax1-NH36 release from pDNA-NP. The parameters were determined and used in the mathematical development of the release model.

Parameters	Description	Unit	TDL (%)		
			0.2	0.5	0.8
$k_b$	Burst constant	$days^{-1}$	4.4513	3.6538	3.6722
$\theta_b$	Fraction of burst release	-	1.0587E-8	0.1914	0.4977
$k_r$	Degradation-relaxation constant	$days^{-1}$	0.2060	0.2792	0.2439
$t_{max}$	Time to achieve 50% of release	$days$	12.7481	15.4318	14.6954
$\theta_r$	Fraction of NP relaxation release	-	0.9999	0.8086	0.5023
$R^2$	Coefficient of determination	-	0.9961	0.9996	0.9969

#### 4.4.5 Plasmid purity and integrity

Figure 4.6 present gel electrophoresis image obtained from different samples of pVAX1-NH36 at different stages of nanoparticle preparation process. These samples were taken to verify initial purity of pVAX1-NH36 and also to evaluate its integrity towards nanoparticle preparation process. Future studies should include transfect *E. coli* with recovered pDNA and produce kanamycin resistance thus demonstrating that released pDNA remained functional. Figure 4.6 presents four channels, where the first one shows the size markers for plasmid over the range of 2,972–12,138 bp. Channel two presents initial pVAX1-NH36 solution used to formulate pDNA-PNP. This solution contains pVAX1-NH36 in its supercoiled form (band of 4,000 bp) and two relaxed isoforms. Channel three and four display samples obtained after pVAX1-NH36 was release from pDNA-PNP for two different batches prepared with 0.5 and 0.8% TDL respectively. Gel image showed single bands representing supercoiled and two relaxed forms of pVAX1-NH36 plasmid consistent with initial plasmid solution bands. Difference in brightness is due to difference of pVAX1-NH36 concentration in each sample. In accordance to electrophoresis gel, plasmid quality over encapsulation experiments was constant without any noticeable damage. Studies of integrity of pure pVAX1-NH36 in aqueous solution during the use of sonication at different potencies were performed and no plasmid damage was observed by using the technique of electrophoresis in agarose gel (data not showed in this work). Wang et al. thoroughly tested structural and functional integrity over sonication experiments and their results suggested that polymer (PLGA) protects plasmid DNA from directly affected by sheering due to high energy of

sonication (Wang *et al.*, 1999). Shi et al. verified plasmid integrity after performing electrophoresis gels confirming that plasmid was amenable to gene transfection (Shi *et al.*, 2014).

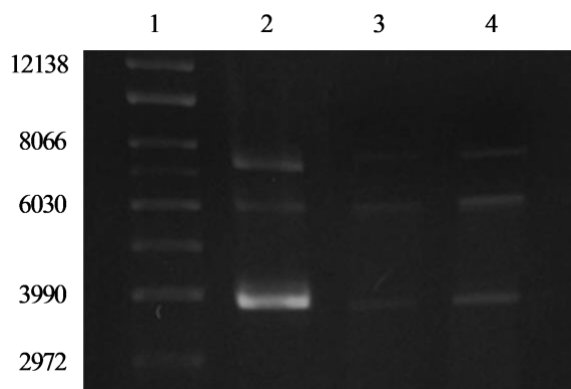


**Figure 4.6.** Agarose gel electrophoresis for pVAX1-NH36 before and after nanoparticle preparation. (1) Size marker for supercoiled plasmid form over the range 2 972 – 12 138 bp. (2) Initial pVAX1-NH36 solution used to formulate the pDNA-NP. (3) Sample acquired from 0.5 % TDL solution after pDNA-NP purification. (4) Sample obtained from 0.8 % TDL solution after pDNA-NP purification.

#### 4.5 Conclusion

PLGA-PEG-FA copolymer was successfully constructed by two conjugation steps and was characterized by FITR. Plasmid pVAX1-NH36 was propagated and efficiently encapsulated into modified polymer PLGA-PEG-FA nanoparticles. Size, polydispersity index, zeta potential, encapsulation efficiency and plasmid load of nanoparticles were determined. These results suggest that with an increase in TDL, diameter of pDNA-PNP, encapsulation efficiency and drug loading increase. However, zeta potential and PDI did not present significant statistical difference, suggesting stability of the particles. Experimental pVAX1-NH36 release profile show a multiphase behavior for all three TDL investigated. A mathematical analysis was introduced to describe experimental release profile by considering simultaneous contributions of initial burst and degradation-relaxation of PNP. Fitting of the release model against experimental data present an excellent correlation. This mathematical analysis could be used to describe and predict the release of plasmid DNA from biodegradable PNP. In addition, pVAX1-NH36 quality over encapsulation experiments was constant without any noticeable plasmid damage.

## CHAPTER 5. CONCLUSIONS

In this research, the preparation parameters for polymeric nanoparticles were evaluated, also, the encapsulation of MB and plasmids. Formulation parameters effects were evaluated for the emulsification and the nanoprecipitation techniques. Within the ranges of the study, in order to obtain smaller size nanoparticles, a low polymer concentration with a greater concentration of PVA, organic to aqueous ratio, sonication amplitude and evaporation speed is required. Injection speed did not affect the sizes and zeta potential of the PNP on the nanoprecipitation technique. The centrifugation speed during purification should be high in order to obtain better yields. Glucose resulted the better cryoprotectant, within the ones used, as it allows PNP to maintain its size and zeta potential through the freezing process.

A combined emulsification technique, consisting of the combination of the single and double emulsification technique was proposed. Size, PDI, zeta potential, MB loading and the encapsulation efficiency of nanoparticles were determined. Using the combined method of preparation resulted in more repeatable and uniform particle sizes. This technique could be used in the formulation of compounds with partial solubility, enabling a better drug loading and improving the physicochemical characteristics of the nanoparticles.

The release kinetics of MB from MB-PNP prepared with all the techniques were analyzed. This study suggest that the MB was encapsulated close to the surface of the nanoparticles. The release profile curve was analysed by considering a mathematical model describing simultaneous contribution of initial burst and diffusion of MB, this model was compared to the individual models. Results show that the initial burst constant and the effective diffusion coefficients are associated to the drug loading of MB in the nanoparticles. The model of the combination of both mechanisms of release describes more accurately the release phenomena than the individual models. This mathematical analysis could be used to describe and predict the release of compounds with intermediate to high solubility from biodegradable nanoparticles.

The photoactivation of MB was explored in aqueous solution and in BEAS-2B cell line. Increments of ROS produced by MB photoactivation are directly related to BEAS-2B cell survival, possibly due to oxidative stress caused on the cells. Production of ROS could be adjusted by modifying MB concentration or the energy fluence. This study suggests that BEAS-

2B cells are more resistant to ROS than cancerous cells, therefore, for PDT of lung cancer, selective cell damage could be achieved.

Plasmid DNA was propagated, purified and efficiently encapsulated in PLGA modified with PEG and FA using the double emulsification technique. Size, PDI, zeta potential, encapsulation efficiency and plasmid loading in nanoparticles were obtained. According to these results, the TDL is proportional to the diameter of the pDNA-PNP, the encapsulation efficiency and the drug loading. Zeta potential and PDI did not presented statistical differences among the different experiments, indicating the stability of the particles. The release study of pDNA from pDNA-PNP presented a multiphase behavior for all three TDL investigated. A mathematical model to predict the release of plasmid DNA was proposed, this model simultaneously accounts for the initial burst and the degradation-relaxation of the nanoparticles mechanisms of release. Fitting of the release model against experimental data present an excellent correlation. This mathematical analysis could be used to describe and predict the release of plasmid DNA from biodegradable PNP. pDNA quality over encapsulation experiments was constant without any noticeable plasmid damage.

In addition, a plasmid containing a GFP gene was encapsulated effectively using PLGA modified with Rh by the double emulsification technique. The *in vitro* release study showed a one-phase release profile over 10-days. H441 cells were treated with pGFP-PNP presenting expression of pGFP, indicating successful uptake and functionality of pGFP after the encapsulation process. Plasmid was encapsulated successfully without losing integrity or functionality.

It is recommended for the future to pursue the research on MB and its application with photodynamic therapies. More experiments with MB and MB-PNP on different cell lines is necessary to obtain further information and then being able on extending this for animal studies.

Since Encapsulation of plasmid DNA has been proven feasible, the pVAX1-NH36 could be tried in different animal models to pursue the formulation of a vaccine against leishmaniasis. Also, different plasmids for gene therapy or vaccinations could be used in further cell and animal studies.

## **APPENDIX A. PHOTOACTIVATION OF METHYLENE BLUE IN BEAS-2B LUNG EPITHELIAL CELLS GENERATES ROS AND COMPROMISES CELL SURVIVAL**

### **A.1 Abstract**

The present studies were conducted to examine the relationship between reactive oxygen species (ROS) generation upon photoactivation of methylene blue (MB) and BEAS-2B cell survival. Initial studies focused on ROS production following laser stimulation of aqueous-dimethyl sulfoxide solutions of MB using 1,3-diphenylisobenzofuran as a probe. We subsequently measured ROS formation and cellular viability of cultured BEAS-2B cells using 2',7'-dichlorodihydrofluorescein diacetate and the MTT assay, respectively. MB alone induced oxidative stress in BEAS-2B cells, with a half maximal inhibitory concentration (IC<sub>50</sub>) of 64 $\mu$ M. MB concentrations below 31.26 $\mu$ M did not induce detectable adverse effects in BEAS-2B cells in the range of energy fluences studied. IC<sub>50</sub> values of MB for radiation fluences of 6J/cm<sup>2</sup>, 18J/cm<sup>2</sup>, and 36J/cm<sup>2</sup> were 55 $\mu$ M, 49 $\mu$ M, and 48 $\mu$ M, respectively. These values were comparable to those of controls and associated with increments in ROS production of 23%, 27%, and 33%, correspondingly. Results suggest that BEAS-2B cells are more resistant to ROS than some cancerous cell lines reported in literature.

### **A.2. Background**

Research in photodynamic therapy (PDT) has been increasing as an alternative and promising non-invasive treatment for cancer and non-cancer diseases. MB has been of great interest in PDT due to its ability to absorb light intensively within the therapeutic window, and upon radiation, it damages biomolecules by producing reactive oxygen species (ROS) (Tardivo *et al.*, 2005). ROS are involved in several biological functions, but when overproduced, the oxidation of biomolecules can cause oxidative stress, hence creating oxidative damage that could cause cell

death (Gomes *et al.*, 2005). Fluorescent probes could be used to detect and measure ROS production in solutions and cells (Gomes *et al.*, 2005; Kolarova *et al.*, 2007; He *et al.*, 2009; Rastogi *et al.*, 2010; Aranda *et al.*, 2013; Deprá de Souza *et al.*, 2016).

### **A.3. Aims**

Production of ROS induced by photoactivation of MB and the human immortalized bronchial epithelial cell (BEAS-2B) survival were compared. 1,3-diphenylisobenzofuran (DPBF) and 2',7'-dichlorodihydrofluorescein diacetate (HDCF-DA) were used as probes for aqueous-solutions and cell-cultures, respectively. Cytotoxic effects of MB irradiated on BEAS-2B cells were analyzed by thiazolyl blue tetrazolium bromide (MTT).

### **A.4. Materials and Methods**

#### **A.4.1. DFBP Probe**

Aqueous-DMSO solutions of DPBF (Sigma) and MB (Química Suastes) were prepared at concentrations of 50  $\mu\text{M}$  of DPBF and 6.25  $\mu\text{M}$  or 31.26  $\mu\text{M}$  of MB. Samples were irradiated every 2 s with an energy fluence of 0.2J/cm<sup>2</sup> using a red laser (660nm, 100mW). UV/VIS absorption spectrums were collected with a Genesis 10S spectrophotometer (Thermo Scientific).

#### **A.4.2. Cell culture**

BEAS-2B cells were cultured in LHC-9 serum-free media (Gibco, Life Technologies) and incubated at 37 °C in a 5% CO<sub>2</sub> environment. Cells were seeded (1.7×10<sup>4</sup> cells/well) on 96-well plates 24 hours prior to experimentation. Cells were treated with MB solution in media at different concentrations (0-156  $\mu\text{M}$ ), and incubated for 3 hours. Then, media was removed and cells were washed three times, two with Dulbecco's phosphate-buffered saline (Gibco, Life Technologies) and one time with media.

#### **A.4.3. *In vitro* PDT treatment and cell survival**

Fresh LCH-9 media was added to cell cultures for PDT treatment (Lam *et al.*, 2001; Mellish *et al.*, 2002; Teichert *et al.*, 2002). Then, BEAS-2B cells were irradiated with energy fluences

ranging between 0 and 36 J/cm<sup>2</sup>. After 36 hours of incubation, a MTT assay was carried to obtain BEAS-2B cell survival (Mellish *et al.*, 2002; Klepac-Ceraj *et al.*, 2011; Van Meerloo *et al.*, 2011).

#### **A.4.4. Determination of intracellular ROS**

BEAS-2B cells were cultured as described in section 3.2. BEAS-2B were treated with HDFC-DA (Biotium) at a final concentration of 5  $\mu$ M. Cells were incubated at 37°C for 40 min followed by *in vitro* PDT treatment as described in section 3.3. Two hours after PDT treatment, fluorescence intensity was quantified by excitation at 485 nm and emission at 528 nm using BioTek.

#### **A.5. Results and Discussion**

ROS production by MB photoactivation in aqueous-DMSO solutions was verified following the DPBF absorbance decay at 417 nm, as presented in Fig. A.1A and Fig. A.1C. These decay is caused by ROS produced in the form of singlet oxygen. DPBF absorbance peak was maintained constant in solutions free of MB and irradiated (results not shown here), confirming that irradiation by itself do not produce ROS in the range of fluences studied. When MB was applied, a proportionality between DPBF absorbance decay and the irradiation time was observed, similar to other studies (Tardivo *et al.*, 2005; Craig *et al.*, 2015). These proportionalities are presented in Fig. 1B and Fig. 1D for MB concentrations of 6.25  $\mu$ M and 31.26  $\mu$ M, respectively. These figures were plotted by considering a first order decay of DPBF (Bonacin *et al.*, 2009; Zhang & Li, 2011; Craig *et al.*, 2015; Deprá de Souza *et al.*, 2016). DPBF decay constants were 0.25 s<sup>-1</sup> and 0.17 s<sup>-1</sup> for the respective concentrations of MB of 6.25  $\mu$ M and 31.26  $\mu$ M. These values are proportional to the ROS generation for each experiment, it is noted that for less concentration of MB, more ROS were produced. This effect could be explained by the formation of dimers, that are less effective generators of ROS (Tardivo *et al.*, 2005; Craig *et al.*, 2015). Also, MB absorbance peak at 665nm decay with the irradiation time, as could be observed in Fig. A.1A and A.1C. These decay could be attributed to a degree of aggregation of MB, also confirming the presence of dimers (Tardivo *et al.*, 2005; Blázquez-Castro *et al.*, 2009).

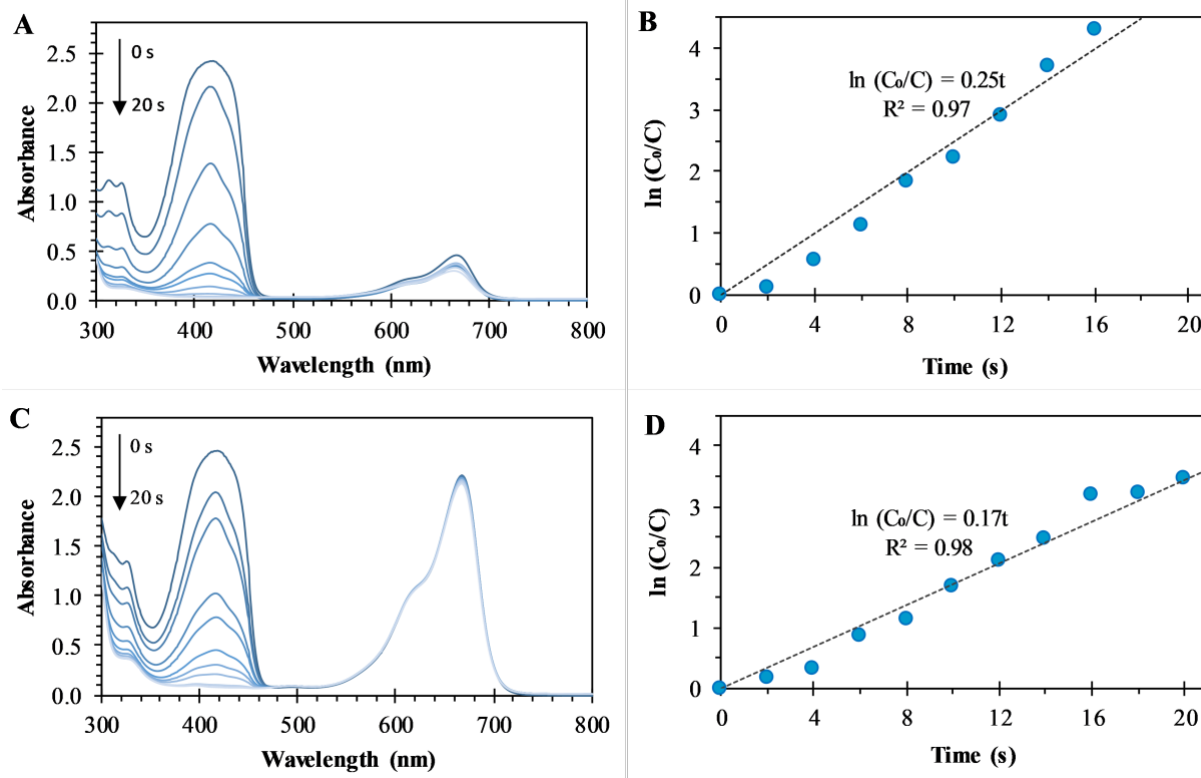


**Figure A.5.1.** DPBF decay after irradiation in the presence of 6.25 μM MB (A) or 31.26 μM MB (C). Proportionality between DPBF absorbance decay and irradiation time in the presence of 6.25 μM of MB (B) and 31.26 μM of MB (D).

ROS produced in BEAS-2B cells were measured by their reaction with DCFH-DA, generating the fluorescent molecule 2,7-dichlorofluorescein (DCF). Fig. A.2A shows a DCF fluorescence increments for different concentrations of MB and different energy fluences. ROS are produced in BEAS-2B cells with no MB and no irradiation. This effect could be attributed to some oxidative stress caused by the cell culture process itself, facilitating the generation of reactive species (Halliwell & Whiteman, 2004). MB in BEAS-2B cells not irradiated produces increments in the oxidative stress, compared with BEAS-2B cells with no MB. However, BEAS-2B cells with MB and laser irradiation produce higher amounts of ROS. Increments in the concentration of MB and energy fluences yield to proportional increments in the ROS produced, within the range studied. BEAS-2B cell survival at different MB concentrations and different energy fluences are presented in Fig. A.2B. No cytotoxic effects on BEAS-2B cells at concentrations up to 31.26 μM of MB and the different energy fluences analyzed were observed. BEAS-2B cell survival decrements were observed at concentrations above 31.26 μM of MB

without irradiation, with a half maximal inhibitory concentration (IC<sub>50</sub>) of 64  $\mu$ M. BEAS-2B cell survival in the presence of MB and irradiation at energy fluences of 6 J/cm<sup>2</sup>, 18 J/cm<sup>2</sup>, and 36 J/cm<sup>2</sup>, resulted in values of IC<sub>50</sub> of 55  $\mu$ M, 49  $\mu$ M, and 48  $\mu$ M, respectively. To reach these IC<sub>50</sub> values, an increase of ROS of 23%, 27%, and 33% with respect to the controls for the respective energy fluences were needed. These results indicate that by increasing the energy fluence, less concentration of MB is required to produce the same amount of ROS (Tardivo *et al.*, 2005). PDT using MB have been reported on CHO cells (McCaughan *et al.*, 2011), RIF-1 murine fibrosarcoma cells (Mellish *et al.*, 2002), B16F1 tumor cells (Cheng *et al.*, 2008), and HeLa tumor cells (Lu *et al.*, 2008). Results for CHO cells are similar to the results obtained in this work with BEAS-2B cells. However, BEAS-2B cells are more resistant to PDT with MB than cancerous cells, where higher cytotoxicity values of MB are reported (Kirsztberg *et al.*, 2005).

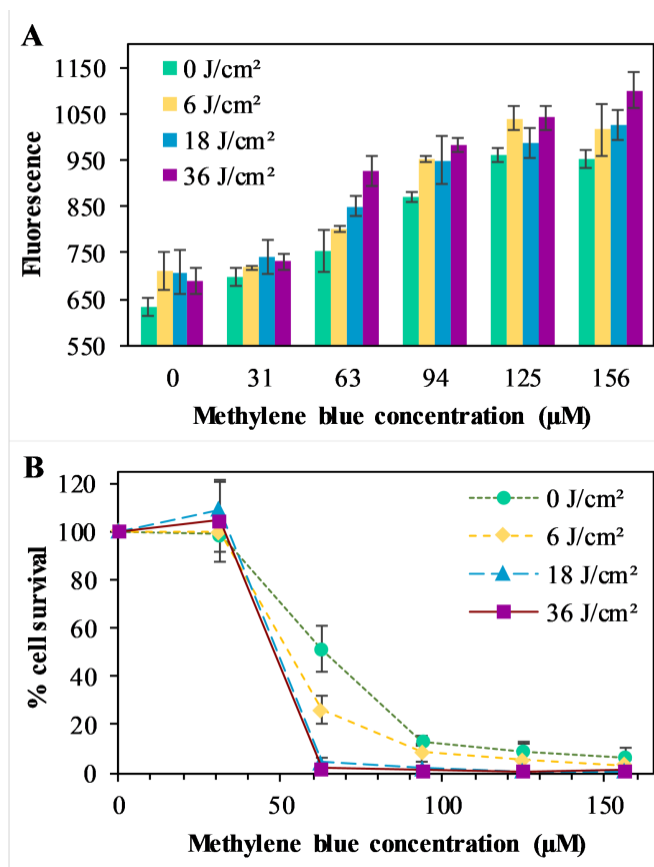


**Figure A.5.2.** (A) ROS production in cells detected by the chemical probe HDFC-DA and (B) cell viability after treatment with MB concentrations ranging from 0 to 156 $\mu$ M in combination with energy fluences of 0J/cm<sup>2</sup> (■), 6J/cm<sup>2</sup> (■), 18J/cm<sup>2</sup> (■), and 36J/cm<sup>2</sup> (■). Data represent the mean with standard deviation for --- replicates?? (n = 3).

## A.6. Conclusions

Several authors have reported the *in vitro* action of MB in PDT for different cell lines. To the best of our knowledge, no data are available on the efficacy of this therapy against BEAS-2B cell lines. Increments of ROS produced by MB photoactivation are directly related to BEAS-2B cell survival. Results suggest that oxidative stress caused by ROS could be adjusted by modifying MB concentration or the energy fluence. Within the results obtained we observed that concentrations above 31  $\mu\text{M}$  of MB are required to produce cellular damage. These dosages are greater to the ones reported in literature for cancerous cells. Therefore, for PDT of lung cancer, selective cell damage could be achieved.

## **APPENDIX B. CELLULAR UPTAKE OF PLGA NANOPARTICLES LOADED WITH PDNA AND GFP PROTEIN EXPRESSION IN H441 CELLS**

### **B.1 Abstract**

Administration of therapeutic agents to cells is more effective delivery vehicles or nanocarriers are used. These nanocarriers can be structured as nanoparticles with specific characteristics and a variety of materials. One of the most successful materials used for gene delivery is PLGA. Coupling of rhodamine and PLGA (PLGA-Rh) facilitates the microscopic visualization of polymeric nanoparticles (PNP). Plasmid DNA containing green fluorescent protein (pGFP) was encapsulated in PLGA-Rh nanoparticles without losing integrity. PLGA-Rh nanoparticles loaded with pGFP (pGFP-PNP) were prepared by using double emulsification-solvent evaporation technique. PLGA-Rh synthesis was verified by FT-IR. Blank nanoparticles (PLGA-Rh PNP) were also prepared, resulting in 125 nm average diameter and displaying zeta potential of -38 mV. An increase in size was observed for pGFP-PNP of 164 nm, and zeta potentials of -49 mV, suggesting successful encapsulation of pGFP. *In vitro* release studies confirmed a single-release profile for the duration of 10-days. GFP expression is seen in H441 transfected with naked plasmid and with pDNA-PNP, confirming the functionality of pGFP.

### **B.2 Introduction**

The use of nanodevices for medical applications is one of the most promising technologies of the last 50 years, when the first nanoparticles were developed for drug delivery and vaccination purposes (Kreuter, 2007b). In gene therapy, nanodevices such as polymeric nanoparticles can protect the integrity of the plasmid DNA from undesirable interactions with other organ tissue, also the use of this nanodevices can allow effective control of the release of this compounds (Peer *et al.*, 2007; Danhier *et al.*, 2012; Gutiérrez-Valenzuela *et al.*, 2016). PLGA has been used in the encapsulation of plasmid DNA (Wang *et al.*, 1999). One of the advantages of PLGA is that it contains uncapped carboxylic acids that can be easily functionalized with other molecules before or after nanoparticles preparation (Gutiérrez-Valenzuela *et al.*, 2016). Coupling of

fluorescent dyes such as rhodamine can be used to perform *in vitro* microscopic visualization (Yang *et al.*, 2006). Polymeric nanoparticles loaded with a plasmid containing the green fluorescent protein gene (pGFP-PNP) were prepared by using the double emulsification-solvent evaporation technique.

### **B.3. Methods**

Plasmid pGFP of 7415 bp was used for these studies. It was replicated using *E. coli* bacteria as a guest in a fermentation process and purified to obtain a pure plasmid. Polymer modifications were performed to obtain PLGA-Rh for labeling purposes. These polymer modifications were verified by using FT-IR. pGFP-PNP were prepared using emulsification-solvent evaporation technique (Gutiérrez-Valenzuela *et al.*, 2016). Particles were purified and freeze-dried. H-441 cells were treated with naked plasmid (using lipofectamine) and with pDNA-PNP for 24 hours. H441 cells were imaged live for GFP fluorescence at 40X magnification using Axiovision inverted microscope 48 hours after treatment.

### **B.4. Results**

Nanoparticles loaded with plasmid pGFP were prepared. Size obtained for PLGA-Rh PNP was 124.5 nm with PDI of 0.022 and zeta potential of -37.9 mV. pGFP-PNP size were 163.7 nm with polydispersity of 0.024 and zeta potential of -48.8 mV. The increment in the size and specially a decrease in zeta potential reflect the presence of pGFP in the nanoparticle. These results are consistent with other works with encapsulated pDNA (Gutiérrez-Valenzuela *et al.*, 2016). A drug loading of 0.08% with encapsulation efficiency (EE) of 10.8% was obtained. *In vitro* release studies for pGFP-PNP were performed (Fig. B.1), a one-phase release can be appreciated over the first 10 days of release suggesting a diffusion mechanism of release. As can be seen in Fig. B.2, GFP expression is seen in H441 cells transfected with naked plasmid and those incubated with pGFP-PNP (Figure B.2, column 3). However, rhodamine label and co-localization with GFP is only seen in cells incubated with pGFP-PNP confirming successful uptake and expression of pGFP (Figure B.2, row 2).

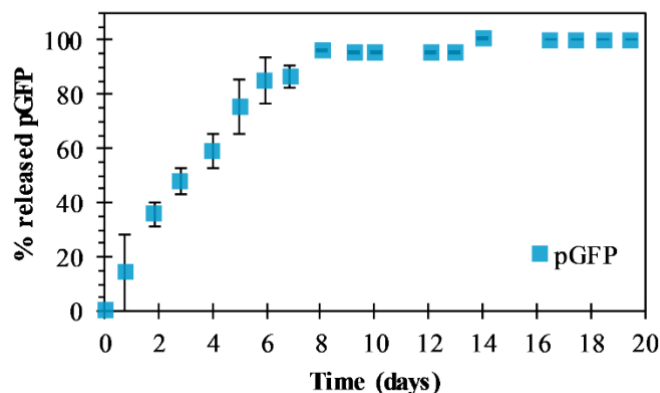


**Figure B.1.** *In vitro* release kinetics of pGFP-PNP.

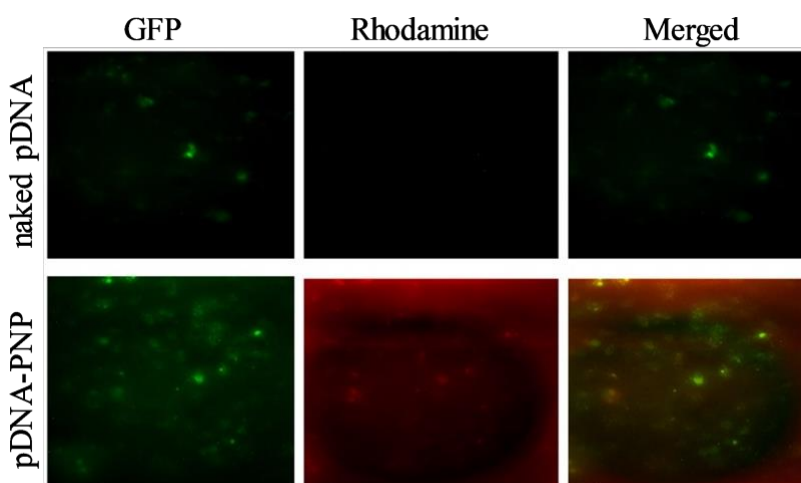


**Figure B.2.** Comparison of internalization between naked and encapsulated plasmid

## B.6. Conclusions

pGFP-PNP characterization showed an average size of 164 nm with a zeta potential of -49 mV. Values obtained for PLGA-Rh PNP were of 125 nm and -38 mV. The increase in size and decrease of zeta potential reflect the presence of pGFP in the nanoparticle. Drug loading obtained was 0.08% with an encapsulation efficiency of 10.4%. An *in vitro* evaluation of drug release kinetics showed a one-phase release profile over 10-days. H441 cells treated with pGFP-PNP displayed expression of pGFP, indicating successful uptake and functionality of pGFP after the encapsulation process. Plasmid was encapsulated successfully without losing integrity or functionality.

## CHAPTER 6. REFERENCES

- Abdelwahed, W., Degobert, G., Stainmesse, S. & Fessi, H. (2006) Freeze-drying of nanoparticles: Formulation, process and storage considerations. *Advanced Drug Delivery Reviews*, **58**, 1688–1713.
- Aranda, A., Sequedo, L., Tolosa, L., Quintas, G., Burello, E., Castell, J. V. & Gombau, L. (2013) Dichloro-dihydro-fluorescein diacetate (DCFH-DA) assay: A quantitative method for oxidative stress assessment of nanoparticle-treated cells. *Toxicology in Vitro*, **27**, 954–963.
- Arica, B. & Lamprecht, A. (2005) In Vitro Evaluation of Betamethasone-Loaded Nanoparticles. *Drug Development and Industrial Pharmacy*, **31**, 19–24.
- Astete, C.E., Kumar, C.S.S.R. & Sabliov, C.M. (2007) Size control of poly(d,l-lactide-co-glycolide) and poly(d,l-lactide-co-glycolide)-magnetite nanoparticles synthesized by emulsion evaporation technique. *Colloids and Surfaces A: Physicochemical and Engineering Aspects*, **299**, 209–216.
- Astete, C.E.F. & Sabliov, C.M. (2006) Synthesis and characterization of PLGA nanoparticles. *J. Biomater. Sci. Polym. Ed.*, **17**, 247–289.
- Basto, P.A. (Pamela A. (2013) Development of polymeric nanoparticle vaccines for immunostimulation. Massachusetts Institute of Technology.
- Batycky, R.P., Hanes, J., Langer, R. & Edwards, D.A. (1997) A theoretical model of erosion and macromolecular drug release from biodegrading microspheres. *Journal of Pharmaceutical Sciences*, **86**, 1464–77.
- Bechet, D., Couleaud, P., Frochet, C., Viriot, M.-L., Guillemin, F. & Barberi-Heyob, M. (2008) Nanoparticles as vehicles for delivery of photodynamic therapy agents. *Trends in Biotechnology*, **26**, 612–21.
- Benfer, M., Reul, R., Betz, T. & Kissel, T. (2012) Folic acid-decorated nanocomposites prepared by a simple solvent displacement method. *Macromolecular bioscience*, **12**, 438–45.
- Bilati, U., Allémann, E. & Doelker, E. (2005) Development of a nanoprecipitation method intended for the entrapment of hydrophilic drugs into nanoparticles. *European Journal of Pharmaceutical Sciences*, **24**, 67–75.
- Blázquez-Castro, A., Stockert, J.C., Sanz-Rodríguez, F., Zamarrón, A. & Juarranz, A. (2009)

- Differential photodynamic response of cultured cells to methylene blue and toluidine blue: role of dark redox processes. *Photochemical & Photobiological Sciences*, **8**, 371–6.
- Boddu, S.H.S. & Vaishya, R. (2012) Preparation and characterization of folate conjugated nanoparticles of doxorubicin using PLGA-PEG-FOL polymer. *Medicinal Chemistry*, **2**, 068–075.
- Boisseau, P. & Loubaton, B. (2011a) Nanomedicine, nanotechnology in medicine. *Comptes Rendus Physique*, **12**, 620–636.
- Boisseau, P. & Loubaton, B. (2011b) Nanomedicine, nanotechnology in medicine. *Comptes Rendus Physique*, **12**, 620–636.
- Bonacin, J., Engelmann, F., Severino, D., Toma, H. & Baptista, M. (2009) Singlet Oxygen Quantum Yields ( $\phi$ ) in Water using Beetroot Extract and an Array of LEDs. *Journal of the Brazilian Chemical Society*, **20**, 31–36.
- Budhian, A., Siegel, S.J. & Winey, K.I. (2007) Haloperidol-loaded PLGA nanoparticles: Systematic study of particle size and drug content. *International Journal of Pharmaceutics*, **336**, 367–375.
- Cannavà, C., Stancanelli, R., Marabeti, M.R., Venuti, V., Cascio, C., Guarneri, P., Bongiorno, C., Sortino, G., Majolino, D., Mazzaglia, A., Tommasini, S. & Ventura, C.A. (2016) Nanospheres based on PLGA/amphiphilic cyclodextrin assemblies as potential enhancers of Methylene Blue neuroprotective effect. *RSC Advances*, **6**, 16720–16729. The Royal Society of Chemistry.
- Chalé-balboa, W.G., Mut-Martin, M., Ramirez-Sierra, M.J., Garcia-Miss, M.R. & Dumonteil, E. (2009) A combination DNA vaccine encoding nucleoside hydrolase 36 and glycoproteine 63 protects female but not male hamsters against *Leishmania mexicana*. *Parasite*, **16**, 227–230. EDP Sciences.
- Chavanpatil, M.D., Khdair, A., Patil, Y., Handa, H., Mao, G. & Panyam, J. (2007) Polymer-surfactant nanoparticles for sustained release of water-soluble drugs. *Pharmaceutical Nanotechnology*, **96**, 3379–3389.
- Cheng, F.Y., Wang, S.P.H., Su, C.H., Tsai, T.L., Wu, P.C., Shieh, D. Bin, Chen, J.H., Hsieh, P.C.H. & Yeh, C.S. (2008) Stabilizer-free poly(lactide-co-glycolide) nanoparticles for multimodal biomedical probes. *Biomaterials*, **29**, 2104–2112.
- Cho, K., Wang, X., Nie, S., Chen, Z.G. & Shin, D.M. (2008) Therapeutic nanoparticles for drug

- delivery in cancer. *Clinical Cancer Research: an official journal of the American Association for Cancer Research*, **14**, 1310–1316.
- Chorny, M., Fishbein, I., Danenberg, H.D. & Golomb, G. (2002) Lipophilic drug loaded nanospheres prepared by nanoprecipitation: effect of formulation variables on size, drug recovery and release kinetics. *Journal of Controlled Release*, **83**, 389–400.
- Choy, J.-H., Jung, J.-S., Oh, J.-M., Park, M., Jeong, J., Kang, Y.-K. & Han, O.-J. (2004) Layered double hydroxide as an efficient drug reservoir for folate derivatives. *Biomaterials*, **25**, 3059–64.
- Cohen-Sela, E., Chorny, M., Koroukhov, N., Danenberg, H.D. & Golomb, G. (2009) A new double emulsion solvent diffusion technique for encapsulating hydrophilic molecules in PLGA nanoparticles. *Journal of Controlled Release*, **133**, 90–5. Elsevier B.V.
- Corrigan, O.I. & Li, X. (2009) Quantifying drug release from PLGA nanoparticulates. *European Journal of Pharmaceutical Sciences*, **37**, 477–485.
- Costa, P. & Sousa Lobo, J.M. (2001) Modeling and comparison of dissolution profiles. *European Journal of Pharmaceutical Sciences*, **13**, 123–33.
- Craig, R.A., McCoy, C.P., De Baróid, Á.T., Andrews, G.P., Gorman, S.P. & Jones, D.S. (2015) Quantification of singlet oxygen generation from photodynamic hydrogels. *Reactive and Functional Polymers*, **87**, 1–6.
- Danhier, F., Ansorena, E., Silva, J.M., Coco, R., Le Breton, A. & Préat, V. (2012) PLGA-based nanoparticles: An overview of biomedical applications. *Journal of Controlled Release*, **161**, 505–522. Elsevier B.V.
- Darabpour, E., Kashef, N. & Mashayekhan, S. (2016) Chitosan nanoparticles enhance the efficiency of methylene blue-mediated antimicrobial photodynamic inactivation of bacterial biofilms: An in vitro study. *Photodiagnosis and Photodynamic Therapy*, **14**, 211–217.
- Deprá de Souza, T., Ziembowicz, F.I., Muller, D.F., Lauermann, S.C., Kloster, C.L., Vianna Santos, R.C., Soares Lopes, L.Q., Ferreira Ourique, A., MacHado, G. & Villetti, M.A. (2016) Evaluation of photodynamic activity, photostability and in vitro drug release of zinc phthalocyanine-loaded nanocapsules. *European Journal of Pharmaceutical Sciences*, **83**, 88–98. Elsevier B.V.
- Dhar, S., Gu, F.X., Langer, R., Farokhzad, O.C. & Lippard, S.J. (2008) Targeted delivery of cisplatin to prostate cancer cells by aptamer functionalized Pt(IV) prodrug-PLGA-PEG

- nanoparticles. *Proceedings of the National Academy of Sciences of the United States of America*, **105**, 17356–17361.
- Diogo, M.M., Queiroz, J.A. & Prazeres, D.M.F. (2003) Assessment of purity and quantification of plasmid DNA in process solutions using high-performance hydrophobic interaction chromatography. *Journal of chromatography. A*, **998**, 109–17.
- Dumonteil, E. (2003) DNA vaccines induce partial protection against *Leishmania mexicana*. *Vaccine*, **21**, 2161–2168.
- Dunne, M., Corrigan, I. & Ramtoola, Z. (2000) Influence of particle size and dissolution conditions on the degradation properties of polylactide-co-glycolide particles. *Biomaterials*, **21**, 1659–68.
- Esmaeili, F., Ghahremani, M.H., Ostad, S.N., Atyabi, F., Seyedabadi, M., Malekshahi, M.R., Amini, M. & Dinarvand, R. (2008) Folate-receptor-targeted delivery of docetaxel nanoparticles prepared by PLGA-PEG-folate conjugate. *Journal of drug targeting*, **16**, 415–423.
- European Technology Platform on NanoMedicine. (2005) Vision Paper and Basis for a Strategic Research Agenda for NanoMedicine. Belgium.
- Feczko, T., Tóth, J., Dósa, G. & Gyenis, J. (2011) Influence of process conditions on the mean size of PLGA nanoparticles. *Chemical Engineering and Processing: Process Intensification*, **50**, 846–853.
- Fioramonti Calixto, G., Bernegossi, J., Freitas, L.M. de, Fontana, C.R. & Chorilli, M. (2016) Nanotechnology-Based Drug Delivery Systems for Photodynamic Therapy of Cancer: A Review. *Molecules*, **21**.
- Fitzgerald, J.F. & Corrigan, O.I. (1993) Mechanisms governing drug release from poly- $\alpha$ -hydroxy aliphatic esters. Diltiazem base release from poly-lactide-co-glycolide delivery systems. Pp. 311–326 in: *Polymeric Delivery Systems*.
- Fredenberg, S., Wahlgren, M., Reslow, M. & Axelsson, A. (2011) The mechanisms of drug release in poly(lactic-co-glycolic acid)-based drug delivery systems-a review. *International Journal of Pharmaceutics*, **415**, 34–52.
- Freitas, S., Merkle, H.P. & Gander, B. (2004) Microencapsulation by solvent extraction/evaporation: reviewing the state of the art of microsphere preparation process technology.

- Gamboa-León, R., Paraguai de Souza, E., Borja-Cabrera, G.P., Santos, F.N., Myashiro, L.M., Pinheiro, R.O., Dumonteil, E. & Palatnik-de-Sousa, C.B. (2006) Immunotherapy against visceral leishmaniasis with the nucleoside hydrolase-DNA vaccine of *Leishmania donovani*. *Vaccine*, **24**, 4863–73.
- Gaspar, V.M., Correia, I.J., Sousa, A., Silva, F., Paquete, C.M., Queiroz, J.A. & Sousa, F. (2011) Nanoparticle mediated delivery of pure P53 supercoiled plasmid DNA for gene therapy. *Journal of Controlled Release*, **156**, 212–22.
- Ghitman, J., Stan, R. & Iovu, H. (2017) Experimental contributions in the synthesis of plga nanoparticles with excellent properties for drug delivery: Investigation of key parameters. *UPB Scientific Bulletin, Series B: Chemistry and Materials Science*, **79**, 101–112.
- Gomes, A., Fernandes, E. & Lima, J.L.F.C. (2005) Fluorescence probes used for detection of reactive oxygen species. *Journal of Biochemical and Biophysical Methods*, **65**, 45–80.
- Govender, T., Stolnik, S., Garnett, M.C., Illum, L. & Davis, S.S. (1999) PLGA nanoparticles prepared by nanoprecipitation: drug loading and release studies of a water soluble drug. *Journal of Controlled Release*, **57**, 171–185.
- Grazia Cascone, M., Zhu, Z., Borselli, F. & Lazzeri, L. (2002) Poly(vinyl alcohol) hydrogels as hydrophilic matrices for the release of lipophilic drugs loaded in PLGA nanoparticles. *Journal of Materials Science: Materials in Medicine*, **13**, 29–32.
- Gutiérrez-Valenzuela, C., Guerrero-Germán, P., Tejeda-Mansir, A., Esquivel, R., Guzmán-Z, R. & Lucero-Acuña, A. (2016) Folate Functionalized PLGA Nanoparticles Loaded with Plasmid pVAX1-NH36: Mathematical Analysis of Release. *Applied Sciences*, **6**, 364. Multidisciplinary Digital Publishing Institute.
- Gutiérrez-Valenzuela, C., Rodríguez-Córdova, R., Hernández-Giottonini, Y., Guerrero-Germán, P. & Lucero-Acuña, A. (2017) Methylene Blue Loaded PLGA Nanoparticles: Combined Emulsion, Drug Release Analysis and Photodynamic Activity. *Microscopy and Microanalysis*, **23**, 1212–1213.
- Halliwell, B. & Whiteman, M. (2004) Measuring reactive species and oxidative damage in vivo and in cell culture: how should you do it and what do the results mean? *British Journal of Pharmacology*, **142**, 231–255.
- Hans, M. & Lowman, A.. (2002) Biodegradable nanoparticles for drug delivery and targeting. *Current Opinion in Solid State and Materials Science*, **6**, 319–327.

- He, X., Wu, X., Wang, K., Shi, B. & Hai, L. (2009) Methylene blue-encapsulated phosphonate-terminated silica nanoparticles for simultaneous in vivo imaging and photodynamic therapy. *Biomaterials*, **30**, 5601–5609. Elsevier Ltd.
- Horcas, I., Fernández, R., Gómez-Rodríguez, J.M., Colchero, J., Gómez-Herrero, J. & Baro, A.M. (2007) WSXM: a software for scanning probe microscopy and a tool for nanotechnology. *The Review of Scientific Instruments*, **78**, 13705. AIP Publishing.
- Huang, H.-C., Yang, Y., Nanda, A., Korla, P. & Rege, K. (2011) Synergistic administration of photothermal therapy and chemotherapy to cancer cells using polypeptide-based degradable plasmonic matrices. *Nanomedicine*, **6**, 459–473.
- Huang, X. & Brazel, C.S. (2001) On the importance and mechanisms of burst release in matrix-controlled drug delivery systems. *Journal of Controlled Release*, **73**, 121–136.
- Iborra, S., Soto, M., Carrión, J., Alonso, C. & Requena, J.M. (2004) Vaccination with a plasmid DNA cocktail encoding the nucleosomal histones of *Leishmania* confers protection against murine cutaneous leishmaniasis. *Vaccine*, **22**, 3865–76.
- Iqbal, M., Zafar, N., Fessi, H. & Elaissari, A. (2015) Double emulsion solvent evaporation techniques used for drug encapsulation. *International Journal of Pharmaceutics*, **496**, 173–190.
- Ismail, R., Allaudin, Z.N. & Lila, M.-A.M. (2012) Scaling-up recombinant plasmid DNA for clinical trial: current concern, solution and status. *Vaccine*, **30**, 5914–20.
- Jain, K. & Jain, N.K. (2015) Vaccines for visceral leishmaniasis: A review. *Journal of immunological methods*, **422**, 1–12.
- Jain, R.A. (2000) The manufacturing techniques of various drug loaded biodegradable poly(lactide-co-glycolide) (PLGA) devices. *Biomaterials*, **21**, 2475–90.
- Jayakumar, R., Chennazhi, K.P., Muzzarelli, R.A.A., Tamura, H., Nair, S.V. & Selvamurugan, N. (2010) Chitosan conjugated DNA nanoparticles in gene therapy. *Carbohydrate Polymers*, **79**, 1–8.
- Kirszberg, C., Rumjanek, V.M. & Capella, M.A.M. (2005) Methylene blue is more toxic to erythroleukemic cells than to normal peripheral blood mononuclear cells: A possible use in chemotherapy. *Cancer Chemotherapy and Pharmacology*, **56**, 659–665.
- Klepac-Ceraj, V., Patel, N., Song, X., Holewa, C., Patel, C., Kent, R., Amiji, M.M. & Soukos, N.S. (2011) Photodynamic effects of methylene blue-loaded polymeric nanoparticles on

- dental plaque bacteria. *Lasers in Surgery and Medicine*, **43**, 600–6. NIH Public Access.
- Kolarova, H., Bajgar, R., Tomankova, K., Nevrelouva, P. & Mosinger, J. (2007) Comparison of sensitizers by detecting reactive oxygen species after photodynamic reaction in vitro. *Toxicology in Vitro*, **21**, 1287–1291.
- Kolarova, H., Nevrelouva, P., Tomankova, K., Kolar, P., Bajgar, R. & Mosinger, J. (2008) Production of reactive oxygen species after photodynamic therapy by porphyrin sensitizers. *General physiology and biophysics*, **27**, 101–105.
- Kreuter, J. (2007a) Nanoparticles—a historical perspective. *International Journal of Pharmaceutics*, **331**, 1–10.
- Kreuter, J. (2007b) Nanoparticles—a historical perspective. *International Journal of Pharmaceutics*, **331**, 1–10.
- Kumari, A., Yadav, S.K. & Yadav, S.C. (2010) Biodegradable polymeric nanoparticles based drug delivery systems. *Colloids and Surfaces B: Biointerfaces*, **75**, 1–18.
- Kunugi, S. & Yamaoka, T. (2012) *Polymers in Nanomedicine*. P. in.: Advances in Polymer Science, Springer Berlin Heidelberg, Berlin, Heidelberg, Heidelberg.
- Lai, W.C., Dixit, N.S. & Mackay, R.A. (1984) Formation of H aggregates of thionine dye in water. *Journal of Physical Chemistry*, **88**, 5364–5368.
- Lam, M., Oleinick, N.L. & Nieminen, A.-L. (2001) Photodynamic therapy-induced apoptosis in epidermoid carcinoma cells. *The Journal of Biological Chemistry*, **276**, 47379–47386. in Press.
- Lao, L.L., Venkatraman, S.S. & Peppas, N.A. (2009) A novel model and experimental analysis of hydrophilic and hydrophobic agent release from biodegradable polymers. *Journal of Biomedical Materials Research Part A*, **90**, 1054–65.
- Lao, L.L., Peppas, N.A., Boey, F.Y.C. & Venkatraman, S.S. (2011) Modeling of drug release from bulk-degrading polymers. *International Journal of Pharmaceutics*, **418**, 28–41. Elsevier B.V.
- Leary, J.F. (2010) Nanotechnology: what is it and why is small so big? *Canadian Journal of Ophthalmology / Journal Canadien d'Ophthalmologie*, **45**, 449–456. Canadian Ophthalmological Society.
- Liang, C., Yang, Y., Ling, Y., Huang, Y., Li, T. & Li, X. (2011) Improved therapeutic effect of folate-decorated PLGA-PEG nanoparticles for endometrial carcinoma. *Bioorganic &*

- Medicinal Chemistry*, **19**, 4057–4066.
- Limayem, I., Charcosset, C. & Fessi, H. (2004) Purification of nanoparticle suspensions by a concentration/diafiltration process. *Separation and Purification Technology*, **38**, 1–9. Elsevier.
- Liu, Y., Li, K., Pan, J., Liu, B. & Feng, S.-S. (2010) Folic acid conjugated nanoparticles of mixed lipid monolayer shell and biodegradable polymer core for targeted delivery of Docetaxel. *Biomaterials*, **31**, 330–8.
- Long, Y., Li, Z., Bi, Q., Deng, C., Chen, Z., Bhattachayya, S. & Li, C. (2016) Novel polymeric nanoparticles targeting the lipopolysaccharides of *Pseudomonas aeruginosa*. *International Journal of Pharmaceutics*, **502**, 232–241.
- Lu, Y., Jiao, R., Chen, X., Zhong, J., Ji, A. & Shen, P. (2008) Methylene blue-mediated photodynamic therapy induces mitochondria-dependent apoptosis in HeLa cell. *Journal of Cellular Biochemistry*, **105**, 1451–1460.
- Lucero-Acuña, A. & Guzmán, R. (2015) Nanoparticle encapsulation and controlled release of a hydrophobic kinase inhibitor: Three stage mathematical modeling and parametric analysis. *International Journal of Pharmaceutics*, **494**, 249–257.
- Lucero-Acuna, J.A. (2013) Synthesis and characterization of polymeric nanoparticle structures for control drug delivery in cancer therapies and temperature effects on drug release. The University of Arizona.
- Makadia, H.K. & Siegel, S.J. (2011) Poly Lactic-co-Glycolic Acid (PLGA) as Biodegradable Controlled Drug Delivery Carrier. *Polymers*, **3**, 1377–1397.
- McCaughan, B., Rouanet, C., Fowley, C., Nomikou, N., McHale, A.P., McCarron, P.A. & Callan, J.F. (2011) Enhanced ROS production and cell death through combined photo- and sono-activation of conventional photosensitising drugs. *Bioorganic and Medicinal Chemistry Letters*, **21**, 5750–5752.
- Van Meerloo, J., Kaspers, G.J.L. & Cloos, J. (2011) Cell Sensitivity Assays: The MTT Assay. Pp. 237–245 in: *Methods in Molecular Biology*.
- Megeed, Z., Cappello, J. & Ghandehari, H. (no date) Controlled Release of Plasmid DNA from a Genetically Engineered Silk-Elastinlike Hydrogel. *Pharmaceutical Research*, **19**, 954–959. Kluwer Academic Publishers-Plenum Publishers.
- Mellish, K.J., Cox, R.D., Vernon, D.I., Griffiths, J. & Brown, S.B. (2002) In vitro photodynamic

- activity of a series of methylene blue analogues. *Photochemistry and Photobiology*, **75**, 392.
- Menon, J.U., Ravikumar, P., Pise, A., Gyawali, D., Hsia, C.C.W. & Nguyen, K.T. (2014) Polymeric nanoparticles for pulmonary protein and DNA delivery. *Acta biomaterialia*, **10**, 2643–52.
- Miladi, K., Sfar, S., Fessi, H. & Elaissari, A. (2016) *Polymer Nanoparticles for Nanomedicines*. P. in.:
- Mora-Huertas, C.E., Fessi, H. & Elaissari, A. (2010) Polymer-based nanocapsules for drug delivery. *International Journal of Pharmaceutics*, **385**, 113–142.
- Mora-Huertas, C.E., Fessi, H. & Elaissari, A. (2011) Influence of process and formulation parameters on the formation of submicron particles by solvent displacement and emulsification-diffusion methods: Critical comparison. *Advances in Colloid and Interface Science*, **163**, 90–122. Elsevier B.V.
- Mu, L. & Feng, S.S. (2003) A novel controlled release formulation for the anticancer drug paclitaxel (Taxol): PLGA nanoparticles containing vitamin E TPGS. *Journal of Controlled Release*, **86**, 33–48.
- Murakami, H., Kobayashi, M., Takeuchi, H. & Kawashima, Y. (2000) Further application of a modified spontaneous emulsification solvent diffusion method to various types of PLGA and PLA polymers for preparation of nanoparticles. *Powder Technology*, **107**, 137–143.
- Nagill, R. & Kaur, S. (2011) Vaccine candidates for leishmaniasis: A review. *International Immunopharmacology*, **11**, 1464–88.
- National Nanotechnology Initiative. (2017a) What It Is and How It Works | Nano. <<http://www.nano.gov/nanotech-101/what>>.
- National Nanotechnology Initiative. (2017b) What It Is and How It Works | Nano.
- Nava-Arzaluz, M.G., Piñón-Segundo, E., Ganem-Rondero, A. & Lechuga-Ballesteros, D. (2012) Single emulsion-solvent evaporation technique and modifications for the preparation of pharmaceutical polymeric nanoparticles. *Recent Patents on Drug Delivery & Formulation*, **6**, 209–23.
- Nie, Y., Zhang, Z., Li, L., Luo, K., Ding, H. & Gu, Z. (2009) Synthesis, characterization and transfection of a novel folate-targeted multipolymeric nanoparticles for gene delivery. *Journal of Materials Science: Materials in Medicine*, **20**, 1849–1857.
- Noury, M. & López, J. (2017) Nanomedicine and personalised medicine: understanding the

- personalisation of health care in the molecular era. *Sociology of Health and Illness*, **39**, 547–565.
- Pagonis, T.C., Chen, J., Fontana, C.R., Devalapally, H., Ruggiero, K., Song, X., Foschi, F., Dunham, J., Skobe, Z., Yamazaki, H., Kent, R., Tanner, A.C.R., Amiji, M.M. & Soukos, N.S. (2010) photodynamic therapy. *Journal of Endodontics*, **36**, 322–328.
- Palatnik-de-Sousa, C.B. (2008) Vaccines for leishmaniasis in the fore coming 25 years. *Vaccine*, **26**, 1709–24.
- Park, H., Yang, J., Lee, J., Haam, S., Choi, I.H. & Yoo, K.H. (2009) Multifunctional nanoparticles for combined doxorubicin and photothermal treatments. *ACS Nano*, **3**, 2919–2926.
- Parveen, S. & Sahoo, S.K. (2008) Polymeric nanoparticles for cancer therapy. *Journal of Drug Targeting*, **16**, 108–123.
- Paszko, E., Ehrhardt, C., Senge, M.O., Kelleher, D.P. & Reynolds, J. V. (2011) Nanodrug applications in photodynamic therapy. *Photodiagnosis and Photodynamic Therapy*, **8**, 14–29. Elsevier B.V.
- Paun, I.A., Moldovan, A., Luculescu, C.R., Staicu, A. & Dinescu, M. (2012) MAPLE deposition of PLGA:PEG films for controlled drug delivery: Influence of PEG molecular weight. *Applied Surface Science*, **258**, 9302–9308.
- Peer, D., Karp, J.M., Hong, S., Farokhzad, O.C., Margalit, R. & Langer, R. (2007) Nanocarriers as an emerging platform for cancer therapy. *Nature nanotechnology*, **2**, 751–760.
- Peracchia, M.T., Gref, R., Minamitake, Y., Domb, A., Lotan, N. & Langer, R. (1997) PEG-coated nanospheres from amphiphilic diblock and multiblock copolymers: Investigation of their drug encapsulation and release characteristics<sup>1</sup>. *Journal of Controlled Release*, **46**, 223–231.
- Perez, C., Sanchez, A., Putnam, D., Ting, D., Langer, R. & Alonso, M. J. (2001) Poly(lactic acid)-poly(ethylene glycol) nanoparticles as new carriers for the delivery of plasmid DNA. *Journal of Controlled Release*, **75**, 211–224.
- Prout, E.G. & Tompkins, F.C. (1944) The thermal decomposition of potassium permanganate. *Transactions of the Faraday Society*, **40**, 488. The Royal Society of Chemistry.
- Rastogi, R.P., Singh, S.P., Häder, D.P. & Sinha, R.P. (2010) Detection of reactive oxygen species (ROS) by the oxidant-sensing probe 2',7'-dichlorodihydrofluorescein diacetate in

- the cyanobacterium *Anabaena variabilis* PCC 7937. *Biochemical and Biophysical Research Communications*, **397**, 603–607.
- Sahana, D.K., Mittal, G., Bhardwaj, V. & Kumar, M.N.V.R. (2008) PLGA nanoparticles for oral delivery of hydrophobic drugs: influence of organic solvent on nanoparticle formation and release behavior in vitro and in vivo using estradiol as a model drug. *Journal of Pharmaceutical Sciences*, **97**, 1530–42.
- Sahoo, S.K., Panyam, J., Prabha, S. & Labhasetwar, V. (2002) Residual polyvinyl alcohol associated with poly ( D , L-lactide-co-glycolide ) nanoparticles affects their physical properties and cellular uptake R esidual polyvinyl alcohol associated with poly ( D , L - lactide-co- glycolide ) nanoparticles affects thei. *Journal of Controlled Release*, **82**, 105–114.
- Saljoughian, N., Zahedifard, F., Doroud, D., Doustdari, F., Vasei, M., Papadopoulou, B. & Rafati, S. (2013) Cationic solid-lipid nanoparticles are as efficient as electroporation in DNA vaccination against visceral leishmaniasis in mice. *Parasite Immunology*, **35**, 397–408.
- Santini, J.T. (2013) Introduction to drug delivery technology. *Chemical Engineering and Processing*, **109**, 19–23,39.
- Schaffert, D. & Wagner, E. (2008) Gene therapy progress and prospects: synthetic polymer-based systems. *Gene therapy*, **15**, 1131–8. Nature Publishing Group.
- Sharma, N., Madan, P. & Lin, S. (2016) Effect of process and formulation variables on the preparation of parenteral paclitaxel-loaded biodegradable polymeric nanoparticles: A co-surfactant study. *Asian Journal of Pharmaceutical Sciences*, **11**, 404–416. Elsevier.
- Shi, J., Votruba, A.R., Farokhzad, O.C. & Langer, R. (2010) Nanotechnology in drug delivery and tissue engineering: from discovery to applications. *Nano Letters*, **10**, 3223–3230.
- Shi, X., Li, C., Gao, S., Zhang, L., Han, H., Zhang, J., Shi, W. & Li, Q. (2014) Combination of doxorubicin-based chemotherapy and polyethylenimine/p53 gene therapy for the treatment of lung cancer using porous PLGA microparticles. *Colloids and Surfaces B: Biointerfaces* , **122**, 498–504.
- Son, S. & Kim, W.J. (2010) Biodegradable nanoparticles modified by branched polyethylenimine for plasmid DNA delivery. *Biomaterials*, **31**, 133–43.
- Song, A., Ji, S., Sook Hong, J., Ji, Y., Gokhale, A.A. & Lee, I. (2016) Encapsulation of

- hydrophobic or hydrophilic iron oxide nanoparticles into poly(lactic acid) micro/nanoparticles via adaptable emulsion setup. *Journal of Applied Polymer Science*, **133**, 1–10.
- Soppimath, K.S., Aminabhavi, T.M., Kulkarni, A.R. & Rudzinski, W.E. (2001) Biodegradable polymeric nanoparticles as drug delivery devices. *Journal of Controlled Release*, **70**, 1–20.
- Tada, D.B., Vono, L.L.R., Duarte, E.L., Itri, R., Kiyohara, P.K., Baptista, M.S. & Rossi, L.M. (2007) Methylene blue-containing silica-coated magnetic particles: A potential magnetic carrier for photodynamic therapy. *Langmuir*, **23**, 8194–8199. American Chemical Society.
- Tang, W., Xu, H., Kopelman, R. & Philbert, M. (2005) Photodynamic Characterization and In Vitro Application of Methylene Blue-containing Nanoparticle Platforms. *Photochemistry and Photobiology*, **81**, 242.
- Tardivo, J.P.J.P., Del Giglio, A., De Oliveira, C.S., Gabrielli, D.S., Junqueira, H.C., Tada, D.B., Severino, D., Turchiello, R.D.F., Baptista, M.S., de Fátima Turchiello, R., Baptista, M.S., De Fattima Turchiello, R. & Baptista, M.S. (2005) Methylene blue in photodynamic therapy: From basic mechanisms to clinical applications. *Photodiagnosis and Photodynamic Therapy*, **2**, 175–191.
- Teichert, M.C., Jones, J.W., Usacheva, M.N. & Biel, M.A. (2002) Treatment of oral candidiasis with methylene blue-mediated photodynamic therapy in an immunodeficient murine model. *Oral Surgery, Oral Medicine, Oral Pathology, Oral Radiology*, **93**, 155–160.
- Tewes, F., Munnier, E., Antoon, B., Ngaboni Okassa, L., Cohen-Jonathan, S., Marchais, H., Douziech-Eyrolles, L., Soucé, M., Dubois, P. & Chourpa, I. (2007) Comparative study of doxorubicin-loaded poly(lactide-co-glycolide) nanoparticles prepared by single and double emulsion methods. *European Journal of Pharmaceutics and Biopharmaceutics*, **66**, 488–492.
- Tuite, E.M. & Kelly, J.M. (1993) Photochemical interactions of methylene blue and analogues with DNA and other biological substrates. *Journal of photochemistry and photobiology. B, Biology*, **21**, 103–24.
- Vauthier, C. & Bouchemal, K. (2009) Methods for the Preparation and Manufacture of Polymeric Nanoparticles. *Pharmaceutical Research*, **26**, 1025–1058.
- Vivero-Escoto, J. & Elnagheeb, M. (2015) Mesoporous Silica Nanoparticles Loaded with Cisplatin and Phthalocyanine for Combination Chemotherapy and Photodynamic Therapy

- in vitro. *Nanomaterials*, **5**, 2302–2316. Multidisciplinary Digital Publishing Institute.
- Wainwright, M. & Crossley, K.B. (2002) Methylene Blue - a Therapeutic Dye for All Seasons? *Journal of Chemotherapy*, **14**, 431–443.
- Wang, D., Robinson, D.R., Kwon, G.S. & Samuel, J. (1999) Encapsulation of plasmid DNA in biodegradable poly(D,L-lactic-co-glycolic acid) microspheres as a novel approach for immunogene delivery. *Journal of Controlled Release*, **57**, 9–18.
- Wen, Y., Pan, S., Luo, X., Zhang, X., Zhang, W. & Feng, M. (2009) A biodegradable low molecular weight polyethylenimine derivative as low toxicity and efficient gene vector. *Bioconjugate Chemistry*, **20**, 322–332.
- Würmseher, M. & Firmin, L. (2017) Nanobiotech in big pharma: a business perspective. *Nanomedicine*, **12**, 535–543.
- Yang, F., Liu, S., Xu, J., Lan, Q., Wei, F. & Sun, D. (2006) Pickering emulsions stabilized solely by layered double hydroxides particles: The effect of salt on emulsion formation and stability. *Journal of Colloid and Interface Science*, **302**, 159–169.
- Yang, J., Lee, C.-H., Park, J., Seo, S., Lim, E.-K., Song, Y.J., Suh, J.-S., Yoon, H.-G., Huh, Y.-M. & Haam, S. (2007) Antibody conjugated magnetic PLGA nanoparticles for diagnosis and treatment of breast cancer. *Journal of Materials Chemistry*. .
- Yang, S.-J., Lin, F.-H., Tsai, K.-C., Wei, M.-F., Tsai, H.-M., Wong, J.-M. & Shieh, M.-J. (2010) Folic acid-conjugated chitosan nanoparticles enhanced protoporphyrin IX accumulation in colorectal cancer cells. *Bioconjugate chemistry*, **21**, 679–89.
- Yoo, H.S. & Park, T.G. (2004a) Folate-receptor-targeted delivery of doxorubicin nano-aggregates stabilized by doxorubicin-PEG-folate conjugate. *Journal of Controlled Release*, **100**, 247–256.
- Yoo, H.S. & Park, T.G. (2004b) Folate receptor targeted biodegradable polymeric doxorubicin micelles. *Journal of Controlled Release*, **96**, 273–83.
- Yu, J., Hsu, C., Huang, C. & Chang, P. (2015) Development of Therapeutic Au – Methylene Blue Nanoparticles for Targeted Photodynamic Therapy of Cervical Cancer Cells. *ACS Applied Materials and Interfaces*, **7**, 432–441.
- Zambaux, M.F., Bonneaux, F., Gref, R., Maincent, P., Dellacherie, E., Alonso, M.J., Labrude, P. & Vigneron, C. (1998) Influence of experimental parameters on the characteristics of poly(lactic acid) nanoparticles prepared by a double emulsion method. *Journal of*

*Controlled Release*, **50**, 31–40.

Zhang, P., Steelant, W., Kumar, M. & Scholfield, M. (2007) Versatile Photosensitizers for Photodynamic Therapy at Infrared Excitation. *Journal of the American Chemical Society*, 4526–4527. American Chemical Society.

Zhang, X.F. & Li, X. (2011) The photostability and fluorescence properties of diphenylisobenzofuran. *Journal of Luminescence*, **131**, 2263–2266.

Zhao, K., Zhang, Y., Zhang, X., Shi, C., Wang, X., Wang, X., Jin, Z. & Cui, S. (2014) Chitosan-coated poly(lactic-co-glycolic) acid nanoparticles as an efficient delivery system for Newcastle disease virus DNA vaccine. *International journal of nanomedicine*, **9**, 4609–19. Dove Press.